Order Number 8804153

Salt redistribution during freezing of saline sand columns with applications to subsea permafrost

Baker, Grant Cody, Ph.D.

University of Alaska Fairbanks, 1987

U·M·I
300 N. Zeeb Rd.
Ann Arbor, MI 48106

PLEASE NOTE:

In all cases this material has been filmed in the best possible way from the available copy. Problems encountered with this document have been identified here with a check mark __✓__.

1. Glossy photographs or pages __✓__
2. Colored illustrations, paper or print _____
3. Photographs with dark background __✓__
4. Illustrations are poor copy _____
5. Pages with black marks, not original copy _____
6. Print shows through as there is text on both sides of page _____
7. Indistinct, broken or small print on several pages __✓__
8. Print exceeds margin requirements _____
9. Tightly bound copy with print lost in spine _____
10. Computer printout pages with indistinct print _____
11. Page(s) _____ lacking when material received, and not available from school or author.
12. Page(s) _____ seem to be missing in numbering only as text follows.
13. Two pages numbered _____. Text follows.
14. Curling and wrinkled pages _____
15. Dissertation contains pages with print at a slant, filmed as received __✓__
16. Other _____

_____

_____

U·M·I

SALT REDISTRIBUTION DURING FREEZING OF SALINE SAND COLUMNS WITH APPLICATIONS TO SUBSEA PERMAFROST

A

THESIS

Presented to the Faculty of the University of Alaska

in Partial Fulfillment of the Requirements

for the Degree of

DOCTOR OF PHILOSOPHY

By

Grant Cody Baker, B.S., M.S.

Fairbanks, Alaska

September 1987

SALT REDISTRIBUTION DURING FREEZING OF SALINE SAND COLUMNS WITH APPLICATIONS TO SUBSEA PERMAFROST

RECOMMENDED:

John P. Jarlin

L. Cannon

D. B. Hawkins

W. D. Harrison

A. P. Weeks

J. P. Zarling

T. E. Osterkamp

Chairman, Advisory Committee

Tom Dawson

Department Head

APPROVED:

Dean, College of Natural Sciences

Director of Graduate Programs

14 July 1987

Date

ABSTRACT

Laboratory experiments were designed to investigate salt redistribution during the freezing of saline sand columns and to obtain information on salt movement in saturated sands and reconstituted subsea permafrost samples. The results of these experiments were combined with results from field investigations of subsea permafrost at Prudhoe Bay, Alaska to develop an improved understanding of salt redistribution during freezing and the movement of salt in the seabed sediments. These processes can produce soil solution salinities in the sediments greater than about 50 ppt. Comparison of spring and fall salinity profiles indicate salt movement with velocities of at least 2 m/year. Laboratory freezing (downward) tests of saline sand columns show significant salt redistribution at growth rates between 0.1 and 2 cm/day. Salt movement was observed with velocities of at least 2 cm/day. Salt movement in the unfrozen soil solution in partially frozen sand appears to be the result of gravity drainage. Freezing upward produced no significant salt redistribution. Salt fingering experiments showed that salt fingers could move with velocities of several cm/hr and suggest that it may be a major mechanism for rapid salt movement in subsea permafrost. Fingers (freshwater) at a thawing fresh ice boundary overlain by thawed saline soil solution displayed

similar rapid movement behavior. Laboratory measurements of the hydraulic conductivity, K, of subsea permafrost samples yielded values that were 10^2 to 10^3 times greater than previously reported in-situ measurements. While it is difficult to apply the laboratory results to subsea permafrost under field conditions, these greater values for K and the large salt fingering velocities suggest that gravity-driven convection, in the form of salt fingering, should be considered as a primary mechanism for rapid salt transport in subsea permafrost.

TABLE OF CONTENTS

TABLE OF CONTENTS (Continued)

TABLE OF CONTENTS (Continued)

LIST OF FIGURES

LIST OF FIGURES (Continued)

LIST OF FIGURES (Continued)

LIST OF FIGURES (Continued)

LIST OF TABLES

LIST OF TABLES (Continued)

ACKNOWLEDGEMENTS

This research was performed under the direction of committee chairman Dr. T. E. Osterkamp, whose suggestions and encouragement were greatly appreciated. I would like to thank my other committee members, Drs. J. Gosink, H. Harrison, D. Hawkins, K. Kawasaki, W. Weeks, and J. Zarling for their valuable contributions.

Computer programs for graphics and computations were developed with many helpful suggestions and consultations from Mr. J. St. Sauver. The field work was a cooperative effort on the part of B. Fisk, V. Gruol, W. Harrison, T. Matava, and T. Osterkamp.

Funding was provided, in part, by the National Science Foundation, Division of Polar Programs, Earth Sciences Section under grant DPP83-12026, and was greatly appreciated. Finally, I would especially like to thank my sweetee, Tina Louise Denton, for her perseverance and support throughout this project.

Chapter 1

INTRODUCTION

1.1 Salt Redistribution During Freezing

Solute redistribution during the solidification of metals has been studied extensively since the early nineteen fifties (Rutter and Chalmers, 1953; Tiller, et al. 1953; Burton, et al., 1953). More recently, salt redistribution during the freezing of seawater and other saline solutions has been investigated and, while many details remain obscure, the problem has been fairly well described (Adams, et al. 1963; Weeks and Lofgren, 1967; Lake and Lewis, 1970; Terwilliger and Dizio, 1970; Grange, et al., 1974; Cox and Weeks, 1975; Grange, et al. 1976; Nakawo and Sinha, 1981).

In contrast, the study of salt redistribution during freezing in soils has received much less attention and there have been few studies directed toward this subject (Banin and Anderson, 1974; Sheeran and Yong, 1975; Sheeran et al., 1976; Hallet, 1978; De Jong, 1981; Mahar, et al., 1983; Kay and Groenevelt, 1983). The effects of freezing rate, solute concentration and soil type on solute redistribution during freezing have yet to be defined.

Salt redistribution during freezing is an important subject in subsea permafrost studies. During the winter season at the ARCO West Dock, Prudhoe Bay, Alaska, the sea ice freezes to the seabed and some distance into the

sediments in the region from the shoreline to about 400 m offshore. From 400 m to about 3 km offshore, the sea ice freezes sporadically to and into the sediments (Osterkamp and Harrison, 1977). In this region, the sediments may become partially frozen (Page and Iskandar, 1978; Harrison and Osterkamp, 1982).

Evidence has been found which indicates that salts rejected during sea ice formation infiltrate the sediments (Page, 1978). Concentrated saline soil solutions have been found immediately below partially frozen sediments. Where the sea ice freezes nearly to the seabed and sub-ice circulation is poor, sea ice formation produces a concentrated brine layer sandwiched between the bottom of the sea ice and the surface of the sediments which can, potentially, infiltrate the sediments (Page and Iskandar, 1978).

Annual sea ice formation and the occurrence of concentrated brines may result in the infiltration of large amounts of salts into the sediments. The freezing of the sediments near the seabed may also cause additional salts to infiltrate deeper into the sediments (Osterkamp, 1975). If the rejected salts are mobile, they may move rapidly until reaching a less permeable barrier, such as fine-grained soil or an impermeable frozen soil layer (permafrost).

The addition of large amounts of salts into the

sediments in the nearshore area can dramatically alter the physical and mechanical properties of the subsea permafrost by decreasing the freezing point of the soil solution. This reduces the amount of pore ice and, consequently, the soil may become partially ice-bonded or non-ice bearing which can decrease strength dramatically. These effects can cause an increase in the hydraulic conductivity of the soil which may allow greater soil solution movement, enhanced heat and salt transfer, and additional pore ice melting. Therefore, it was considered possible that the infiltration of salts into the sediments may play a key role in the thawing of subsea permafrost.

Since the addition of salts may have such a significant effect on the mechanical and physical properties of subsea permafrost and on transport processes occurring in it, it is important to understand the mechanism(s) for salt movement. In offshore oil exploration and development, the proper design and construction of offshore structures, such as gravel islands, roads, and pipelines, must take into account the effect of salt and salt movement within the subsea permafrost.

Previous research conducted on identifying the mechanism(s) of salt transport in subsea permafrost has been inconclusive (Osterkamp, 1975; Harrison and Osterkamp, 1982; Swift et al., 1983; Swift and Harrison, 1984). One reason

for the present study was to obtain new data and to try to develop new insights into the possible mechanism(s) of salt transport in subsea permafrost.

1.2 Objectives

The objectives of this study were:

1) To investigate salt redistribution in the nearshore subsea permafrost in the layer characterized by annual freezing and thawing at the seabed.

2) To investigate salt redistribution during the freezing of saline sand columns in the laboratory.

3) To investigate the implications of these salt redistribution studies in interpreting field data on subsea permafrost.

1.3 Work Plan

Both field work and laboratory experiments were performed. The purpose of the field work was to obtain data for in-situ soil solution salinity, water content, and temperature profiles of the nearshore subsea permafrost in the zone of annual freezing and thawing. These data were then used to design the necessary laboratory experiments for the freezing of saline sand columns. The experiments were conducted, primarily, to determine salt redistribution during downward freezing at various growth rates.

Examination of the initial results of the laboratory freezing experiments prompted additional laboratory tests conducted on freezing direction and salt fingering.

Finally, the laboratory results were utilized to interpret and analyze the field data in an attempt to develop new insight into the possible mechanism(s) of salt transport in subsea permafrost in the nearshore region of annual freezing and thawing of the sediments.

1.4 Thesis Organization

Topics discussed in this study are diverse in nature and include a wide range of measurements, methods, procedures, calibrations, etc. To preserve continuity between discussions, the thesis organization will be the same as that of the work plan. The next chapter (Chapter 2) will present the field data and its analysis and interpretation. Chapter 3 will present the laboratory data and its analysis and interpretation. Chapter 4 presents the results and provides interpretation of special laboratory tests on salt fingering. Chapter 5 will be a synthesis of the laboratory results and an examination of their implications for subsea permafrost. The final chapter (Chapter 6) will be a summary of the work presented by this thesis.

Chapter 2

SALT REDISTRIBUTION IN NEARSHORE SUBSEA PERMAFROST BY ANNUAL FREEZING OF THE SEDIMENTS NEAR THE SEABED

2.1 Field Site Description

The field site was located at the ARCO West Dock, Prudhoe Bay, Alaska along a line originating at the North Prudhoe Bay State Number 1 well head (which no longer exists) and bearing N31.5E as shown in Figure 2.1. This has been the area and approximate line investigated by Osterkamp and Harrison (1976), Sellman et al. (1976), Osterkamp and Harrison (1985), and Matava (1986) and will be referred to as the West Dock Line (WDL).

The onshore area is characterized by ice-rich tundra flatlands. The mean annual surface temperature (MAST) is about -10 °C (Lachenbruch, 1982). It is a region of continuous permafrost with depths greater than 600 meters (Osterkamp and Payne, 1981) and subsea permafrost extending a few tens of kilometers offshore (Osterkamp, et al., 1985). The onshore permafrost acts as a barrier to surface water percolation and results in a generally wet condition of the area in the summer.

Formation of nearshore subsea permafrost is a result of shoreline regression in permafrost areas. This was caused by a rise in sea level until about 3000 to 4000 B.P. and is presently caused by shoreline erosion (Mackay, 1972). Warm

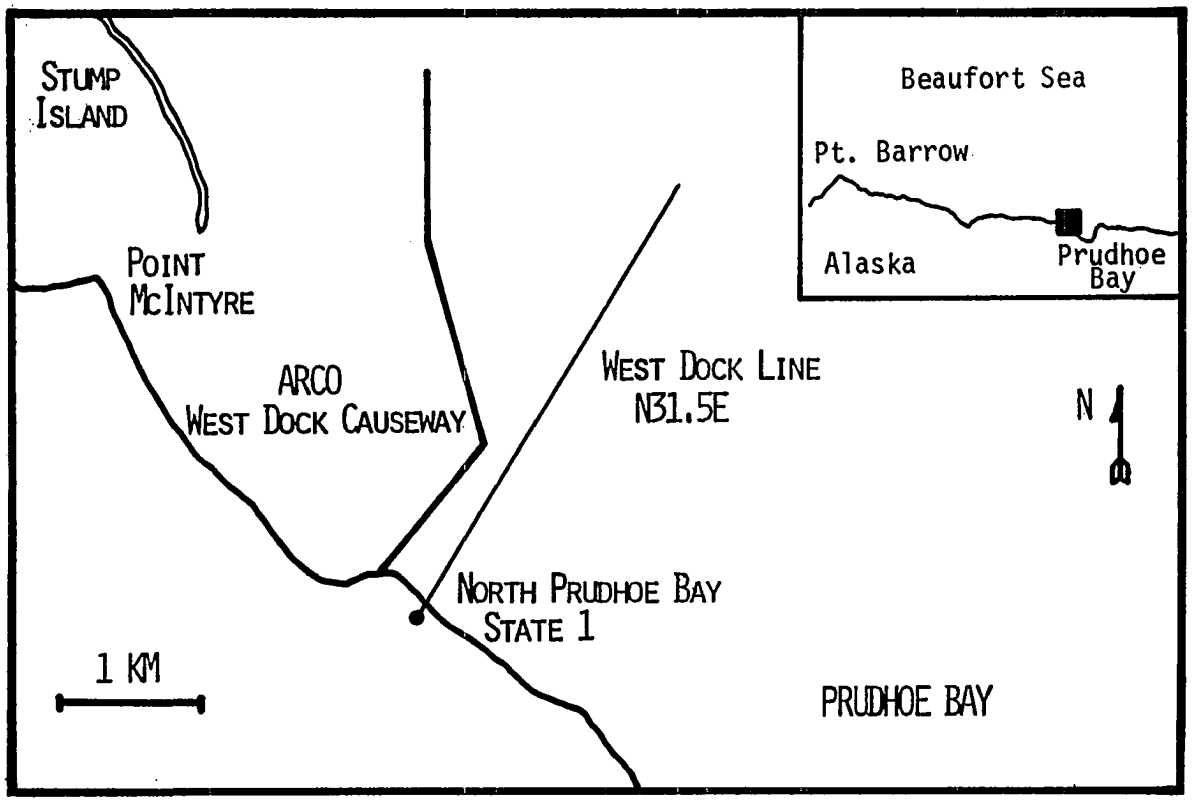

Fig. 2.1: Map showing the location of the field study site, near the ARCO West Dock, Prudhoe Bay, Alaska.

seawater and wave action during summer storms are major causes of shoreline erosion. Because of the low topography and high ice content of the top 10 m of soil in the area, relatively high shoreline erosion rates can occur. The shoreline has been reported to be regressing at about 1 m/yr (Alexander and others, 1975; Hopkins and Hartz, 1978). This has resulted in the formation of subsea permafrost (transgression of the sea over permafrost) in most of the continental shelf of the Beaufort Sea (Hopkins and Sellman, 1983).

The nearshore region is herein defined as that region from the shoreline to about 3 km offshore. The seawater depth in this region is about two meters or less.

During the winter of each year, the sea ice freezes directly to or nearly to the seabed (Osterkamp and Harrison, 1977). Consequently, the thermal and chemical boundary conditions at the seabed in this region are different from those of the deeper water regions that exist farther offshore (Osterkamp, 1975). Therefore, it may be expected that heat and salt transport processes in this region may differ from those in regions farther offshore.

Drilling programs by Osterkamp and Harrison (1976), Hopkins and Hartz (1978), and Sellman and Chamberlain (1980) have indicated that the area offshore has a 1 to 10 m sequence of Holocene marine sediments (muddy sands) which

overlie sandy gravels or glacial outwash (Hopkins and Hartz, 1978). The sediments above the ice-bonded permafrost table have been characterized as silty gravelly sands for distances up to 3 km offshore by Osterkamp and Harrison (1976), a description which agrees with that of Sellman and Chamberlain (1980).

2.2 Ice-Bonded Permafrost Table

Results of the work by Osterkamp and Harrison (1976), Sellman, et al. (1977), and Osterkamp and Harrison (1985) have been combined to define the depth to the ice-bonded permafrost table (IBPT) along the WDL. Their results on subsea permafrost distribution, sea ice conditions, sediment salinity conditions, and temperature profiles, were used to classify the nearshore subsea permafrost at Prudhoe Bay into two zones as follows:

1) 0 to 400 m offshore.

In this zone, the sea ice freezes annually to the seabed and some distance into the sediments. The rejected salts from sea ice formation may infiltrate the sediments and freezing of the sediments may also cause additional salts to be forced deeper into the sediments.

Depth to the IBPT increases slowly to about 3 or 4 m at 400 m offshore. There is a seasonal active layer that reaches to the IBPT which is analogous to an active layer

onshore in that it freezes and thaws each year.

2) 400 m to about 3 km from shore.

In this region, the sea ice freezes to the seabed in some places and nearly to it in others. Where the sea ice almost freezes to the seabed, concentrated brines rejected from the sea ice during its growth may accumulate beneath the sea ice on the seabed. Infiltration of these cold and saline brines into the sediments is thought to occur (Page and Iskandar, 1978). If the concentration of the brines is greater than that of the soil solution, then partial freezing of the sediments may occur.

It is thought that the sediments immediately above the IBPT are thawed. The IBPT is mechanically very distinct and is referred to as the phase boundary because it is a contact between the frozen and thawed sediments.

Two different behaviors are displayed by the IBPT profile in this zone. From about 400 m to 440 m offshore, the depth of the IBPT increases rapidly and nearly linearly from about 4 m to about 14 m. This implies a rate of thaw of about 0.25 m/year assuming a shoreline regression of about 1 m/year. This portion of the IBPT has been referred to as the "ramp" (Osterkamp and Harrison, 1985).

From about 440 m to about 3.4 km offshore, the IBPT profile has a parabolic shape described by the equation (Harrison and Osterkamp, 1982)

$$Y = a\,(x-x_o)^{1/2} \qquad (2.1)$$

where: Y = depth (m) of the IBPT below the seabed

x = distance (m) from shore (x > 440 m)

a = 1.147 $m^{1/2}$

x_o = 276 m.

At the IBPT, the temperature is fairly constant at about -2.4 °C.

The depth of thaw of the sediments in the parabolic region can be predicted by a simple Stefan heat conduction model. Negative temperatures at the IBPT indicate that salt transport to the IBPT is occurring at a rate which cannot be explained by a salt diffusion mechanism and suggest convection by porewater motion (Harrison and Osterkamp, 1978).

It was suggested by Osterkamp and Harrison (1985) that the transport of salt from the ocean into the sediments is a key feature of subsea permafrost evolution. A potentially important salt transport mechanism was gravity-driven convection of the soil solution within the thawed layer of the sediments (Harrison and Osterkamp, 1978). The driving force for this mechanism was assumed to be the release of buoyant relatively-fresh soil solution by thawing at the IBPT. Subsequent investigations have shown that this may not be the case (Swift et al., 1983; Swift and Harrison,

1984) and suggest that there may be an unidentified process involved (Swift and Harrison, 1984).

In the nearshore region, it is apparent that the chemical and thermal conditions at the seabed, and IBPT depth, change dramatically with distance offshore. Annual sea ice formation results in large amounts of salts being made available which can infiltrate the sediments. Salt redistribution in the sediments during freezing may force these salts deeper. The presence and movement of these salts form the basis by which the thawing of the subsea permafrost may eventually be explained.

2.3 Field Methods and Procedures

2.3.1 Introduction

It was suggested by Osterkamp (1975) that freezing of the sediments near the seabed could potentially force high salinity brine deeper into the sediments. Subsequent research (Osterkamp and Harrison, 1977, and Page and Iskandar, 1978) confirmed that in the nearshore areas where the sea ice froze to or nearly to the seabed, salt (rejected during sea ice formation) was being transported into the sediments. However, additional temperature and salinity data of the sediments were needed in order to develop a more detailed understanding of the process of salt rejection and redistribution during sediment freezing. Therefore,

temperature logging and sampling of the sediments were conducted along the WDL out to about 3 km offshore. The samples were analyzed for soil type, water content, and salinity of the soil solution.

2.3.2 Work Schedule

There were three field seasons in which soil sampling and temperature measurements were conducted; spring 1984, fall 1984, and spring 1985. Table 2.1 gives the work schedule and a description of the activities for each field season. These provided a sampling program that represented a complete cycle of yearly thawing and freezing. The spring and fall were chosen as the times for the field seasons since they represent the time of the maximum depth of freezing and thawing, respectively. Other considerations, such as these being the only times with reasonable weather and sea ice conditions were also factors considered in scheduling the field research.

2.3.3 Sediment Temperature Measurement

Temperature logging access tubing was placed in the sediments using the methods and procedures described by Osterkamp and Harrison (1981 and 1982), and Osterkamp (1984). The drill rod was driven with a Cobra™ gasoline-powered jackhammer, and an electric Bosch Breaker hammer

Table 2.1

Field program work schedule

Dates	Activities
May 21, 1984 to June 2,1984	1) Sampling of the sediments near the seabed from 400 m to 3 km offshore. 2) Placement of temperature holes in this region. 3) Hole heating of some temperature holes. 4) Temperature logging.
October 10, 1984 to November 3, 1984	1) Sampling of the sediments near the seabed from 10 m to about 450 m offshore. 2) Placement of temperature holes in this region. 3) Temperature logging of holes placed in both spring and fall.
May 27, 1985 to June 2, 1985	1) Sampling of the sediments near the seabed from 10 m to about 450 m offshore.

(model number 11304) with a Honda 3000 watt gasoline-powered generator for the power supply.

The holes were located by using standard surveying methods described by Osterkamp and Harrison (1976) and were allowed to equilibrate for at least a day after drilling before the first temperature logging.

Resistance measurements of the thermistor sensors on the temperature logging cables were made with a Leeds and Northrup Wheatstone Bridge Model Number 4289. The procedures used for determination of the temperature were similar to those described by Osterkamp and Harrison (1982) and Osterkamp (1984).

Two different logging cables were constructed, each having two thermistors in parallel. This was to reduce the possible heating effects that could be incurred during resistance measurements. One cable used Fenwall type 2-GB 38SM2-H-76 thermistors. The second cable used Fenwall type 2-GC 32SM2-H-73 thermistors.

The method for calibration of all temperature logging cables used was similar to that described by Osterkamp (1984) which requires resistance measurements at three known temperatures. Two of the calibration temperatures were obtained with a constant temperature bath (Forma Scientific model number 2161). An ice bath was used to obtain a third calibration temperature.

A few of the holes were heated in an attempt to determine the ice content. The methods and procedures used were similar to those described by Osterkamp and Harrison (1980).

2.3.4 Sediment Sampling

Both SIPRE cores and Shelby tube samples of the sediments were obtained. Two different diameter Shelby tubes [2-inch (5.08 cm) and 2 3/8-inch (6.03 cm)] with a length of 30-inches (76.2 cm) were used and were purchased from Diamond Drill Contracting Co.

The sampling procedure was similar to that described by Osterkamp and Harrison (1976). The Shelby tubes were driven into the sediments with the gasoline powered jackhammer for the spring 1984 field season. For all subsequent field seasons, the electric Bosch hammer was used.

After the sampler had been driven into the sediments to the desired depth, the sampler was pulled with a jacking rig. This apparatus was similar to that described by Osterkamp and Harrison (1982) for pulling drill rod. After pulling, the Shelby tube was removed from the drill rod and placed immediately in a sample extruder (Diamond Drill Part No. 011380). The sample was extruded and segmented into samples approximately 5 cm in length. Each sample was

placed in a Nalgene sample jar which was sealed and packaged before being sent to the laboratories of the Geophysical Institute in Fairbanks for analyses.

SIPRE sample cores, measuring 3-inches in diameter, were taken with a portable gasoline driven Tecumseh 3 h.p. driving head that requires two persons to operate safely. After coring, the sample cores were removed from the core barrel and immediately segmented and placed into sample jars.

2.3.5 Sample Preparation

Over 700 field samples were analyzed for gravimetric water content and soil solution salinity. The method used was similar to that described by Kay and Groenevelt (1983) for their nitrate analysis. A portion of about 100 grams from each sample was selected and oven dried at about 105 ^{o}C. The sample was then rewetted with distilled water in a ratio of 2:1 (distilled water:dry sample) by weight. The samples were allowed to soak for about 24 hours before the electrical conductivity of the diluted soil solution was measured. This distilled water:dry soil ratio gave adequate excess solution for an electrical conductivity measurement which required a minimum of 5 ml per measurement. It also allowed adequate mixing and assured a uniform salt concentration throughout the diluted soil

solution. It was assumed that the salts precipitated during drying were reabsorbed with addition of the distilled water. Investigative tests showed that this assumption was justified and that the amount of unabsorbed salts was small and induced negligible error in calculations.

2.3.6 Electrical Conductivity Measurements

Electrical conductivity measurements of the soil solutions were made with a Beckman RC-19 electrical conductivity bridge. The accuracy of the Beckman bridge is rated at 0.25 percent of the reading.

A Beckman pipette type electrical conductivity cell (G-20) was used. The cell constant was checked periodically with NaCl solutions and was found to be 20.02 cm^{-1} $\pm$ 0.02 cm^{-1}. A decade capacitance box (General Radio Type 1419-K) rated up to 1 micro-farad was used to assist balancing electrical conductivity measurements when the capacitance balancing capability of the Beckman bridge was exceeded.

The electrical conductivity cell was adapted for precise temperature measurement by placing a YSI thermistor (type 46007) inside, near the platinum plates of the cell. Thermistor resistance was measured with a Hewlett Packard multimeter (HP3465B). This enabled the precise temperature (within $\pm$ 0.01 °C) of the solution to be determined at the time of the electrical conductivity measurement.

2.3.7 Electrical Conductivity and Salinity Relation

It was established by Page and Iskandar (1978) that the composition of subsea permafrost soil solution was similar to seawater. For this research, it was assumed that the electrical conductivity and salinity relation for the soil solution of subsea permafrost would be similar to that of seawater. Artificial seawater solutions were prepared and their electrical conductivities measured for the salinity range from 0 to about 212 ppt. Algorithms for the conversion of electrical conductivity to salinity (and vice-versa) for this salinity range were developed. This enabled the measured electrical conductivities of the soil solutions to be converted to salinities. The detailed procedure and the algorithms are given in Baker (1987).

2.3.8 Salinity and Freezing Temperature Relation

For brine in contact with ice, the brine salinity, S_b (ppt) can be determined from the freezing temperature, T_F (^oC), from the equilibrium phase diagram for the solution. Assur (1960), based on data of Nelson and Thompson (1954) determined the following relation for seawater at one atmosphere,

$$S_b = 1000 \left[1 - \left(\frac{54.1126}{T_F}\right)\right]^{-1}. \qquad (2.2)$$

Solving Eq. 2.2 for T_F gives

$$T_F = - 54.1126 \left(\frac{S_b}{1000 - S_b}\right). \qquad (2.3)$$

Equations 2.2, and 2.3, are valid for the salinity range from 0 to 124.68 ppt. For the salinity range from 124.68 to 230.77 ppt, Assur (1960) gives

$$\frac{S_b}{1000 - S_b} = - 0.0103085\ T_F + 0.06240. \qquad (2.4)$$

Solving Eq. 2.4 for T_F gives

$$T_F = 6.05326 - 97.00732 \left(\frac{S_b}{1000 - S_b}\right). \qquad (2.5)$$

Solving Eq. 2.5 for S_b gives

$$S_b = 1000\ [(-0.0103085\ T_F + 0.06240)^{-1} + 1]^{-1}. \qquad (2.6)$$

Doherty and Kester (1974) made very precise measurements of S_b and T_F for seawater and gave the following relation

$$T_F = - 0.0137 - 0.051990\ S_b - 0.00007225\ S_b^2 \qquad (2.7)$$

at atmospheric pressure. Solving for S_b gives

$$S_b = (A - B\ T_F)^{1/2} - C \qquad (2.8)$$

where:

A = 129260.9428

B = 13840.8304

C = 359.7924.

Equations 2.7 and 2.8 are valid for the salinity range from 4 to 40 ppt and Eq. 2.7 has an accuracy to within $\pm$ 0.002 °C.

The relation developed by Doherty and Kester (1974) was based on actual seawater measurements and is preferred over Assur's, which was based on the 6 major ion constituents in seawater, for the salinity range from 4 to 40 ppt. Therefore, the referenced equations given in Table 2.2 were used for the determination of S_b from T_F and T_F from S_b. The S_b and T_F intervals of their validity are given.

Table 2.2

Equations for relating salinity and freezing temperature for seawater

Salinity Interval (ppt)	Temperature Interval (°C)	Equation Number	
		T_F to S_b	S_b to T_F
$0 \leq S_b < 4$	$0 < T_F < -0.217$	2.2	2.3
$4 \leq S_b \leq 40$	$-0.217 \leq T_F \leq -2.209$	2.8	2.7
$40 < S_b \leq 124.68$	$-2.209 < T_F \leq -7.708$	2.2	2.3
$124.68 < S_b \leq 230.77$	$-7.708 < T_F \leq -23.049$	2.6	2.5

2.3.9 Calculation of Soil Properties

The bulk gravimetric water content, W_B (percent), is defined as:

$$W_B = 100\ (M_W/M_{SL}) \qquad (2.9)$$

where M_W is the mass of the water and M_{SL} is the mass of the dry soil (no soil solution salts). Dry soil is generally defined as soil dried to equilibrium in an oven at 105 °C (Hillel, 1980).

When determining W_B of very saline solutions, such as those associated with subsea permafrost, the mass of the salt, M_S, can be significant, and must be accounted for in calculations of W_B.

For W_B calculations, the following additional symbols are defined.

M_{SA} = total mass of sample

$$M_{SA} = M_{SL} + M_S + M_W \qquad (2.10)$$

M_{DS} = mass of dried sample

$$M_{DS} = M_{SL} + M_S \qquad (2.11)$$

M_{DW} = mass of distilled water added to dried sample

M_{SW} = mass of diluted sample (sample with distilled water added)

$$M_{SW} = M_{SL} + M_S + M_{DW} \qquad (2.12)$$

$C_B(S,T)$ = electrical conductivity of the bulk

soil solution salinity at temperature T

$C_D(S,T_M)$ = measured electrical conductivity of the diluted soil solution at measured temperature T_M

S_B = salinity of the bulk soil solution (ppt),

$$S_B = 1000 \left(\frac{M_s}{M_s + M_w}\right) \qquad (2.13)$$

and,

S_D = salinity of the diluted soil solution (ppt)

$$S_D = 1000 \left(\frac{M_s}{M_s + M_{Dw}}\right). \qquad (2.14)$$

From laboratory measurements, M_{sA}, M_w, M_{Ds}, M_{sw}, and $C_D(S,T_M)$ are known. Solving Eq. 2.11 for M_{sL} yields,

$$M_{sL} = M_{Ds} - M_s. \qquad (2.15)$$

Solving Eq. 2.14 for M_s yields,

$$M_s = \frac{S_D M_{Dw}}{1000 - S_D}. \qquad (2.16)$$

The following procedure was used to determine W_B assuming that the composition of the soil solution of subsea permafrost was the same as seawater. Also, it was assumed that all salts were present as soil solution, i.e. no solid salts present. This assumption is reasonable for temperatures warmer than about -8 °C at which $Na_2SO_4 \cdot 10H_2O$ begins to precipitate.

S_D was determined from $C_D(S,T_M)$ by the procedure

described in Section 2.3.7. Substitution of values for S_D and M_{DW} into Eq. 2.16 determines M_S. Substitution of values for M_{DS} and M_S into Eq. 2.15 determines M_{SL}. W_B was then determined by substitution of values for M_W and M_{SL} into Eq. 2.9.

In addition, S_B was determined by substitution of values for M_S and M_W into Eq. 2.13. Also, $C_B(S,T)$ was determined from S_B using the procedure discussed in Section 2.3.7.

A similar method was followed to determine W_B using a measured value of $C_B(S,T_M)$. First, S_B was determined from $C_B(S,T_M)$ using the procedure described in Section 2.3.7. Solving Eq. 2.13 for M_S gives

$$M_S = \frac{S_B M_W}{1000 - S_B}. \qquad (2.17)$$

M_{SL} was then determined by substitution of values for M_{DS} and M_S into Eq. 2.15. Finally, substitution of values for M_{SL} and M_W into Eq. 2.9 determined W_B.

In partially frozen sandy soils, the unfrozen gravimetric water content, W_U, can be determined, if the unfrozen soil solution salinity, S_U, is known. S_U can be determined if S_B, and the soil temperature, T_S, are known.

In addition to the assumptions given above, it is assumed that T_S is equal to the freezing temperature, T_F, and S_U is equal to the brine salinity, S_b, from the

equilibrium phase diagram for the soil solution (in this case seawater). Also, it is assumed that soil particle surface effects are negligible, and that all salts are present in the unfrozen soil solution (no salts in the ice). The procedure for determining S_b from T_F is described in Section 2.3.8.

The unfrozen gravimetric water content, W_U (percent), is defined as

$$W_U = 100\ (M_U/M_{SL}) \qquad (2.18)$$

where M_U is the mass of the unfrozen water.

Substitution of S_U for S_B and M_U for M_W into Eq. 2.13 and solving for M_U gives,

$$M_U = \frac{M_S\ (1000 - S_U)}{S_U}. \qquad (2.19)$$

Substitution of values for M_S and S_U into Eq. 2.19 gives M_U. W_U is then determined by substitution of values for M_U and M_{SL} into Eq. 2.18.

2.3.10 Calculation of Unfrozen Soil Solution Content

The unfrozen soil solution content by volume, V_U, of frozen soil can be determined if S_B and S_U are known. This means that it can be determined for those sample cores for which a temperature profile was obtained. V_U will be

defined for soils as the ratio of the unfrozen soil solution volume to the volume of unfrozen soil solution and ice. Note that it will not be based on the volume of soil. This is the same definition for the brine content by volume, v_b (ppt), used by Weeks (1962) for NaCl solutions and is given by the relation

$$v_b = 1000 \left(\frac{S_i/\rho_b S_b}{S_i/\rho_b S_b + (1 - S_i/S_b)/\rho_i} \right) \qquad (2.20)$$

where:

S_i = bulk ice salinity (ppt)

S_b = brine salinity (ppt)

ρ_i = pure ice density (g/cm^3)

ρ_b = brine density (g/cm^3).

Pounder (1965) gives the following expression for ρ_i (g/cm^3)

$$\rho_i = 0.917 - 1.403 \times 10^{-4} T \qquad (2.21)$$

where T is the temperature in °C. It is assumed that the ice does not contain any salt, i.e. all salt is rejected during ice formation and exists as brine.

Zubov (1945) gives the following expression for ρ_b (g/cm^3) for seawater

$$\rho_b = 1.0000 + 0.0008 S_b. \qquad (2.22)$$

For ice-bearing soils,

$$S_i = S_B \tag{2.23}$$

$$S_b = S_U \tag{2.24}$$

$$\rho_b = \rho_U \tag{2.25}$$

and,

$$V_b = V_U. \tag{2.26}$$

Substitution of Eqs. 2.23, 2.24, 2.25, and 2.26 into Eq. 2.20 gives

$$V_U = 1000 \left(\frac{S_B/\rho_U S_U}{S_B/\rho_U S_U + (1 - S_B/S_U)/\rho_i} \right). \tag{2.27}$$

The procedure for determining S_B and S_U is described in Section 2.3.9. ρ_i is determined from Eq. 2.21. ρ_U is determined by substitution of Eqs. 2.24 and 2.25 into Eq. 2.22. Substitution of values for S_B, S_U, ρ_U, and ρ_i into Eq. 2.27 gives V_U.

2.4 Field Results and Discussion

2.4.1 Introduction

The results of the field program include analysis of the grain size distribution of the sediments, location of the mechanically ice-bonded permafrost table, particularly in the region from the shoreline to about 400 m offshore, bulk and unfrozen soil solution salinity, bulk and unfrozen gravimetric water content, sediment temperatures, rate of change of salinity with time, and unfrozen soil solution

volume profiles of the sediments. These profiles were used to develop a better understanding of the effects of sediment freezing and thawing on salt redistribution in the sediments near the seabed.

The field data will be published as a separate report because of its voluminous nature (Baker et al., 1987) and only that data necessary for the thesis research will be presented.

2.4.2 Sediment Description

A combination of soil samples from several sample cores obtained along the WDL was used as a representative soil sample for grain size distribution analysis. Sediment samples from 0.2 to 2 m below the seabed at sites located from 100 m and farther offshore were combined, washed with distilled water, oven dried at 105 °C, and then sieved. Prior to this process, the individual sediment samples were observed to be quite uniform and so the grain size distribution for the combined samples should be representative of the sediments for the depth interval of 0.2 to 2 m below the seabed. Figure 2.2 shows the grain size distribution curve obtained by sieve analysis of the sediments. The sediments are gravelly sands containing about 12 percent gravel, 85 percent sand, and about 3 percent silt or finer, silt being defined as those particles

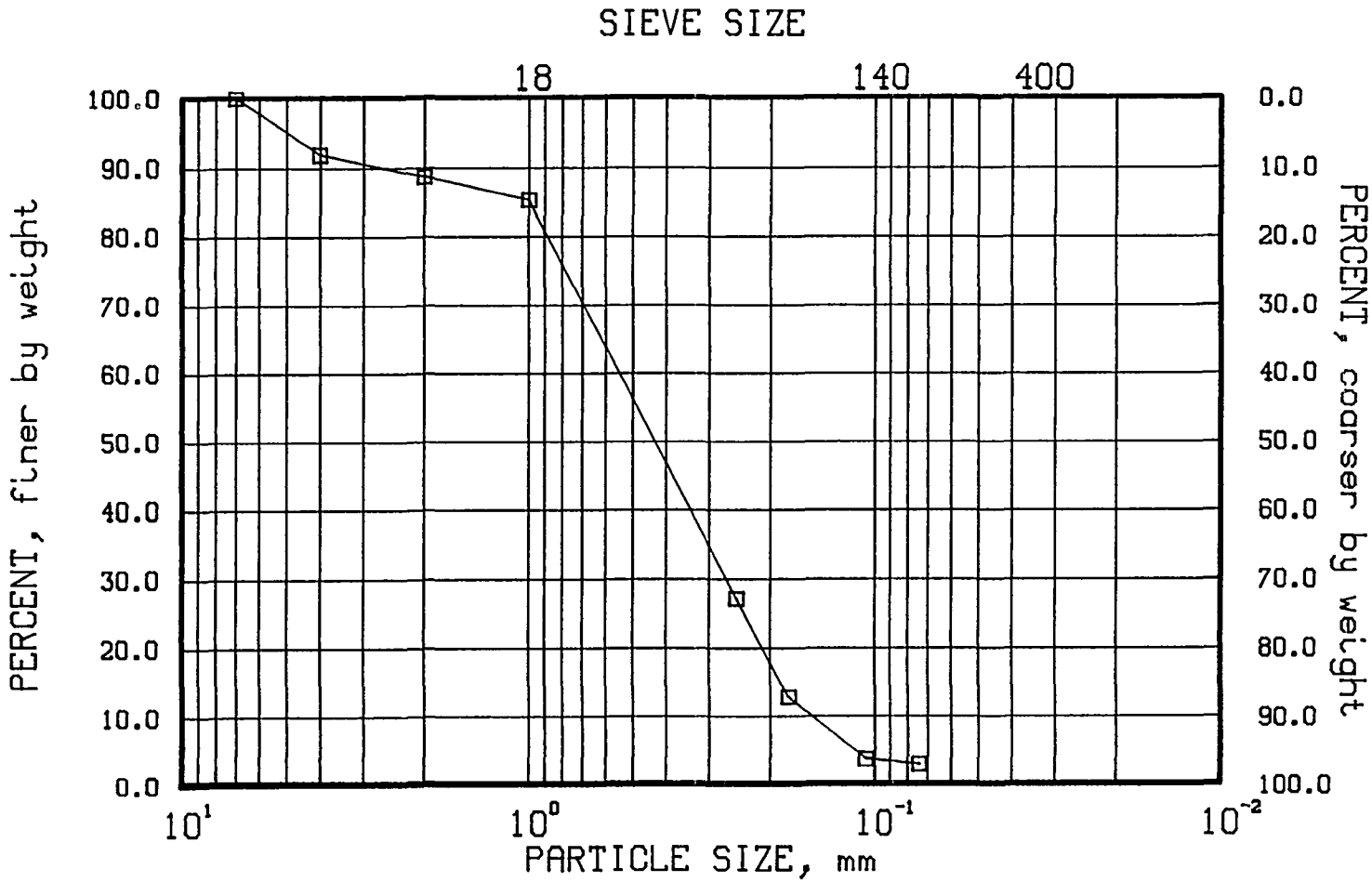

Fig. 2.2: Particle size distribution curve for subsea permafrost sediments near the seabed near the ARCO West Dock, Prudhoe Bay, Alaska.

with size less than 140 mesh or about 105 microns.

The top 0.20 m or so of the sediments included about 15 percent silt or finer and about 85 percent sand. In the region out to about 3 km offshore, the top 0.20 m layer is the only portion of the sediments thought to contain sufficient fines to be frost susceptible. A frost susceptible soil is defined as a soil containing at least 3 percent particles with size less than 20 microns (Casagrande, 1932).

2.4.3 Ice-Bonded Permafrost Table

Figures 2.3, 2.4, and 2.5 show the ice-bonded permafrost table (IBPT) and seabed profile along the WDL at different scales. At each site there are two symbols placed on the figures. The top symbol represents the seabed depth and the lower symbol represents the IBPT depth. Values for the IBPT and seabed depths are given in Table 2.3 which includes data obtained from previous studies.

The distance between the ice surface and the seabed may vary each year and between seasons by as much as 20 or 30 cm because the ice may be resting on the seabed and thereby be raised above hydrostatic level (Matava, 1986). Therefore, the relative positions of the seabed and IBPT, which were measured from the ice surface and obtained during different field seasons, may differ vertically by this

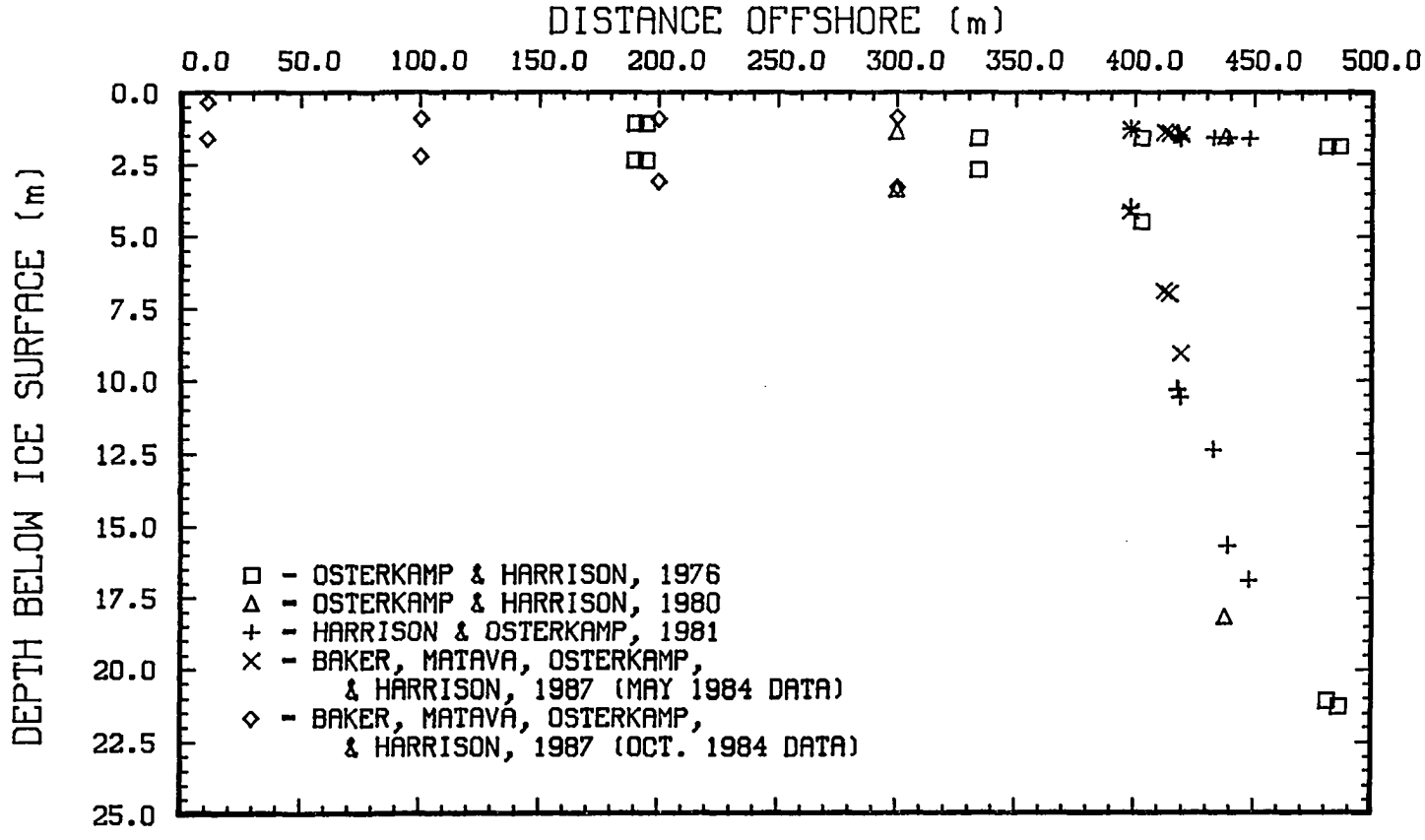

Fig. 2.3: Depth of the ice-bonded subsea permafrost table and seabed below the ice surface from 0 to 500 m offshore near the ARCO West Dock, Prudhoe Bay, Alaska. For each site offshore, there are two symbols shown. The upper symbol indicates the seabed location and the lower symbol indicates the ice-bonded permafrost table location.

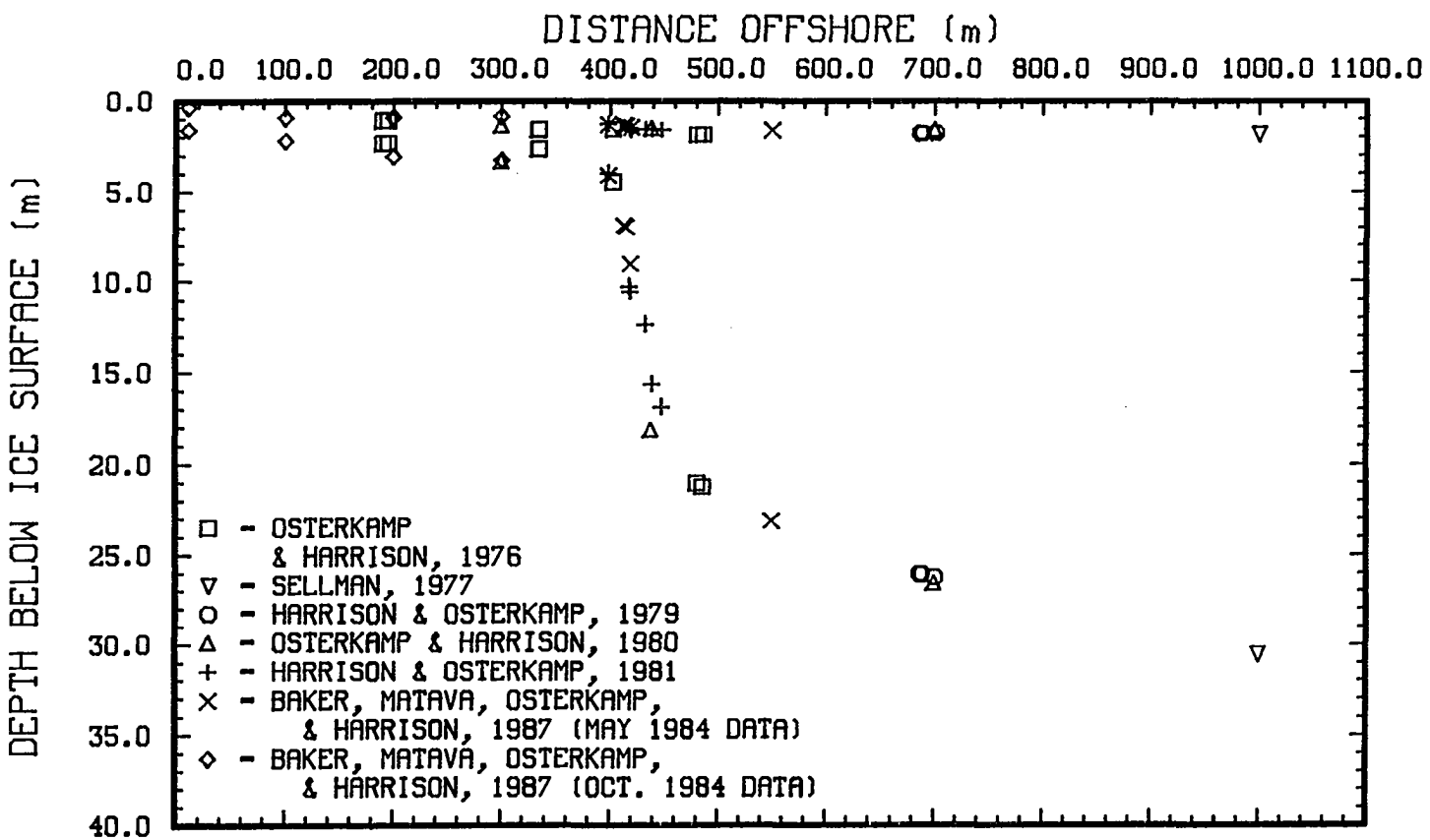

Fig. 2.4: Depth of the ice-bonded subsea permafrost table and seabed below the ice surface from 0 to 1 km offshore near the ARCO West Dock, Prudhoe Bay, Alaska. For each site offshore, there are two symbols shown. The upper symbol indicates the seabed location and the lower symbol indicates the ice-bonded permafrost table location.

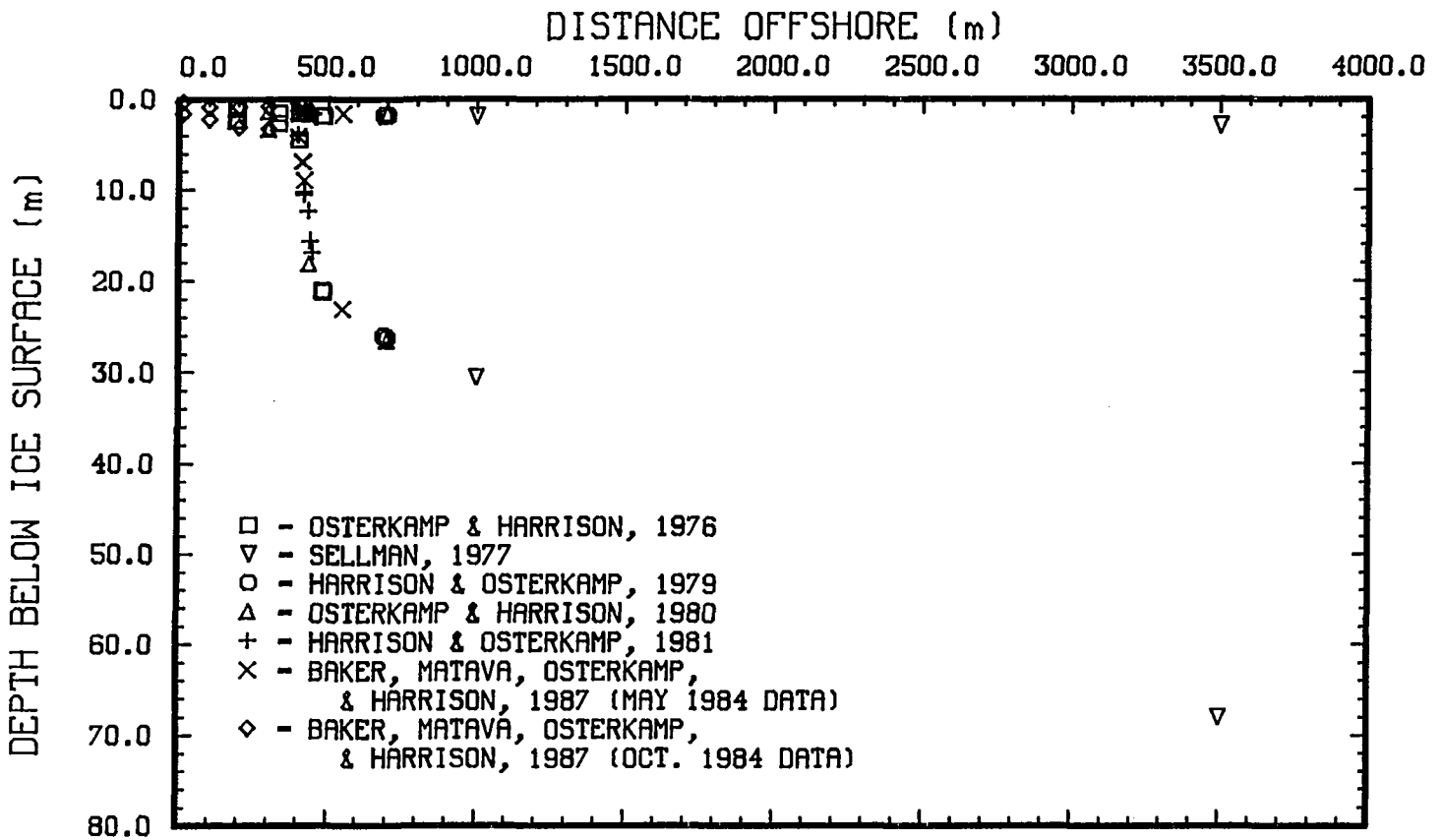

Fig. 2.5: Depth of the ice-bonded subsea permafrost table and seabed below the ice surface from 0 to 3.5 km offshore near the ARCO West Dock, Prudhoe Bay, Alaska. For each site offshore, there are two symbols shown. The upper symbol indicates the seabed location and the lower symbol indicates the ice-bonded permafrost table location.

Table 2.3

Depth of ice-bonded subsea permafrost table and seabed

DISTANCE OFFSHORE (m)	DEPTH FROM ICE SURFACE TO SEABED (m)	DEPTH FROM ICE SURFACE TO IBPT (m)	DEPTH FROM SEABED TO IBPT (m)	REFERENCE
10.8	0.36	1.63	1.27	7
100.3	0.94	2.24	1.30	7
190.0	1.10	2.38	1.28	1
195.0	1.10	2.38	1.28	1
200.0	0.93	3.10	2.17	7
300.0	1.37	3.37	2.00	4
300.1	0.87	3.30	2.43	7
334.0	1.60	2.70	1.10	1
398.0	1.27	4.01	2.74	5
398.2	1.32	4.16	2.84	6
403.0	1.60	4.50	2.90	1
412.6	1.40	6.93	5.53	6
414.6	1.42	7.02	5.60	6
418.0	1.51	10.32	8.81	5
419.0	1.63	10.58	8.95	5
419.4	1.49	9.08	7.59	6
433.0	1.58	12.39	10.81	5
438.0	1.53	18.18	16.65	4
439.0	1.59	15.68	14.09	5
448.0	1.61	16.91	15.30	5
481.0	1.90	21.10	19.30	1
486.0	1.90	21.30	19.50	1
550.2	1.65	23.19	21.54	6
687.0	1.80	26.10	24.30	3
689.0	1.82	26.12	24.30	3
701.0	1.80	26.30	24.50	3
700.0	1.62	26.62	25.00	4
1000.0	1.85	30.60	28.75	2
3500.0	2.86	68.00	65.14	2

References:

1. Osterkamp and Harrison, 1976
2. Sellman, 1977
3. Harrison and Osterkamp, 1979
4. Osterkamp and Harrison, 1980
5. Harrison and Osterkamp, 1981
6. Baker, Matava, Osterkamp, and Harrison, 1987 (May 1984 data)
7. Baker, Matava, Osterkamp, and Harrison, 1987 (October 1984 data)

amount. The distance offshore was measured from the break in slope of the shoreline, although a narrow beach, 1 to 2 m in width was present in the area of the study site.

The IBPT gradually increases in depth below the seabed, almost linearly, from about 1.3 m at 10.8 m offshore to about 2.8 m at 398 m offshore. Similarly, the seabed depth also increases, in a nearly linear manner, from about 0.4 m to about 1.3 m.

Between about 398 m to 448 m offshore, the IBPT depth dramatically increases, almost linearly, to about 15 m. This coincides with a noticeable increase in the seabed depth from about 1.3 m to about 1.6 m between about 398 m and about 419 m offshore and then remains nearly constant to about 448 m offshore. It is believed that the annual ice cover freezes, sporadically, to the seabed beyond 398 m offshore. It is important to note the association of the decoupling of the annual ice cover from the seabed with the dramatic increase in the depth of the IBPT. Both the thermal and chemical boundary conditions at the seabed are different from those in the region closer than 400 m offshore. In particular, there is an increase in the mean annual seabed temperature (MASBT) beyond 400 m offshore (Osterkamp and Harrison, 1977). It is believed that the increase in MASBT and decoupling of the sea ice from the seabed are mainly responsible for the increase in depth of

the IBPT in the region from about 400 m to 450 m offshore. This point will be discussed further in Section 2.4.5.

Beyond about 448 m to about 3500 m offshore, the IBPT increases less dramatically to about 65.1 m while the seabed depth increases gradually to about 2.9 m.

Table 2.4 gives the IBPT temperatures for the region out to 3500 m offshore including data from other studies. The fall measurements show that the IBPT temperature decreases from about -2.44 to -4.03 °C from 10.3 m to 300.1 m offshore. At 398.2 m offshore, the spring IBPT temperature is about -4.46 °C. Both spring and fall temperature profiles were not taken in the region out to 398.2 m offshore and so seasonal variation of these temperatures cannot be determined.

In the spring, between 412.6 m and 3.5 km offshore, the IBPT temperature remains fairly constant at about -2.41 °C with a standard deviation of $\pm$0.07 °C. It is believed that these IBPT temperatures remain fairly constant throughout the year in this region as shown at 550.2 m offshore. Table 2.4 shows that temperature data from this study agrees very well with that of previous studies.

It is possible to predict the IBPT depth below the seabed based on a knowledge of the thermal and chemical boundary conditions, and sediment properties, such as ice content. This will be discussed in detail in Section 2.4.5.

Table 2.4

Values for the temperature of the ice-bonded permafrost table and distance offshore near the ARCO West Dock, Prudhoe Bay, Alaska

DISTANCE OFFSHORE (m)	IBPT TEMPERATURE (°C)	TIME OF YEAR	REFERENCE
10.3	-2.44	FALL	7
100.3	-3.14	FALL	7
200.0	-3.40	FALL	7
300.1	-4.03	FALL	7
398.2	-4.46	SPRING	6
412.6	-2.43	SPRING	6
414.6	-2.42	SPRING	6
414.6	-2.53	FALL	7
418.0	-2.42	SPRING	5
419.4	-2.50	SPRING	6
433.0	-2.33	SPRING	5
438.0	-2.45	SPRING	4
439.0	-2.38	SPRING	5
448.0	-2.40	SPRING	5
481.0	-2.48	SPRING	1
550.2	-2.33	SPRING	6
550.2	-2.33	FALL	7
689.0	-2.42	SPRING	3
700.0	-2.44	SPRING	4
1000.0	-2.45	SPRING	2
3500.0	-2.30	SPRING	2

References:

1. Osterkamp and Harrison, 1976
2. Lachenbruch and Marshall, 1978
3. Harrison and Osterkamp, 1979
4. Osterkamp and Harrison, 1980
5. Harrison and Osterkamp, 1981
6. Baker, Matava, Osterkamp, and Harrison, 1987 (May 1984 data)
7. Baker, Matava, Osterkamp, and Harrison, 1987 (October 1984 data)

2.4.4 Sediment Freezing Near the Seabed

2.4.4.1 Fall Data

There were a number of observations, including drilling and sampling operations, that suggested the sediments were partially frozen during the fall 1984 field season. Subsequent analyses of the data confirmed these observations and will now be discussed.

During the fall 1984 field season, sediment cores to depths on the order of 2 m were obtained out to about 451.8 m offshore. Drilling indicated that sediments were partially frozen from the seabed to a depth of about 0.2 to 0.3 m. Below this layer, the sediments felt thawed and in some cases almost soupy until a lower partially frozen layer was reached. For example, at 300.1 m offshore, drilling indicated the sediments were partially frozen to a depth of about 0.2 m, thawed to a depth of about 1.3 m, and then partially frozen to the IBPT at 2.43 m. These drilling observations indicate that the second partially frozen zone extends to the IBPT out to at least 400 m offshore.

The sediment characteristics at site PB301.1 are discussed here as representative of the sediment conditions during the fall in the region from the shoreline to about 400 m offshore. Figure 2.6 shows the bulk soil solution salinity, S_B, profile for site PB301.1. The top 0.2 to 0.3

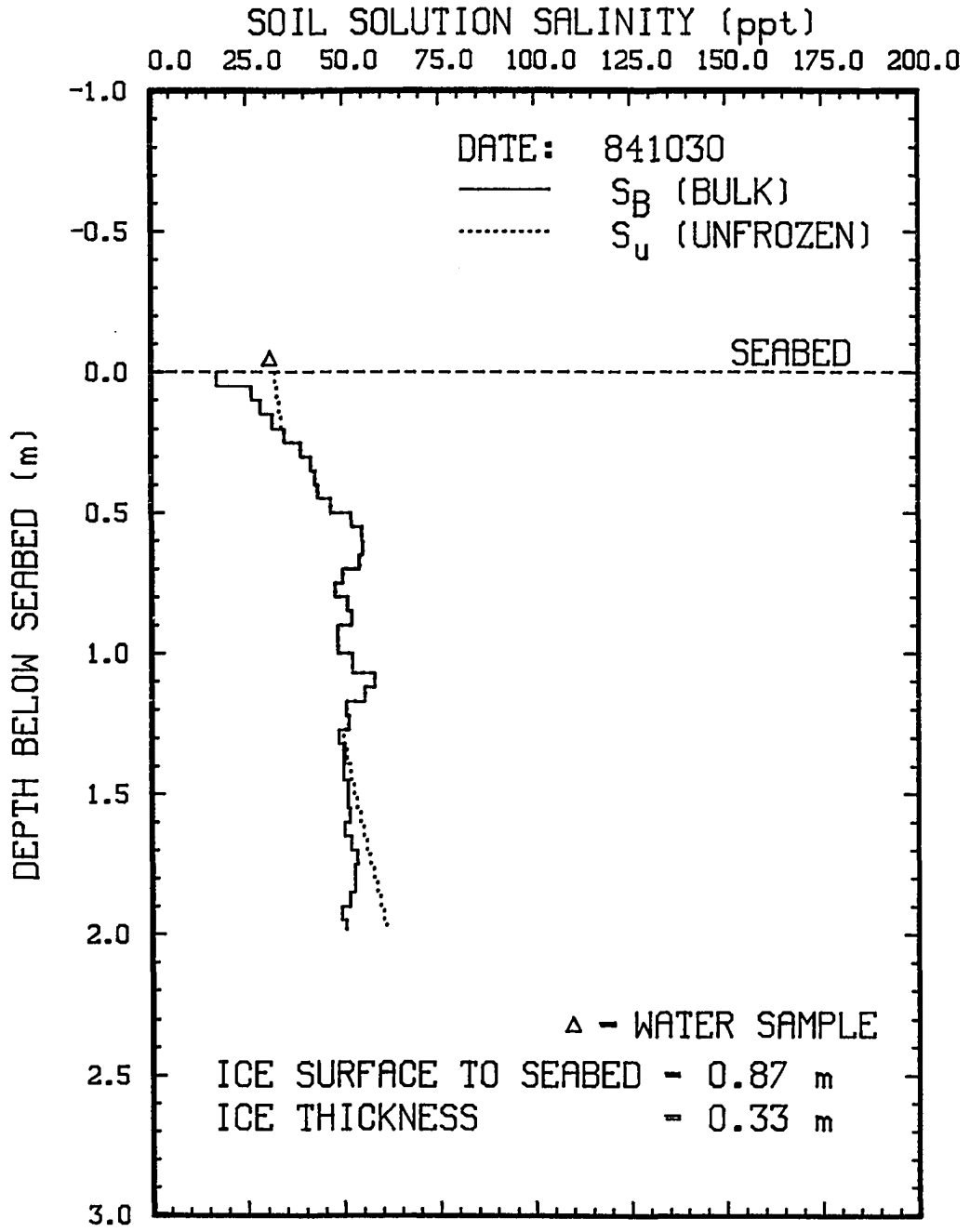

Fig. 2.6: Bulk and unfrozen soil solution salinity vs. depth for site PB301.1.

m or so of the sediments has relatively low S_B values (less than about 35 ppt) and the top 0.15 m has S_B values less than the overlying seawater possibly suggesting freezing of the sediments with salt rejection and/or soil solution drainage. Below about 0.4 to 0.5 m, fairly large and relatively constant S_B values averaging about 52 ppt are observed.

For those sediment sampling sites for which a temperature profile was obtained, the unfrozen soil solution salinity, S_U, and unfrozen gravimetric water content, W_U, profiles were determined. Figure 2.6 shows the S_U profile for site PB301.1 with the S_B profile. Comparison of these two profiles can be used to identify frozen zones. If ice is present, values for S_B will be less than those for S_U. Therefore, a partially frozen or ice-bearing zone is indicated wherever the S_U profile indicates greater salinity values than the S_B profile.

A comparison of the S_B and S_U profiles indicates that the top 0.2 m or so of the sediments is partially frozen and overlies a thawed layer to about 1.2 m. Below the thawed layer, the sediments becomes partially frozen again which agrees with drilling observations.

The S_U profiles are based on the temperature profiles whereas the S_B profiles were determined from direct measurements. Both sets of data, although determined by

independent methods, agree with each other and with drilling observations for the location of the partially frozen layers. If the bulk salinity values were only a few percent different, the top frozen layer would not appear or would be much deeper than drilling and S_B profiles indicate.

Close agreement between the location of the partially frozen regions determined from the S_B and S_U profiles, and the drill logs also confirms that the assumption made in calculating S_U, that the pore ice does not contain salt (all salt was rejected to the unfrozen soil solution), is justified. If the pore ice did contain more than a few percent of the salt present, the boundaries of the frozen regions determined by the two methods would not agree as well as they do.

Figure 2.7 shows the bulk gravimetric water content, W_B, and unfrozen gravimetric water content, W_U, profiles for site PB301.1. There are relatively high W_B values in the top 0.2 m of the sediments which may be taken to indicate the presence of ice lenses and suggest that it is partially frozen. In fact, ice lenses were observed in the top few centimeters of the sediments during drilling and sampling. These lenses were characteristically about 0.5 to 1 cm in length and width and about 1 mm thick. They were angled between 0 to about 30 degrees from the vertical.

Figure 2.8 shows the fall temperature profile for site

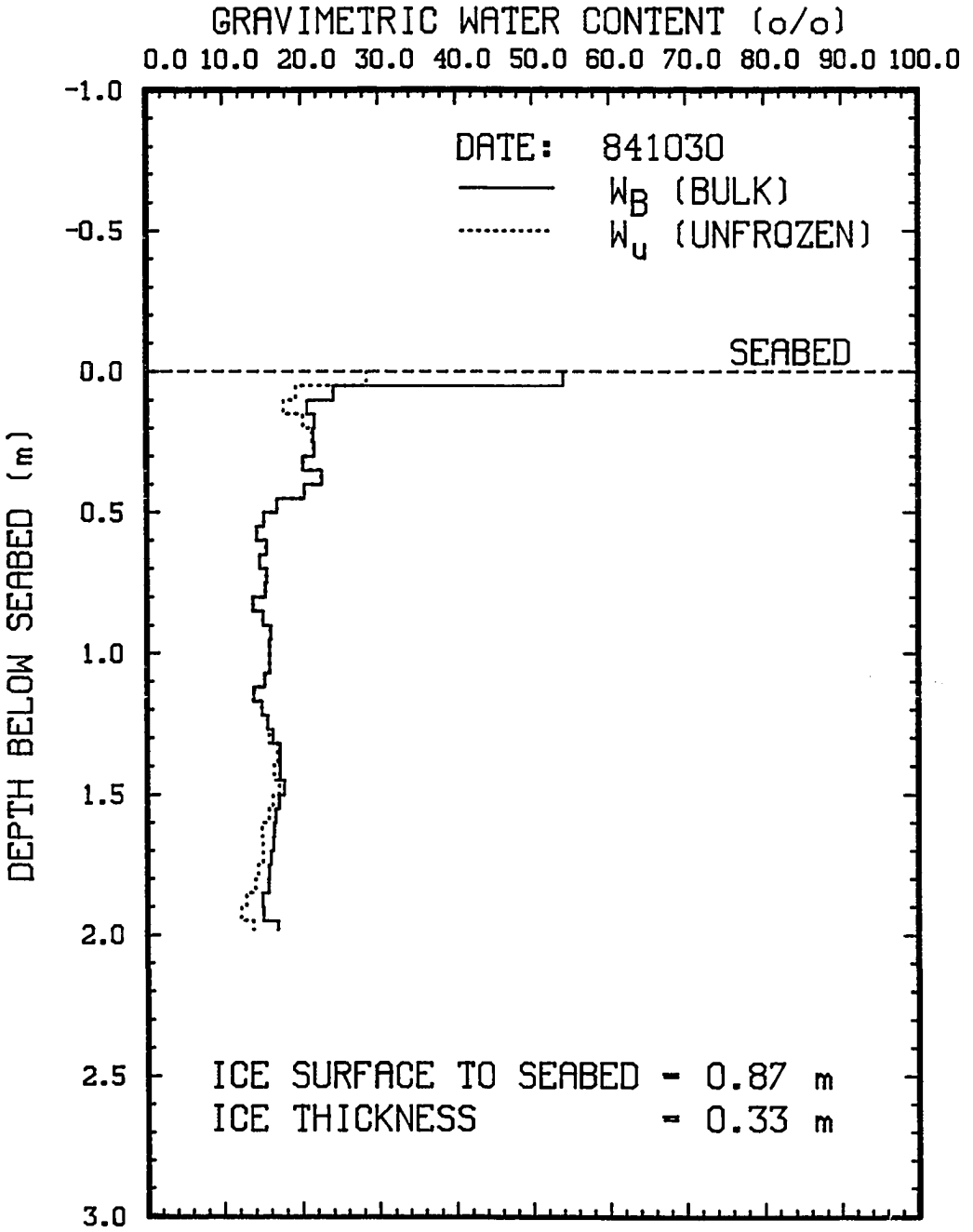

Fig. 2.7: Bulk and unfrozen gravimetric water content vs. depth for site PB301.1.

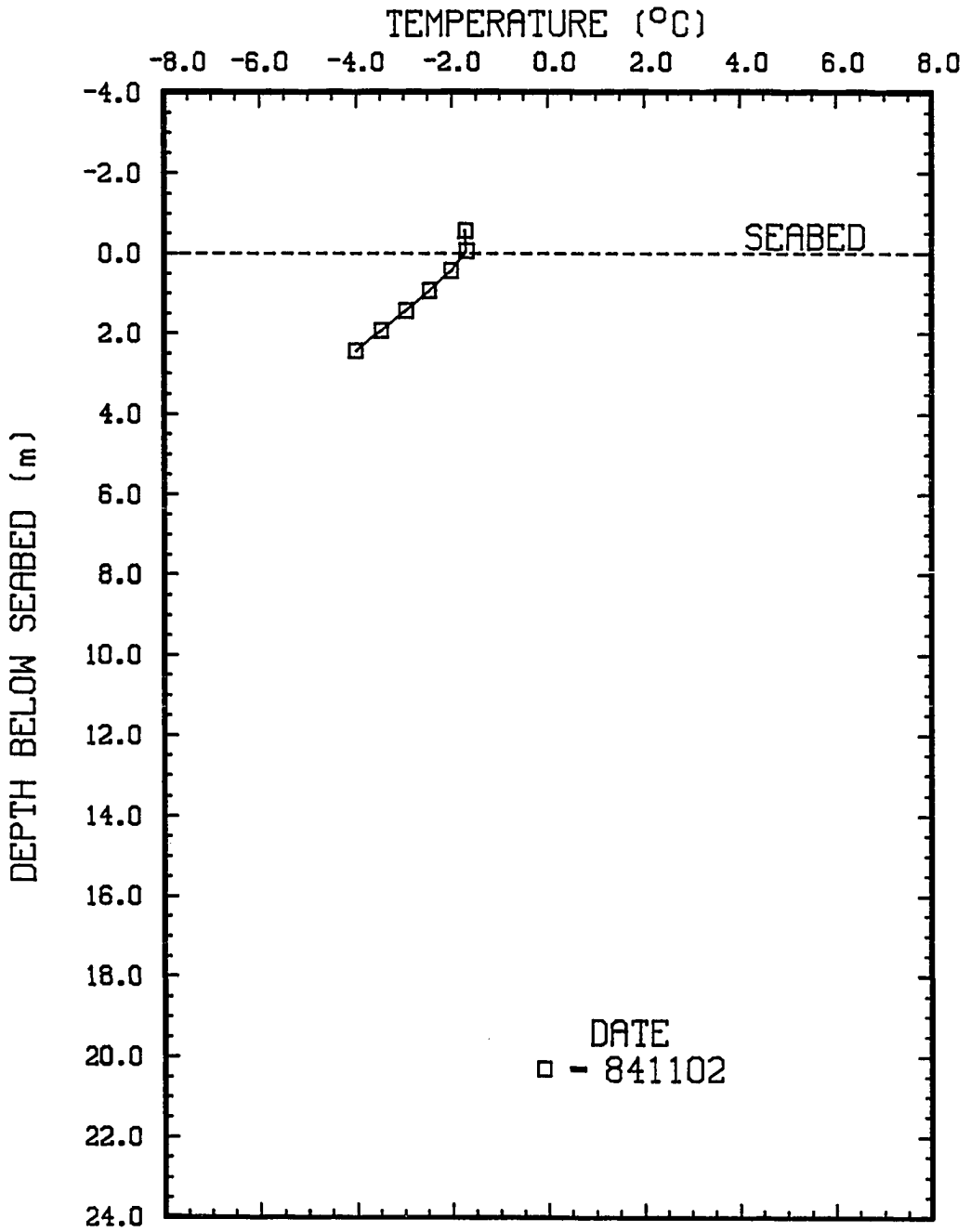

Fig. 2.8: Temperature vs. depth for site PB300.1.

PB301.1. Temperatures of about -1.74 °C and -4.027 °C were found at the seabed and IBPT, respectively.

The unfrozen soil solution content, V_u, profiles were determined for those sample cores for which a temperature profile was taken. These profiles clearly identify the ice-bearing and thawed regions of the sediments. Figure 2.9 shows the V_u profile for site PB301.1. It clearly shows that the top 0.2 m or so of the sediments is partially frozen. Below this depth, there is a thawed region underlain by another partially frozen region.

Values for V_u show that the unfrozen soil solution represents a substantial amount of the pore volume. In general, values for V_u in the fall were greater than about 400 ppt at about 10 m offshore and increased with distance offshore. The ice content (ppt) is 1000 - V_u, assuming no air present. Figure 2.9 shows that there is some ice in the sediments near the seabed and near the bottom of the profile.

Previous literature has not noted the existence of the partially frozen layer of sediments near the seabed in the fall although observations of frozen sediments near the seabed have been made in the spring at sites where there was up to 0.5 m of water under the ice (Osterkamp, personal communication). It is somewhat of a curiosity since the seawater above it is not frozen nor are the sediments

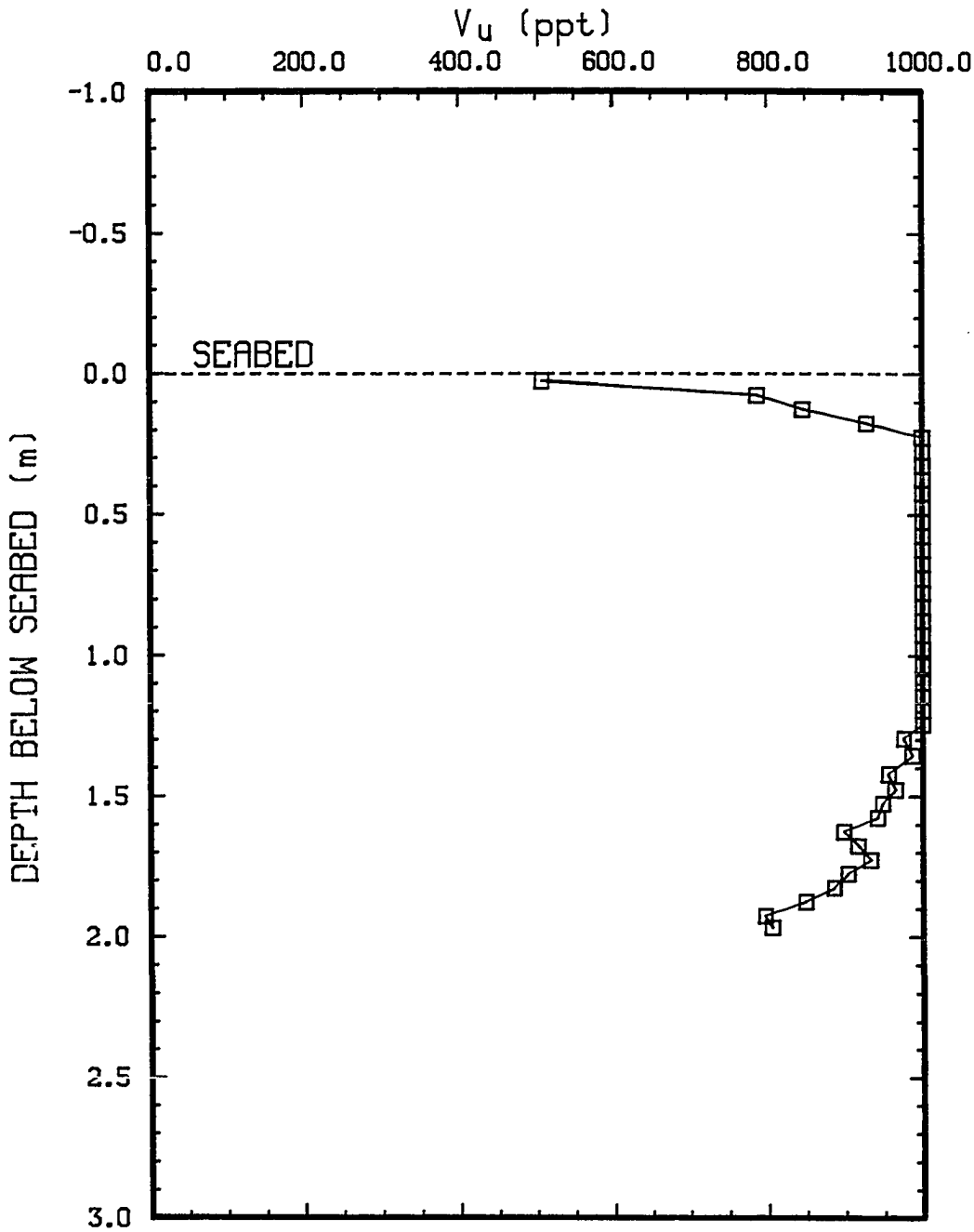

Fig. 2.9: Unfrozen soil solution content vs. depth for site PB301.1.

immediately below it. The model below gives an explanation for the development of this layer.

It is assumed that the top layer of the sediments has a soil solution salinity of the seawater in Prudhoe Bay during the summer when it is ice-free. This was determined from chloride concentration data to be about 28.9 ppt (ARCO, personal communication, 1985). During sea ice formation, cold concentrated brines are rejected to the underlying seawater which decreases its freezing temperature. Consequently, the layer of the sediments near the seabed may freeze, if the salinity of the sediments is less than the overlaying seawater, and reject salts to a lower level in the sediments. This decreases the freezing temperature of the soil solution sufficiently so that this lower region in the sediments remains thawed until additional freezing occurs.

This point can be illustrated with a simple Stefan phase boundary problem. It is assumed that the sensible heat is negligible, the seabed and phase boundary temperatures are constant, the temperature gradient in the freezing zone is linear, and the density of ice and of the soil solution are the same. The depth of freezing, X (m), is given by

$$X = \sqrt{\frac{2\, k_F\, (T_F - T_s)\, t}{L_s}} \qquad (2.28)$$

where:

k_F = thermal conductivity of partially frozen sediments (J/m-yr-°C)

T_F = freezing temperature of sediments (°C)

T_s = seabed temperature (°C)

L_s = volumetric latent heat of sediments, (J/m^3)

t = time (years) seabed subjected to temperature T_s (assuming a step change).

The thermal conductivity of the partially frozen sediments, k_F, can be expressed by the weighted geometric mean equation given by Lachenbruch et al. (1982) as

$$k_F = k_i^A \, k_w^B \, k_G^{1-A-B} \qquad (2.29)$$

where:

A = volume fraction of ice in partially frozen sediments, m^3 ice/m^3 sediments

B = volume fraction of unfrozen soil solution in sediments, m^3 unfrozen soil solution/m^3 sediments

1-A-B = volume fraction of mineral grains in sediments, m^3 mineral grains/m^3 sediments

k_i = thermal conductivity of ice, J/m-yr-°C

k_w = thermal conductivity of water, J/m-yr-°C

k_G = thermal conductivity of mineral grains, J/m-yr-°C

It is assumed that effects of salts on k_F are negligible in that it is assumed that the thermal conductivity of the soil solution is equal to the thermal conductivity of water.

The porosity, ϵ, is approximated by

$$c \simeq A + B \qquad (2.30)$$

and is assumed to be constant.

At Prudhoe Bay, Alaska (Lachenbruch, 1982),

$c \simeq 40$ percent,

$k_o \simeq 1.375 \times 10^8$ J/m-yr-°C.

Lachenbruch (1982) also gives the following values for k_i and k_w;

$k_i \simeq 7.19 \times 10^7$ J/m-yr-°C

$k_w \simeq 1.768 \times 10^7$ J/m-yr-°C.

At site PB301.1, the seawater salinity above the seabed is about 31 ppt. From Eq. 2.8, the freezing temperature of this solution is determined to be about -1.73 °C and will be assumed to be equal to T_s.

The freezing temperature of the seawater in Prudhoe Bay during the summer is about -1.61 °C (for a salinity of 28.9 ppt) which is taken to be T_f. This gives

$T_f - T_s = 0.12$ °C.

An average value for the unfrozen soil solution content, V_u, can be estimated from Figure 2.8 to be about 800 ppt. This gives

$$A = (1 - 0.8) \times 0.4 = 0.08$$

and,

$$B = 0.8 \times 0.4 = 0.32.$$

The latent heat of fusion for 28.9 ppt salinity seawater, L, is estimated to be about 3.335×10^8 J/m³. The latent heat of fusion of sediments is approximated by assuming that it is equal to the latent heat of the ice formed within it. This means that for the partially frozen sediments,

$$L_s \simeq L \times A = 2.668 \times 10^7 \text{ J/m}^3.$$

Substitution of values for A, B, k_i, k_w, and k_o into Eq. 2.29 gives

$$k_F = 6.77 \times 10^7 \text{ J/m-yr-}^\circ\text{C}.$$

It was assumed that sea ice formation had been in progress for about 30 days before the sample core at site PB301.1 was obtained. This gives

$$t = 0.0822 \text{ years}.$$

Substitution of values for L_s, k_F, T_F, T_s, and t into Eq. 2.28 gives

$$X = 0.22 \text{ m}$$

which is approximately the thickness of observed frozen

layer thickness (about 0.2 to 0.3 m). Agreement between the predicted and observed values for X reinforces credence in the process described above as the mechanism for the formation of the top frozen layer.

It can also be shown that salt rejection during sea ice formation is probably sufficient to cause the salinity of the seawater to increase from about 28.9 to about 31 ppt. At site PB301.1, the seabed depth below the ice surface is 0.87 m. The ice thickness is 0.33 m which gives the thickness of the underlying water to be 0.54 m.

The maximum increase in salinity of the seawater due to ice formation can be determined if it is assumed that water circulation (by tides, winds, etc.) is terminated once ice formation begins. This essentially makes the system closed. It is also assumed that there is about 80 percent salt rejection and/or drainage during formation of sea ice with a salinity of about 6 ppt. In this case, ice formation could cause a salinity increase of about 13.0 ppt which is more than sufficient to raise the salinity from about 28.9 to about 31 ppt (salinity difference of 2.1 ppt).

Realistically, seawater motion (due to tidal action and currents) beneath the ice probably does occur for a considerable time before sea ice formation restricts movement of the seawater. Therefore, it is reasonable to assume that the increase in seawater salinity due to sea ice

formation at site PB301.1 would be less than 13.0 ppt, but sufficient to raise the salinity to 31 ppt as was observed at the time of sampling.

2.4.4.2 Spring Data

Sediment sample cores were obtained during spring 1984 and spring 1985. Temperature measurements of the sediments were made during spring 1984. Analyses of the data suggested that salt, rejected from sea ice formation and sediment freezing, infiltrated the sediments. These analyses will now be discussed.

Figures 2.10 and 2.11 show spring S_B profiles for sites PB301.0 and PB450.8, respectively, and are typical to about 450 m offshore. Comparison of the spring S_B profiles with fall S_B profiles shown in Figures 2.11 and 2.12 for sites PB450.8 and PB451.8, respectively, reveals distinctly higher S_B values in the spring. This indicates that the salt rejected and/or draining during sea ice formation and sediment freezing has infiltrated deeper into the sediments. In addition, the lower S_B values in the fall throughout the profile depths of about 2 m imply salt transport velocities of at least 2 m/year through this depth.

It also appears that salt rejection during freezing of the sediments has caused the formation of very saline layers in the sediments. Consequently, the spring S_B profiles are

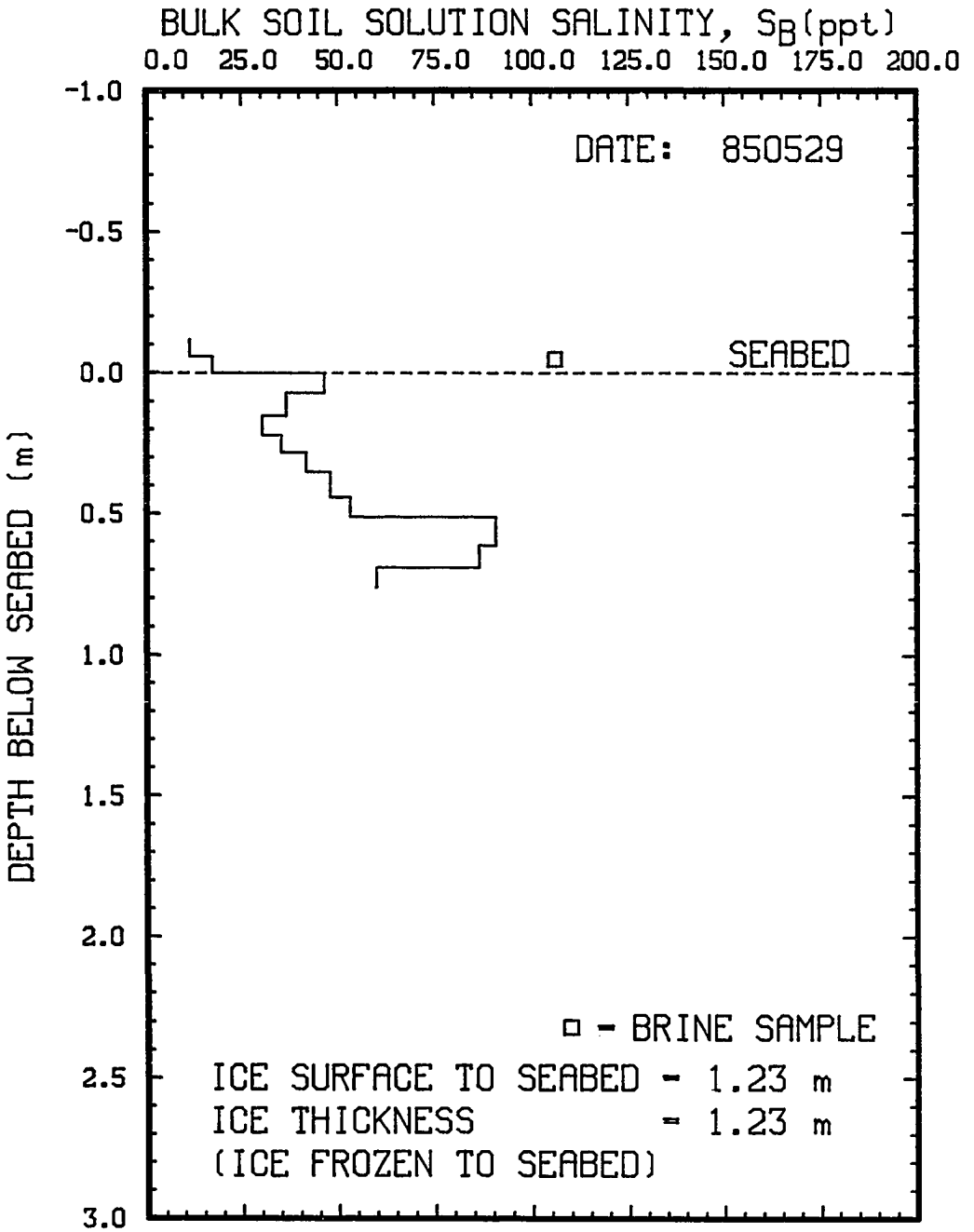

Fig. 2.10: Bulk soil solution salinity vs. depth for site PB301.0.

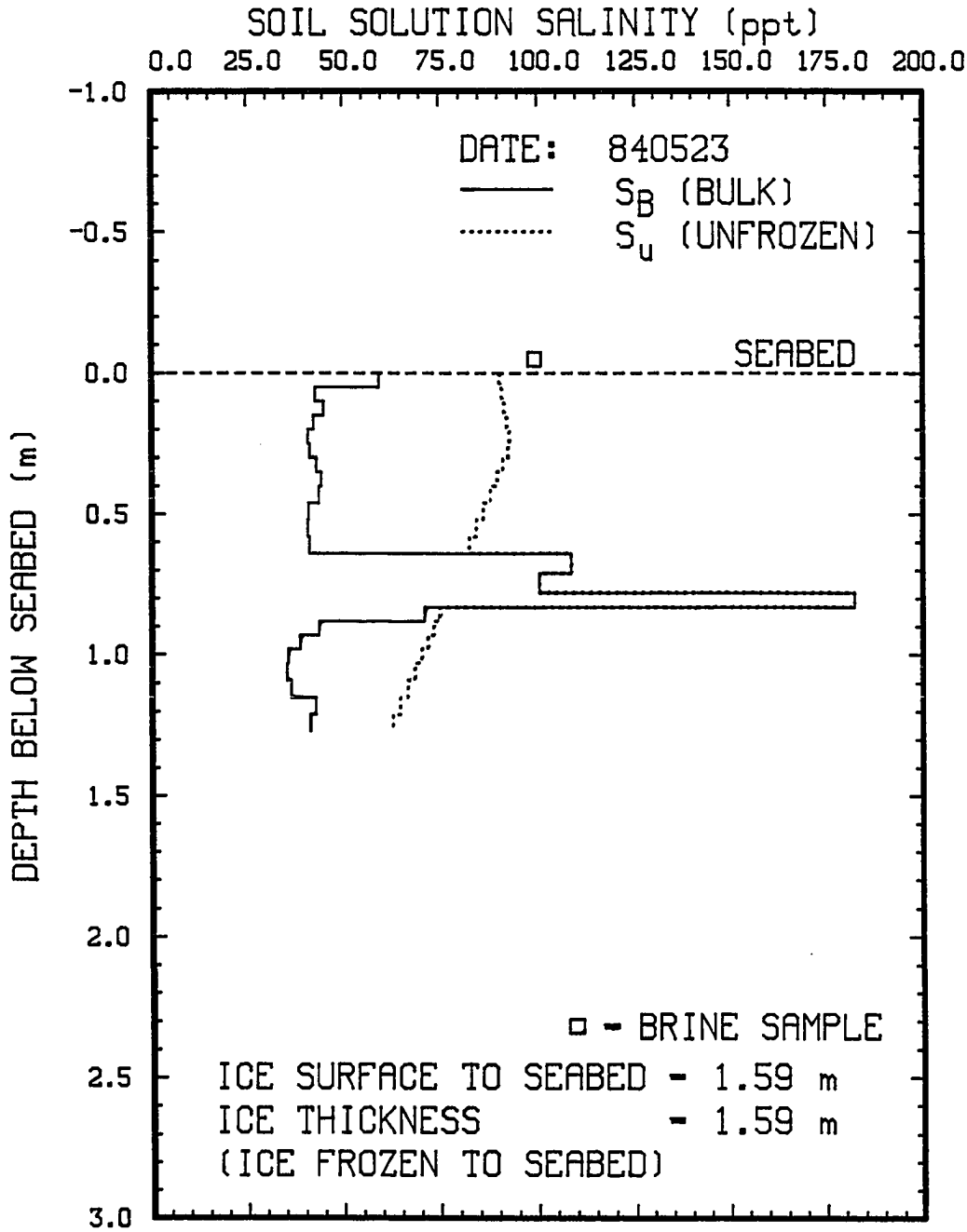

Fig. 2.11: Bulk and unfrozen soil solution salinity vs. depth for site PB450.8.

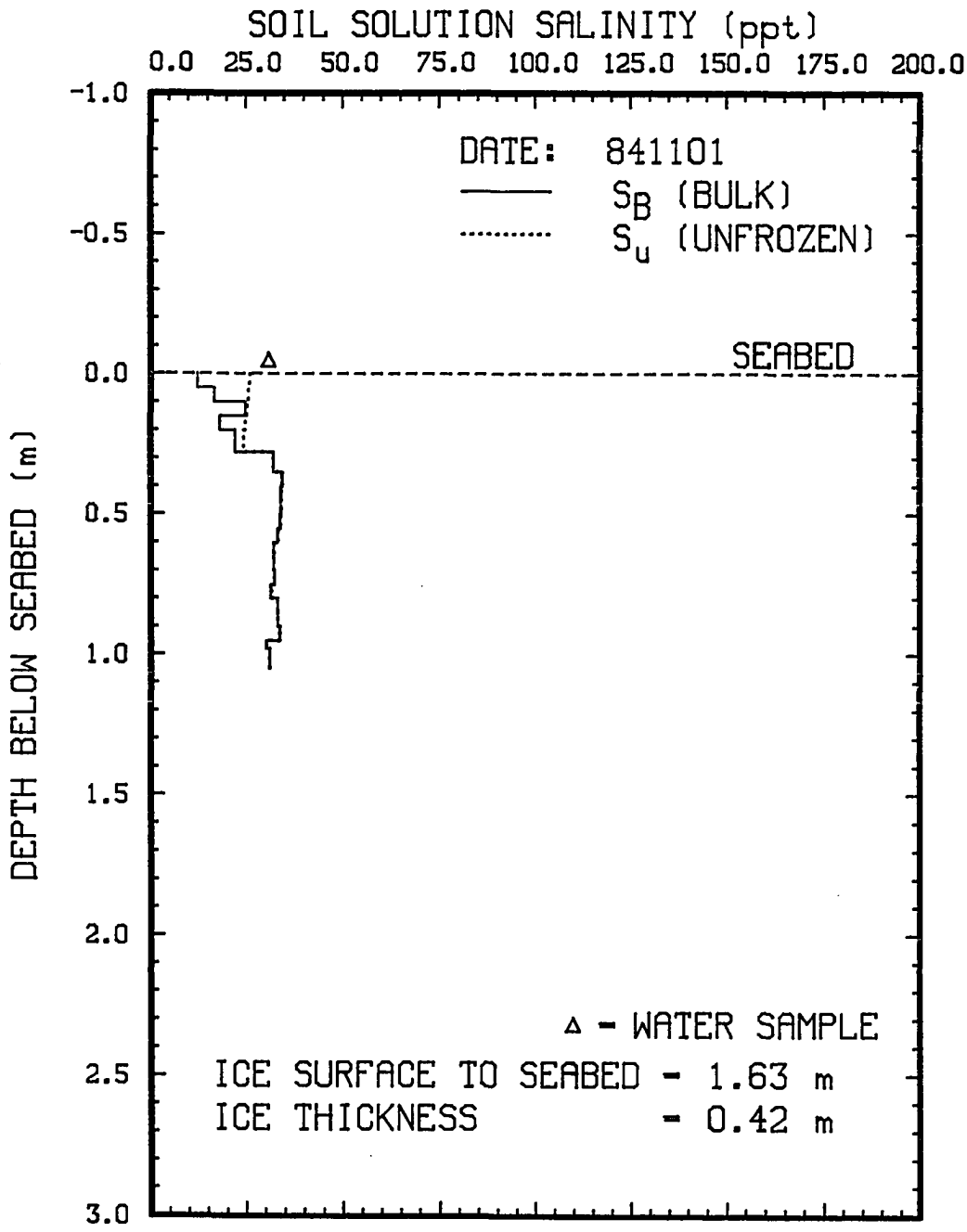

Fig. 2.12: Bulk and unfrozen soil solution salinity vs. depth for site PB451.8.

much more erratic than in the fall. There appears to be at least one highly saline layer in the top meter of the sediments at almost all of the sites in the region out to about 452 m offshore. These saline layers are commonly about 0.1 m to 0.2 m thick. At site PB301 one such layer is located between about 0.51 m and 0.69 m below the seabed and has a S_B value of about 90 ppt. Spring temperature profiles for this site were not obtained and, consequently, S_U profiles could not be determined and used to detect the unfrozen layers if present. Although, if it is assumed that the temperatures at site PB301 are at least as cold as those at site PB399.8, then the sediments are partially frozen for the full depth of the sample core.

A similar saline layer was observed at a depth between 0.64 m and 0.83 m at site PB450.8. This layer has S_B values as high as 182.3 ppt. It appears to be thawed and sandwiched between a frozen layer above and below (determined from comparison of the S_B and S_U profiles). This may be an illustration of a type of banding (alternating thawed and frozen layers) created in the following manner.

During initial sea ice formation, the top 0.2 or 0.3 m of the sediments begins to freeze as described above. As freezing progresses during the winter, a layer beneath the top freezing layer of the sediments may become very saline due to salt infiltration caused by both sea ice formation

and freezing of the sediments near the seabed. As sediment temperatures decrease, the fresher region below the saline thawed layer begins to freeze (assuming it is nucleated) and forms a second frozen layer (this lower layer may already be partially frozen and is discussed further below).

As freezing of the top layer progresses, the rejected salt will become restricted in its downward movement by the lower partially frozen layer which may be expected to have a relatively low hydraulic conductivity (hydraulic conductivity decreases with increasing ice content). This highly saline layer may remain thawed even at low sediment temperatures so long as the salt is restricted in its movement and concentrates in the soil solution of the confined layer. This freezing procedure results in the formation of a very saline, thawed layer sandwiched between two freezing layers and is clearly illustrated by the S_B and S_U profiles shown in Figure 2.11 for site PB450.8. Apparently, in contrast to site PB450.8, the freezing conditions at site PB301 were such that the salt concentration in the saline layer was insufficient to prevent freezing since it is thought that the entire sample core was partially frozen.

Additional evidence (temperature data) has been found that suggests the existence of a lower partially frozen layer in contact with the IBPT in the region out to at least

414.6 m offshore. Figure 2.13 shows both spring and fall temperature profiles at site PB414.6. At this site, the temperature profile extends to the IBPT. There is a region that extends from a depth of about 3 m to the IBPT for which the fall and spring temperature profiles are nearly identical indicating the possible presence of ice. The temperature within this region is close to the expected freezing point at about -2.4 °C and supports the possibility that this region may be partially frozen. The depth of seasonal temperature oscillation should be deeper for this site as suggested by the temperature profiles at sites PB450.8 and PB550.2, shown in Figures 2.14 and 2.15, respectively. At these sites the depth at which the spring and fall temperature profiles coincide is about 6.3 m and 9.3 m, respectively. The temperatures at these depths are about -2.2°C and -1.8 °C, respectively, and are warmer than at the corresponding point at site PB414.6. This suggests that, at these sites, the presence of a partially frozen layer in contact with the IBPT should not be expected. Based on drill log, salinity, and temperature data of this study and previous data (Osterkamp and Harrison, 1982, Harrison and Osterkamp, 1982), it is believed that beyond about 440 m offshore the sediments above the IBPT are thawed and do not contain ice except near the seabed and at the IBPT.

If a partially frozen layer does exist above the IBPT

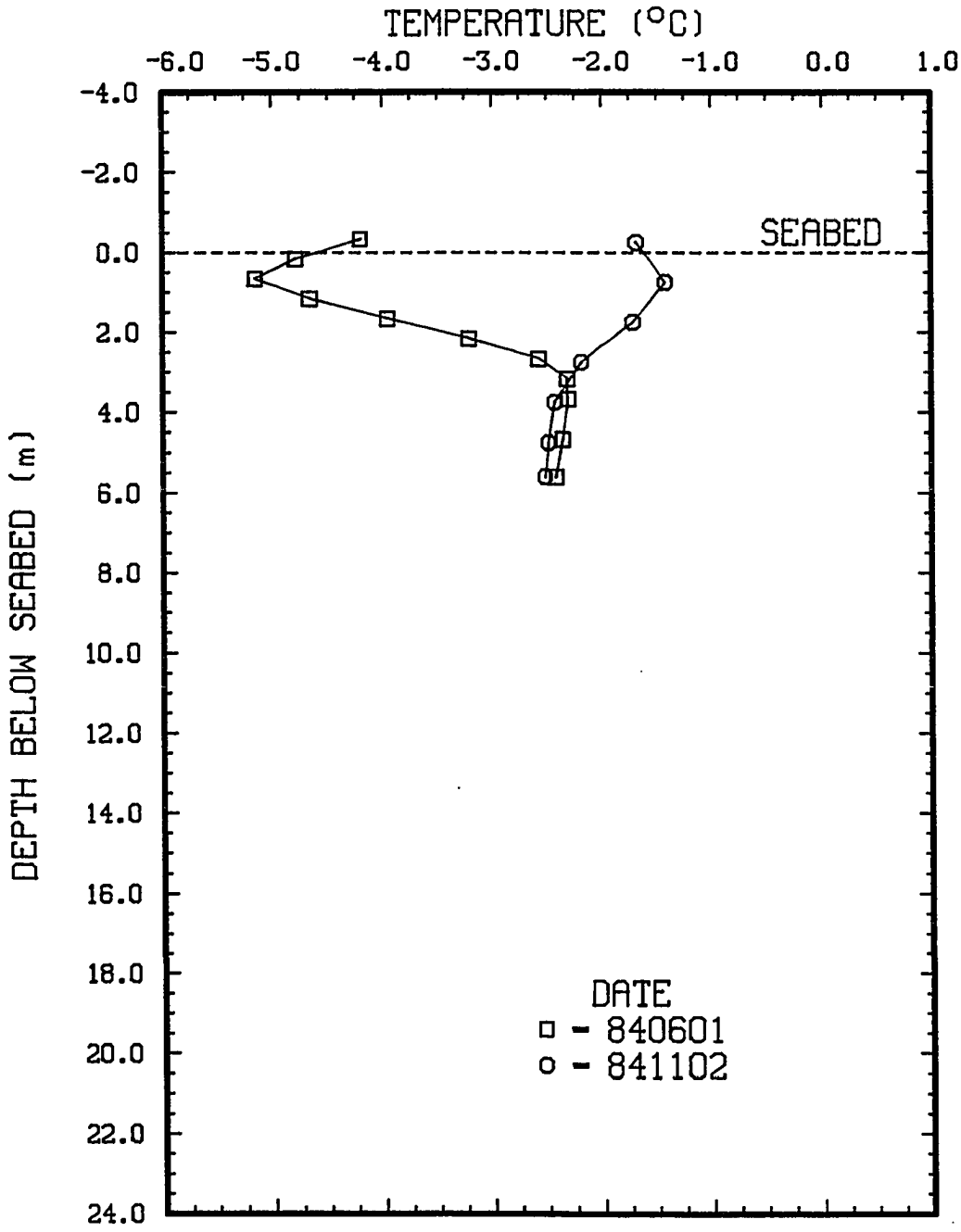

Fig. 2.13: Temperature vs. depth for site PB414.6.

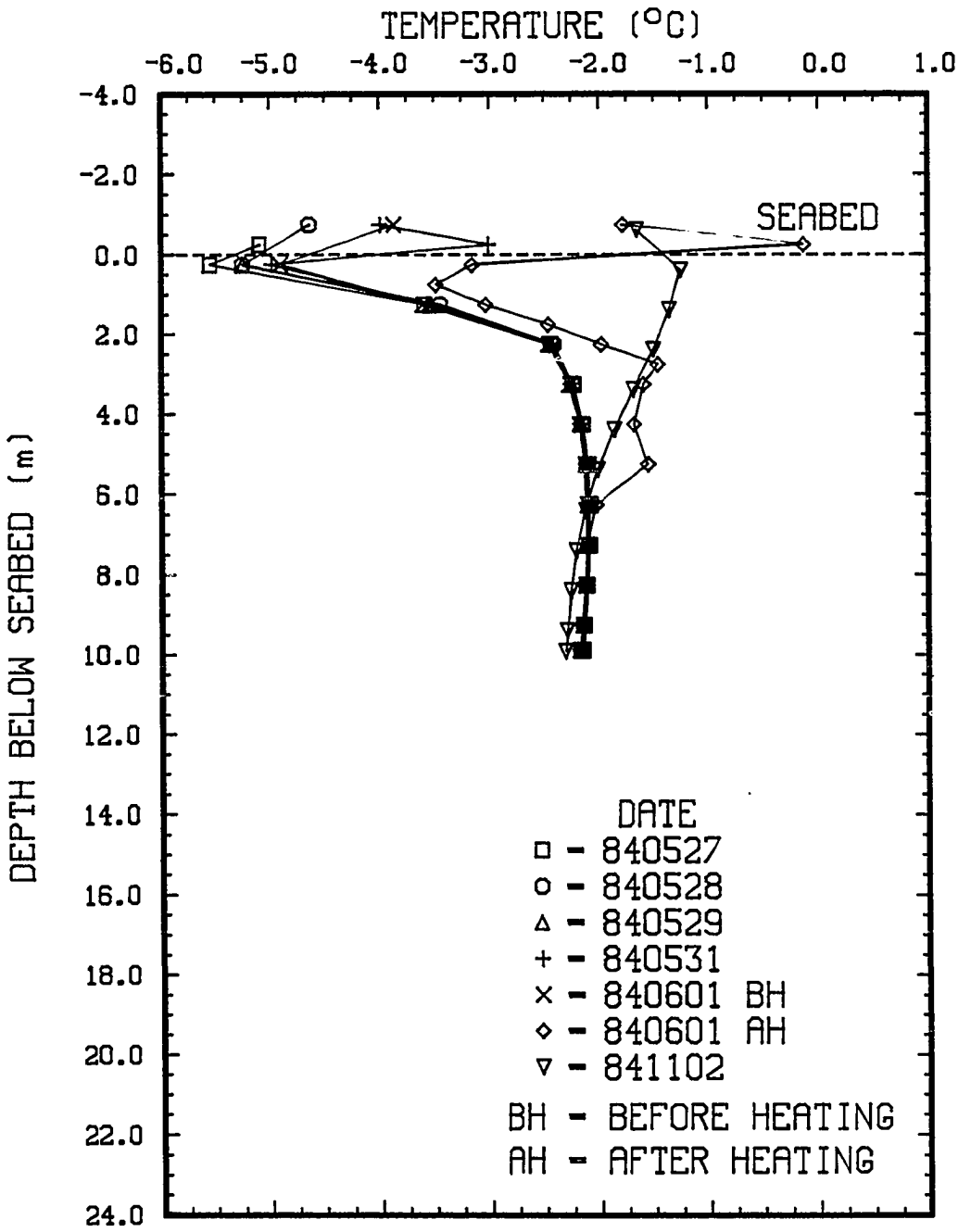

Fig. 2.14: Temperature vs. depth for site PB450.8.

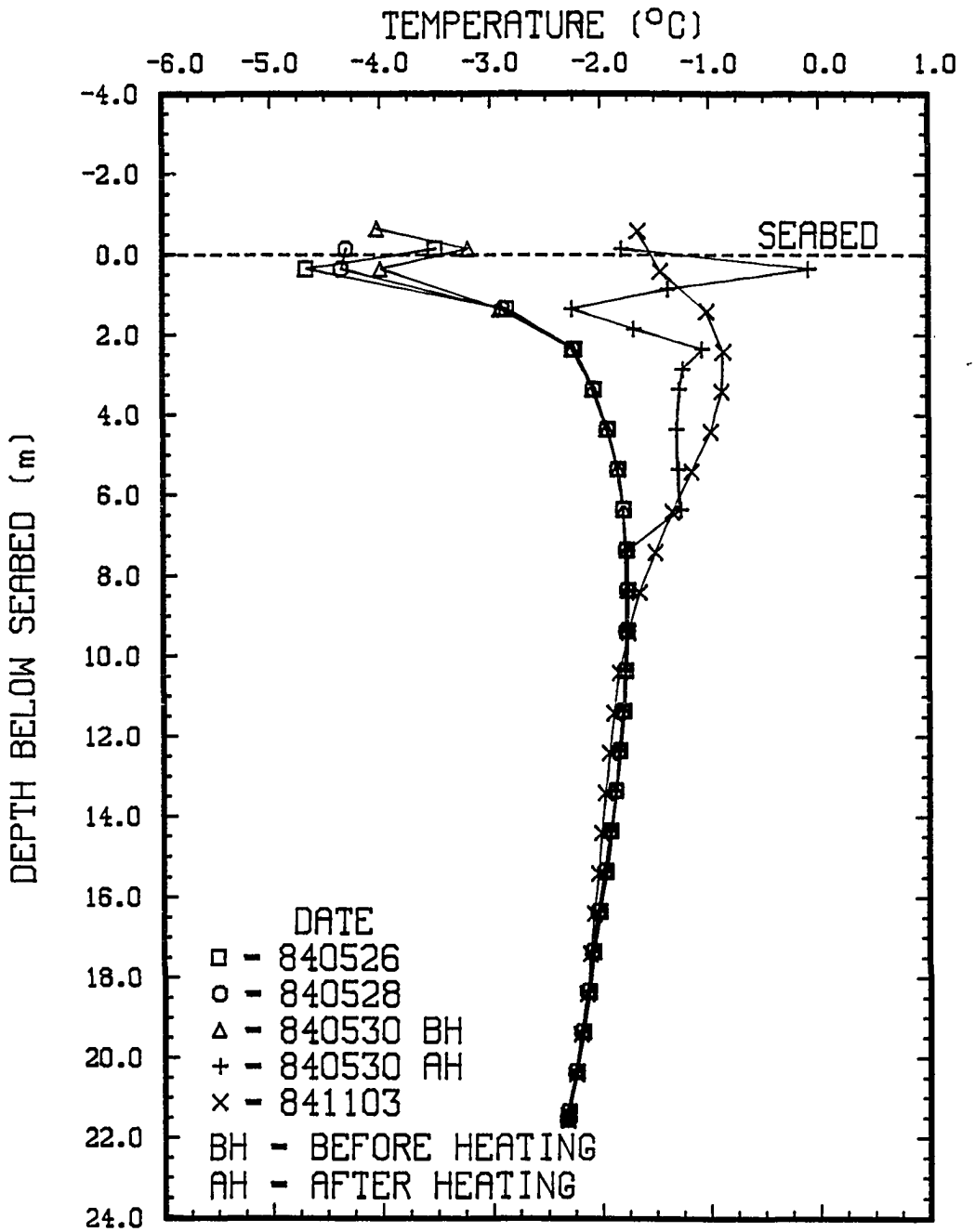

Fig. 2.15: Temperature vs. depth for site PB550.2.

in the region out to about 414.6 m offshore, it may be an indication that annual freezing and thawing may not be occurring at a well defined boundary, but over the entire partially frozen region. During freezing, this partially frozen layer may act as a restriction to salt movement and may be partially responsible for the banding described above.

Generally, in the spring, the ice content of the sediments decreased and temperature increased with distance offshore, as expected. Values for V_U increased from about 300 ppt at site PB399.8 to about 900 ppt at site PB2973.7. This corresponds to the ice content decreasing from about 700 ppt to 100 ppt. Ice was only present in the top few tenths of a meter at site PB2973.7 as shown by the V_U profile in Figure 2.16.

Figure 2.17 shows the S_B and S_U profiles for site PB2973.7. The S_B profiles become much smoother and density stable at sites greater than about 450 m offshore. The salinity profile is described as density stable since the salinity and, consequently, density increases with depth (density changes due to the small temperature gradient are negligible).

Hole heating experiments indicated that ice content decreased with distance offshore. Temperature profiles at several sites were taken immediately before and after

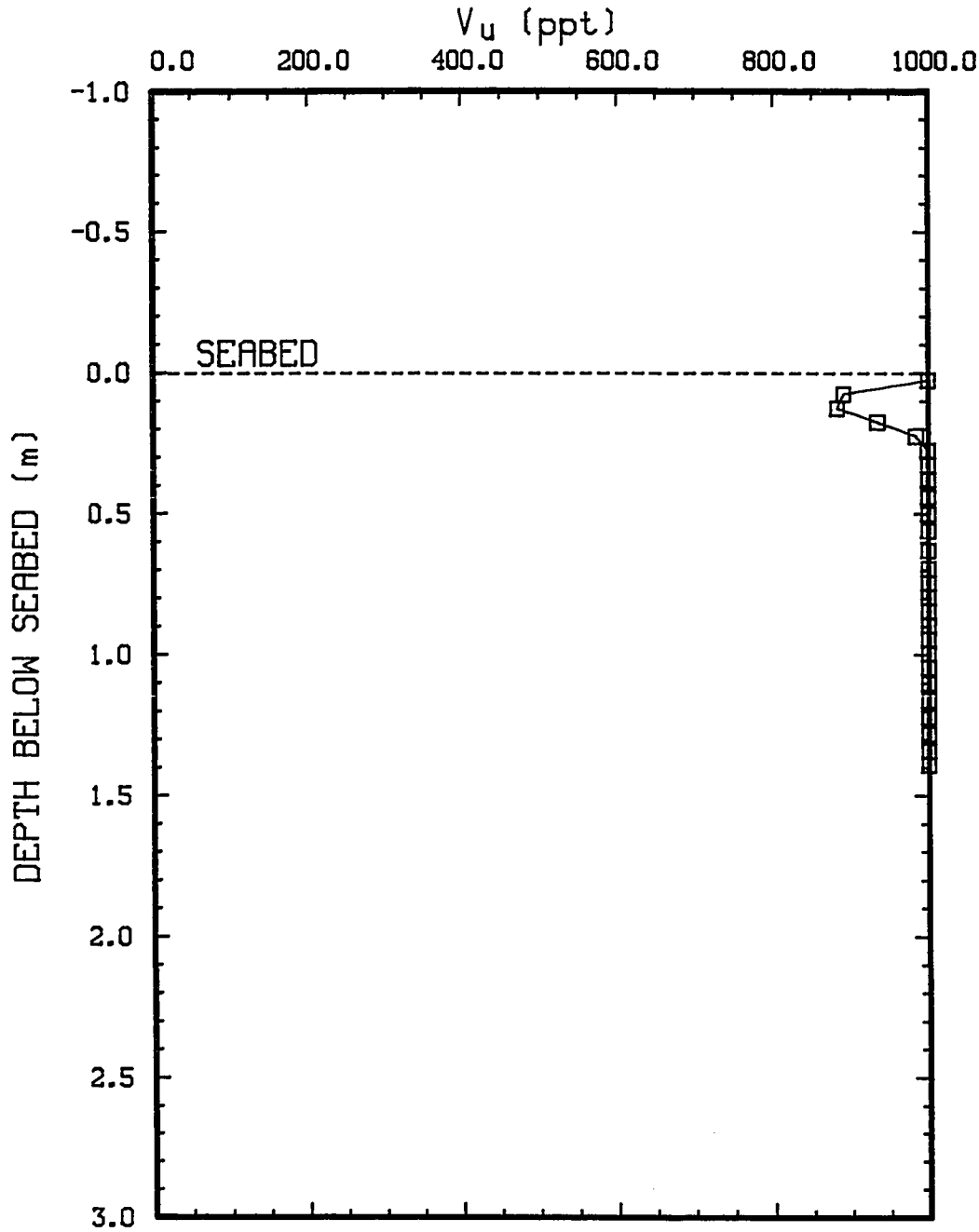

Fig. 2.16: Unfrozen soil solution content vs. depth for site PB2973.7.

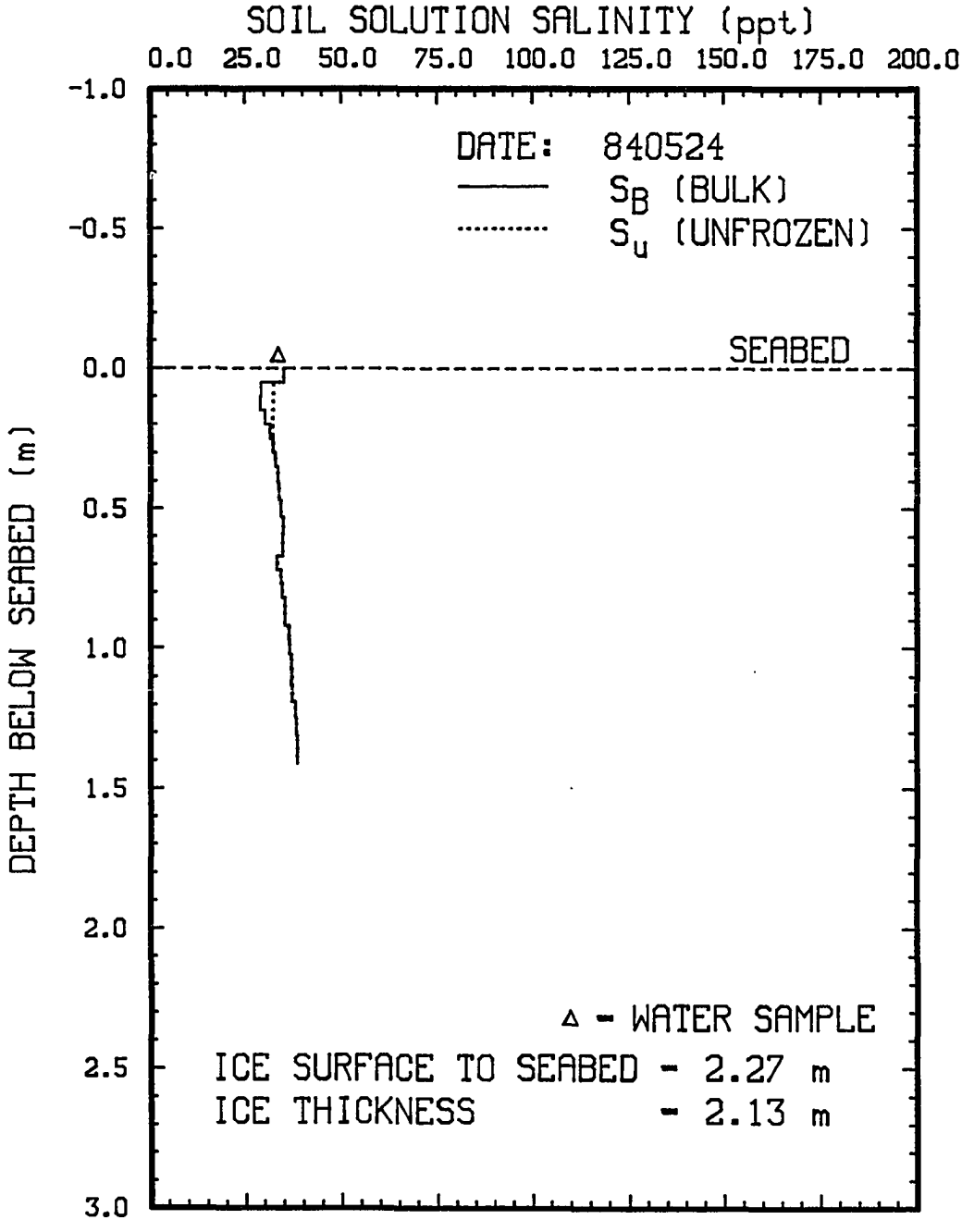

Fig. 2.17: Bulk and unfrozen soil solution salinity vs. depth for site PB2973.7.

heating and are shown in Figures 2.14, 2.15, and 2.18 for sites PB450.8, PB550.2, and PB2971.7, respectively. These holes were heated for the same amount of time using the same equipment. The increase in the sediment temperature due to heating appears to increase with distance offshore and indicates a decrease in ice content with distance offshore.

For site PB450.8, V_u profiles before and after heating are shown in Figures 2.19 and 2.20, respectively. The frozen portion of the sediments is clearly shown. Heating appears to increase values for V_u consistently throughout the profile. The increase in values for V_u due to heating increases with distance offshore. The farthest offshore sites, including PB554.1, PB1168, and PB2974 were essentially thawed completely by the heating. This is another indication that the ice content decreases with distance offshore.

2.4.4.3 Comparison of Fall and Spring Data

A comparison of the spring and fall data show several similarities and differences. Interpretation of the results of the comparison revealed characteristics of salt transport in the subsea permafrost sediments near the seabed. Some of these are:

1) In the region out to about 400 m offshore, fall S_B profiles appear to be much smoother and density stable

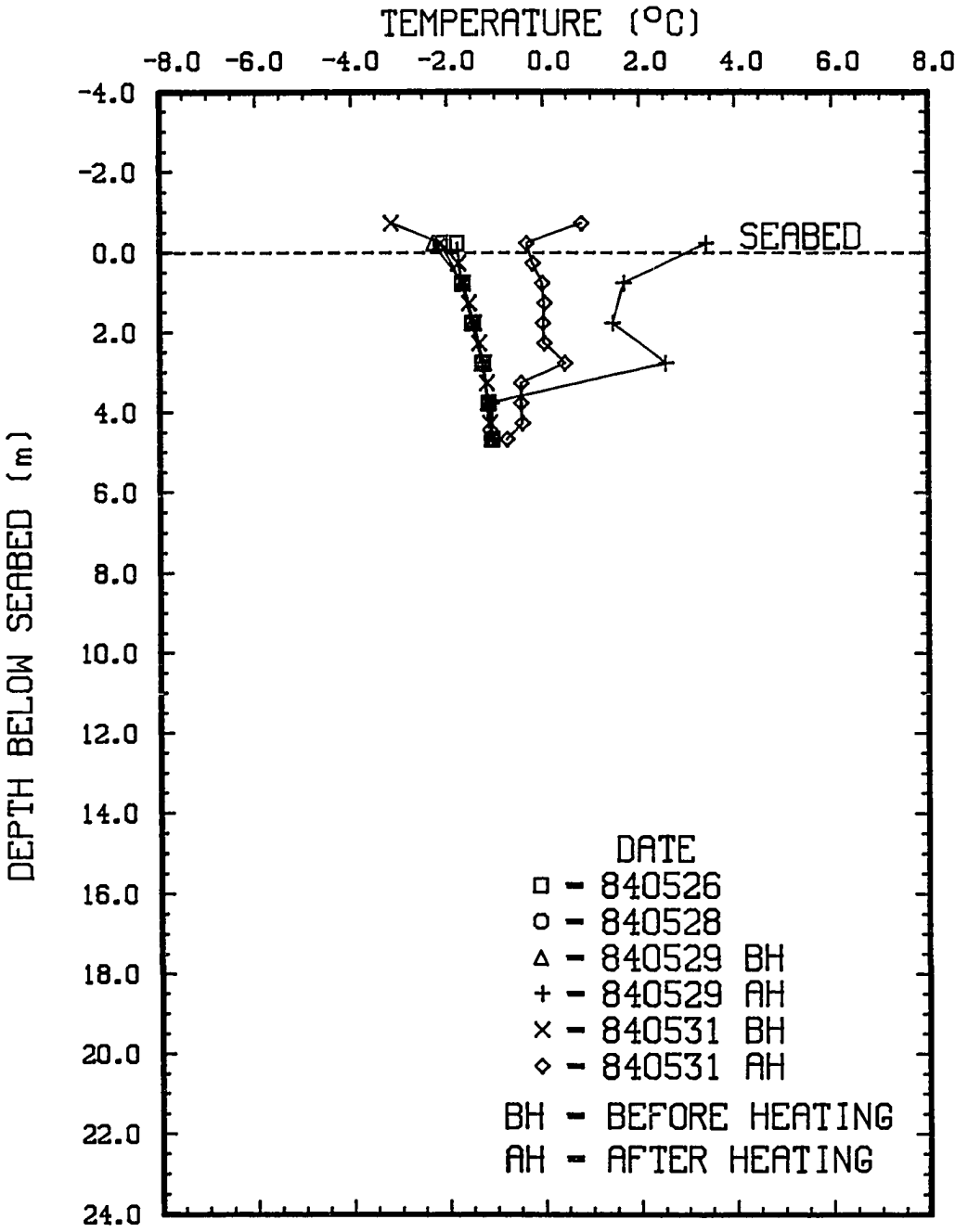

Fig. 2.18: Temperature vs. depth for site PB2971.7.

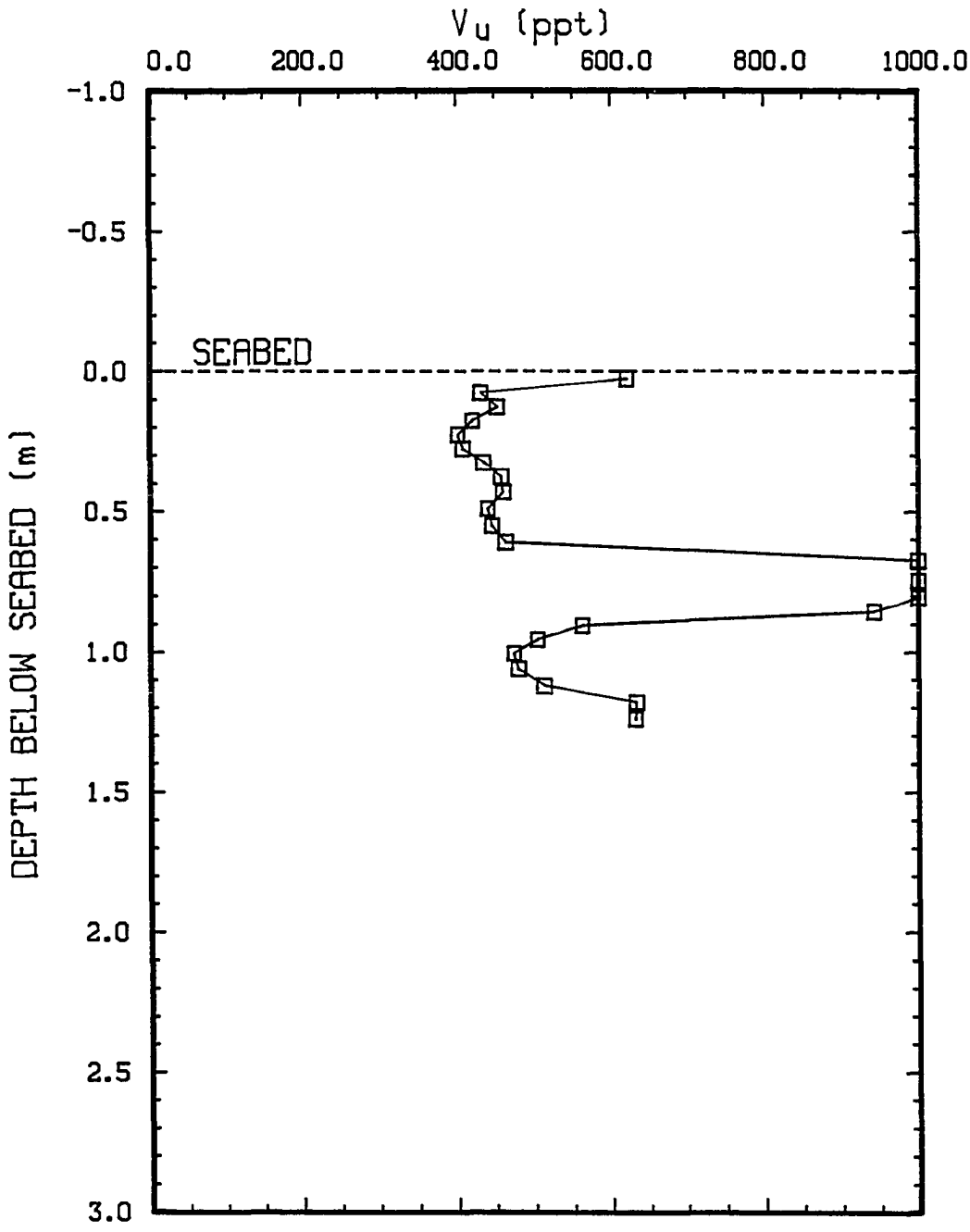

Fig. 2.19: Unfrozen soil solution content vs. depth before heating for site PB450.8.

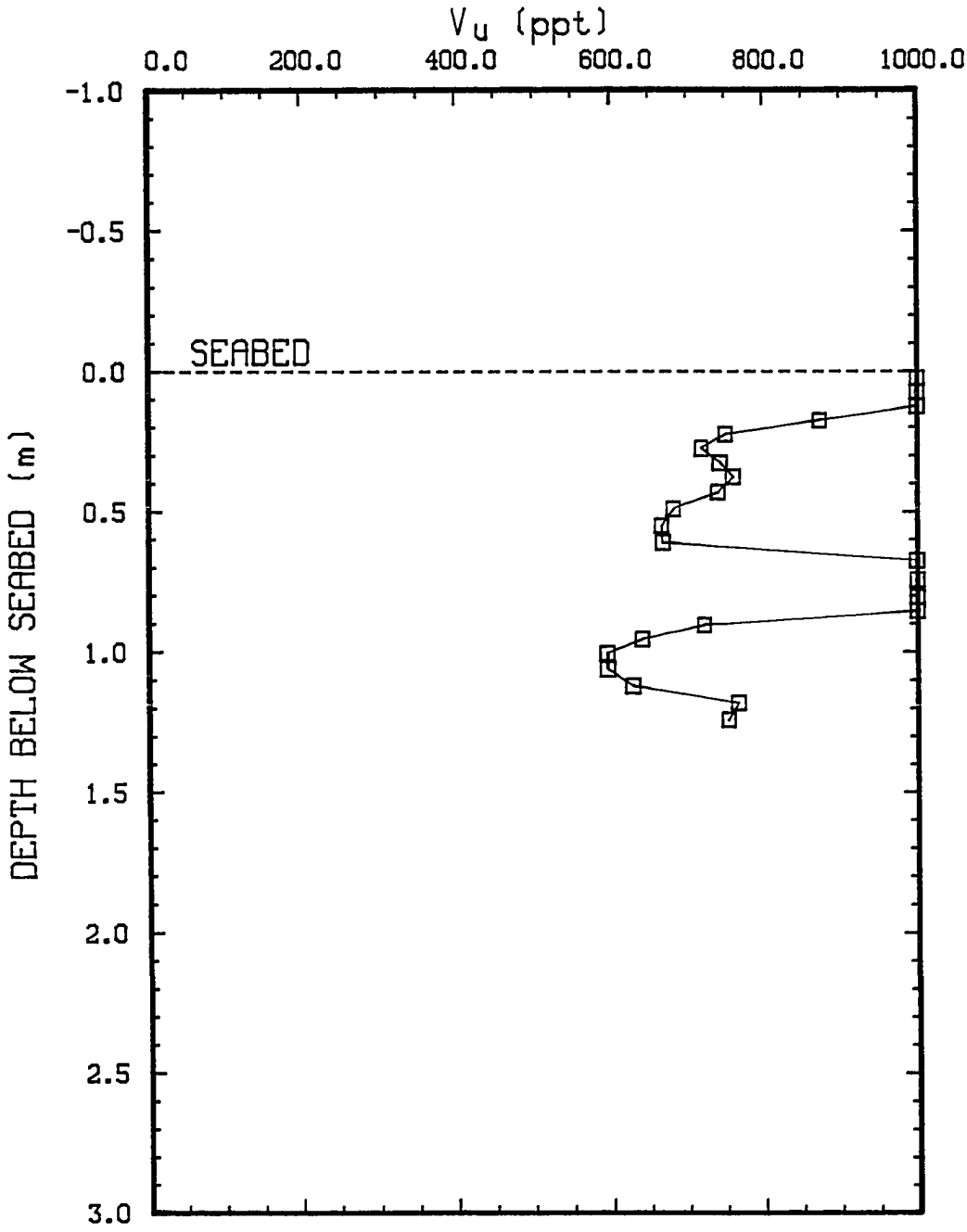

Fig. 2.20: Unfrozen soil solution content vs. depth after heating for site PB450.8.

compared to the spring profiles. This is probably a result of the dramatic increase in the soil solution salinity caused by the rejected and drained salt infiltrating the sediments as sea ice forms and grows into the sediments during the winter. The results are erratic S_B profiles. During the summer, thawing or partially thawing of the sediments allows greater mobility of the soil solution and, consequently, greater salt transport resulting in smoother S_B profiles in the fall.

2) During both the spring and fall, values for V_U in the partially frozen regions are relatively large. This is especially true for the partially frozen top layer described for the fall sample cores. Since the hydraulic conductivity should increase with increasing V_U values, this may imply that the hydraulic conductivity may be sufficient for the soil solution to be relatively mobile for salt transport by gravity drainage.

3) The distance from the ice surface to the seabed increased substantially by about 0.20 to 0.30 m between the fall and spring seasons. Apparently, sea ice initially froze to the seabed and was followed by a temporary rise in the sea level due to storms or other activity. When the thickened ice lowered, it refroze to the seabed. This occurred several times and resulted in a type of sediment banding of the ice near the seabed. Each time the sea ice

froze to the seabed a band of soiled ice was formed. Figure 2.21 is a photograph of a core sample of the sea ice near the seabed showing the multiple bands in the bottom 0.20 m or so of the core. Similar results have been reported by Matava (1986).

Profiles of the salinity change with time, $\partial S/\partial t$, of the sediments as a function of depth were determined for those sites which had at least two sample cores taken, each during a different field season. $\partial S/\partial t$ was defined as the salinity difference between sample cores divided by the time between sampling (field seasons) and is expressed in units of ppt/sec.

Figure 2.22 shows the $\partial S/\partial t$ profile at about 301 m offshore and is typical of the $\partial S/\partial t$ profiles for the freeze-up period from fall to spring. The increase in the soil solution salinity during the winter months due to salt infiltration is clearly shown. Values for $\partial S/\partial t$ ranged from about 0 to 2.5 X 10^{-6} ppt/sec throughout the depth of the core and were as high as 5 X 10^{-6} ppt/sec at other sites.

Figure 2.23 shows the $\partial S/\partial t$ profile for site PB451.8 for the thawing season (from spring to fall). It clearly shows a decrease in the soil solution salinity for the entire hole to a depth of about 1 m, particularly, at depths greater than 0.5 m which has $\partial S/\partial t$ values as low as about -11 X 10^{-6} ppt/sec. This is an indication that salt

Fig. 2.21: Photograph of sea ice core showing bands of soiled ice. Numbers shown have units of centimeters.

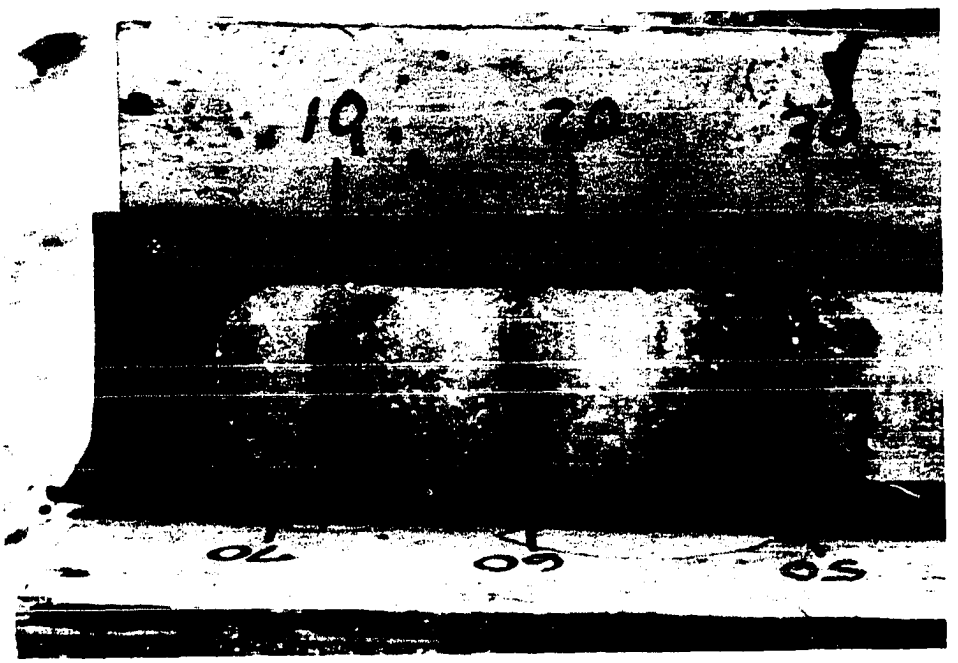

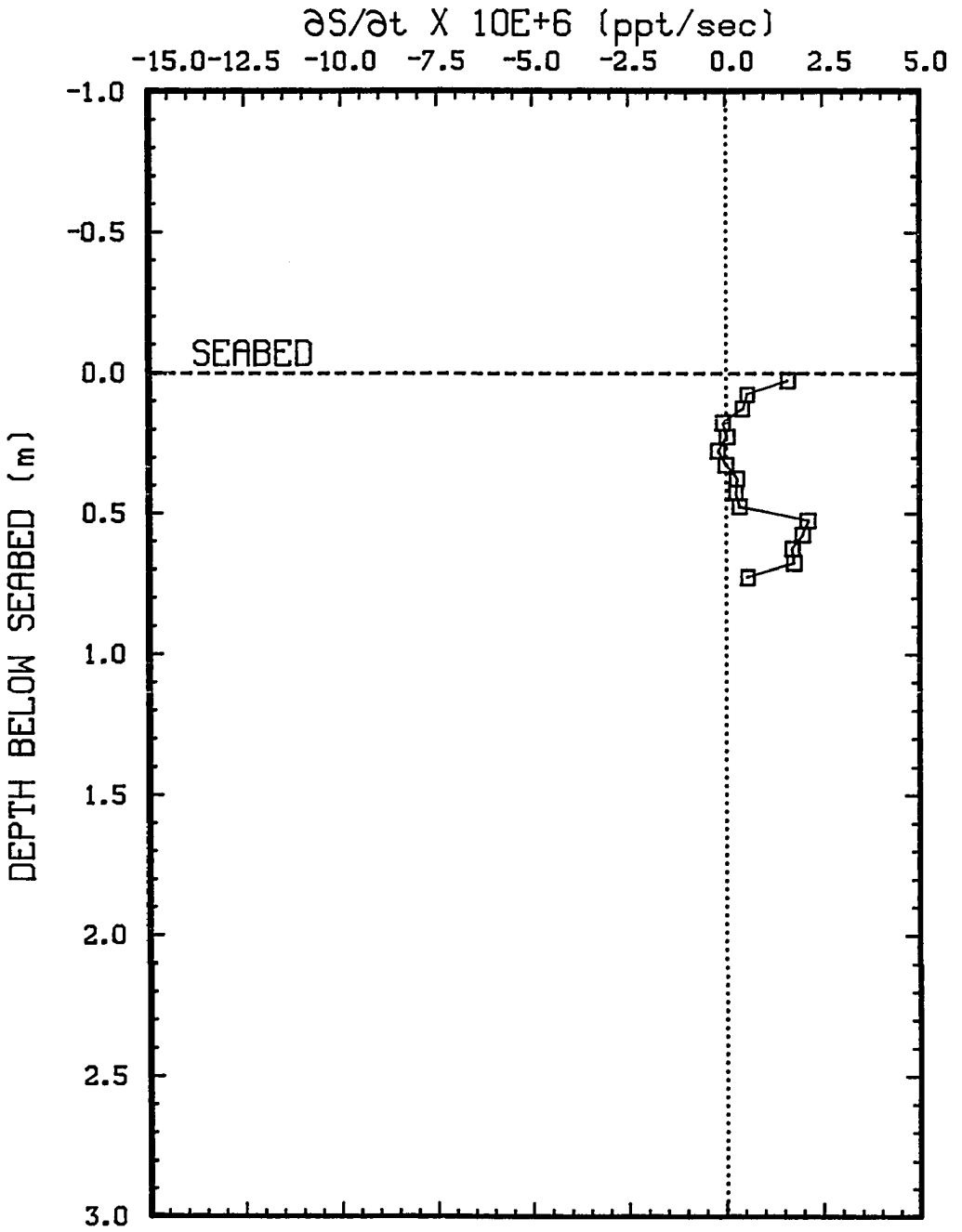

Fig. 2.22: Rate of change of salinity with time between sites PB301.1 (cored on 841030) and PB301.0 (cored on 850529).

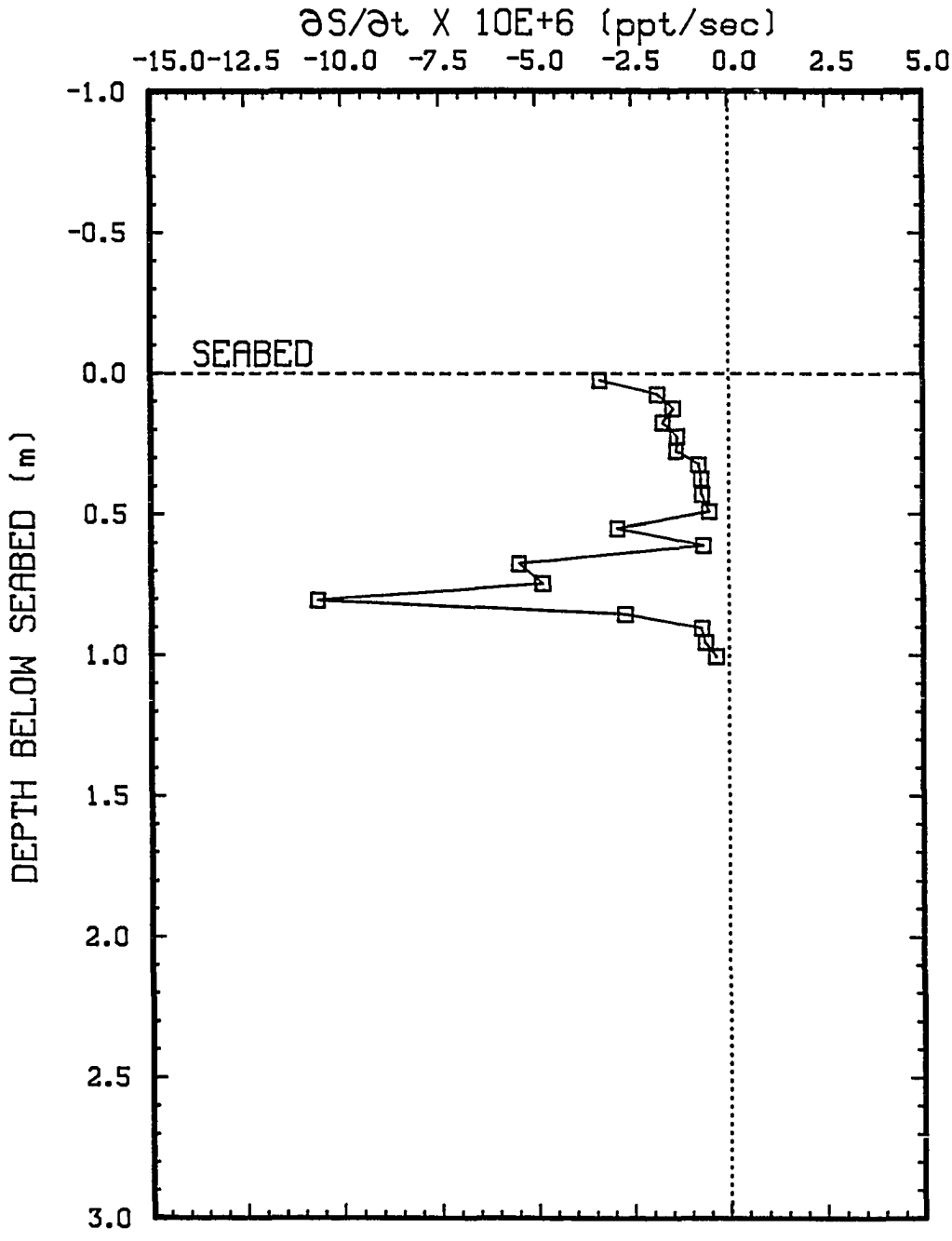

Fig. 2.23: Rate of change of salinity with time between sites PB450.8 (cored on 840523) and PB451.8 (cored on 841101).

transport, which is probably downward, occurs during the summer months and implies a salt velocity of at least 1 m/year at this site. These results were similar to those at other sites where the sediment sample core depth was about 2 m and implies a salt velocity of at least 2 m/year for these other sites.

2.4.5 Sediment Thawing Near the Seabed

2.4.5.1 Predicting the Near-Shore Ice-Bonded Permafrost Table Depth

The Stefan equation in the form

$$X = \sqrt{\frac{2\, k_T\, (T_s - T_T)\, t}{L_s}} \qquad (2.31)$$

where:

X = depth of thaw, m

k_T = thermal conductivity of the thawed sediments, J/m-yr-°C

T_s = temperature at the seabed, °C

T_T = temperature at the IBPT, °C

t = time, years

L_s = latent heat of the sediments, J/m³

was used to predict the IBPT depth (active layer depth) along the WDL out to about 400 m offshore. It is assumed that sensible heat effects are negligible, the temperature gradient in the thawing zone is linear, the seabed and phase boundary temperatures are constant, and the density of ice

is the same as the soil solution. The mean seabed temperatures show a distinctive increase at about 400 m offshore which also corresponds to a noticeable increase in the seabed depth below the sea ice surface of about 0.5 meters. In the region from shore to about 400 m offshore, the seabed depth below the sea ice surface is about 1 to 1.5 meters and the mean annual seabed temperature is about -3.4 °C (at 190 m offshore) [Osterkamp and Harrison, 1977]. The fall 1984 data show that the IBPT temperature decreases from about -2.4 °C at 10 m offshore to about -4.0 ° C at about 300 m offshore. In the spring, the IBPT temperature at site PB398.2 was -4.457 °C. The following assumptions were made:

1) In the region out to 400 m offshore, the sediments refreeze to the IBPT every year. This was confirmed by drilling observations.

2) The absolute unfrozen soil solution content, V_{wu}, at site PB399.8 is about 0.4 to a depth of about 2 m in the spring. For sites closer to shore it was assumed (since data is not available) that in the spring (maximum freezing) the unfrozen soil solution content was the same as at site 399.8. Although, it should be noted that the actual unfrozen soil solution content may be higher or lower depending on the freezing conditions and salt movement at each site.

3) The dependency of the volumetric latent heat on

salt content was neglected. This is justified by noting that these effects are most apparent in the spring when the soil solution salinity is highest and decrease during the summer as thawing and salt movement decreases the soil solution salinity.

The latent heat of the sediments is then given by

$$L_s = L_v (1 - V_{AU}) \quad (2.32)$$

where:

L_v = the volumetric latent heat of the sediments with V_U equal to 0, J/m^3

L_s = the actual volumetric latent heat of the sediments, J/m^3

V_{AU} = absolute unfrozen soil solution volume, m^3/m^3

$1 - V_{AU}$ = absolute volumetric ice content, m^3 ice/ m^3 ice and unfrozen soil solution

Osterkamp and Harrison (1982) give the following values for k_T and L_v for Prudhoe Bay.

$$k_T = 6.1 \times 10^7 \text{ J/m-yr-}^\circ\text{C} \quad (2.33)$$

$$L_v = 12.0 \times 10^7 \text{ J/m}^3$$

Substitution of known values for L_v and V_{AU} into Eq. 2.32 gives,

$$L_s = 7.2 \times 10^7 \text{ J/m}^3. \quad (2.34)$$

The average summer seawater temperature of Prudhoe Bay

at the ARCO West Dock (average for the months of July, August, and September, which gives t = 0.25 years) is +2.6 °C (ARCO, personal communication, 1985). For sites PB10.8, PB100.3, PB200.0, PB300.1, and PB399.8, the IBPT or active layer depth was determined from Eq. 2.31 using values for T_s, and T_T associated with each site. Values used for K_T and L_s were those given by Eqs. 2.33 and 2.34, respectively. Table 2.5 gives the calculated value for the IBPT depth, X, and the measured value, X_M, for each of the above sites. Values used for T_T and T_s are also given. It was assumed that V_{AU} = 1.0 (completely thawed) by the end of the summer.

Table 2.5

Summary of calculated and measured values for the ice-bonded permafrost table depth and distance offshore near the ARCO West Dock, Prudhoe Bay, Alaska

Site	IBPT Temperature T_T (°C)	Temperature Difference $T_s - T_T$ (°C)	Calculated IBPT Depth X (m)	Measured IBPT Depth X_M (m)
PB10.8	-2.443	5.043	1.46	1.27
PB100.3	-3.143	5.743	1.56	1.31
PB200.0	-3.398	5.998	1.59	2.17
PB300.1	-4.027	6.627	1.68	2.43
PB399.8	-4.457	7.056	1.73	2.84

At site PB10.8, it was assumed that the summer IBPT

temperature was about the same as in the fall which was -2.443 °C. The discrepancy between the calculated and measured values for the IBPT depth for sites PB10.8 and PB100.3 could be explained by small errors in the values used for T_s and T_T. In addition, this difference may be explained if the sediments immediately above the IBPT do not completely thaw during the summer, in other words, they are partially frozen ($V_{AU} < 1.0$) in the fall as observed during sampling. Consequently, this would essentially reduce the latent heat of the sediments and increase the depth of thaw predicted by Eq. 2.31. This effect would become more pronounced for the sites beyond 100 m offshore since the depth of the active layer increases with distance offshore.

The temperatures used for T_T were those taken in the fall 1984 and may be warmer than those of the spring. However, the difference is not considered significant enough to alter the conclusion of these calculations: the approximate depth of the IBPT can be predicted by the Stefan equation if the sediment properties, such as V_{AU}, and temperature are known.

In the region beyond about 450 m offshore, the IBPT depth, X (m), has been shown to be predicted by (Osterkamp and Harrison, 1985)

$$X = 1.147\ m^{1/2}\ (x - 276\ m)^{1/2} \qquad (2.35)$$

where x (m) is the distance offshore. Equation 2.35 shows that X has a $(time)^{1/2}$ dependency and is a typical Stefan solution for simple phase boundary propagation problems. This type of time dependence for thawing also holds when there are substantial amounts of unfrozen soil solution present (Osterkamp, personal communication). It is assumed that the rate of shoreline regression is 1 m/year.

In the region from about 400 m to 450 m offshore, the IBPT depth seems to be a transition zone in response to the changes in the mean annual seabed temperature (MASBT) and IBPT temperature that occur in this region. It is believed that the MASBT becomes warmer than the mean annual IBPT temperature so that thawing at the IBPT is occurring. Unfortunately, there are insufficient temperature data for the seabed and IBPT in this region to confirm these hypotheses. A partially frozen zone immediately above the IBPT may also exist in part of this offshore region.

2.5 Summary and Conclusions

The field work enabled S_B, W_B, and temperature profiles of the sediments near the seabed to be determined which were used to determine the unfrozen sediment properties, such as, S_U, W_U, and V_U. Observations during drilling and sampling operations suggested freezing of the sediment near the seabed and was confirmed by interpretation

of the sediment property profiles. There is good agreement between the S_B, S_U, W_B, W_U, temperature profiles, and drill log data describing the partially frozen regions of the sediments. The fall salinity profiles are generally smoother and more density stable than those of the spring. The erratic salinity profiles of the spring are probably a reflection of the rejected salts during sea ice formation infiltrating the sediments and of gravity drainage of the unfrozen soil solution in the partially frozen zones. A comparison of the spring and fall S_B profiles imply salt transport velocities of at least 2 m/year in these subsea permafrost sediments.

The top 0.20 m or so of the sediments are frozen in the early fall which is probably caused by temperature changes of the overlaying seawater associated with changes in composition and the formation of sea ice. This frozen layer contains small ice lenses angled from about 0 to 30 degrees from the vertical indicating that the layer is frost susceptible.

Temperature profiles confirm earlier results by Osterkamp and Harrison (1982) that there is a nearly constant IBPT temperature of about -2.4 °C beyond about 400 m to about 3.5 km offshore. A comparison of the spring and fall temperature profiles indicate that the thawing interface may be described as a thawing zone, up to several

meters thick, above the IBPT in the region out to about 414.6 m offshore. Temperature increases caused by hole heating indicate that the sediment ice content decreases with distance offshore.

Ice-bearing zones in the sediments are clearly identified by the V_U profiles. Values for V_U are substantial throughout the year, particularly in the fall. This may suggest that the presence of ice may not be sufficient to prevent convective instabilities in the soil solution and, hence, unfrozen soil solution drainage in the partially frozen zone may occur.

Significant amounts of salts are infiltrating the thawed or partially thawed subsea permafrost sediments during the freezing season. This was shown by positive $\partial S/\partial t$ values for this period. Near zero or negative $\partial S/\partial t$ values for the thawing season suggests salt is being transported to lower regions in the sediments during this period.

The depth to the IBPT along the WDL out to about 400 m offshore can be predicted, approximately, by the Stefan equation if sediment properties, such as V_{AU}, and temperatures at the seabed and IBPT are known. Previous work by others (Harrison and Osterkamp, 1982; Osterkamp and Harrison, 1982) showed that the depth of the IBPT could be approximated by a simple Stefan solution from about 450 m to

3 km offshore.

The abrupt increase in the depth of the IBPT in the region from about 400 m to 450 m offshore corresponds to a decoupling of the sea ice from the seabed and is associated with MASBT becoming warmer than IBPT temperatures which remain fairly constant in this region at about -2.4 °C. Closer to shore, the MASBT appears to be colder than IBPT temperatures.

Chapter 3

SALT REDISTRIBUTION DURING FREEZING OF SALINE SAND COLUMNS

3.1 Introduction

Preliminary interpretation of the field data indicated that salt was being rejected during seabed freezing and moving to lower levels in the seabed. Velocities of salt movement were determined to be at least 2 m/yr. While it was known that salt movement was occurring, the exact mechanism(s) for this movement was not understood. Therefore, laboratory tests were conducted to help identify and give a better understanding of the mechanism(s) of salt redistribution and transport during freezing.

The following section is a review of the pertinent literature including research previously conducted on salt redistribution during freezing. BPS theory (Burton, Prim, and Slichter, 1953), which describes the freezing of a solid from its melt that contains impurities and a brief discussion on hydraulic conductivity of frozen soils, are also presented.

3.2 Literature Review

There has been relatively little work performed on salt redistribution during freezing in soils. The exact mechanisms for salt redistribution and how the soils are affected are largely unknown owing to the vast differences

in soils, soil moisture content, soil solution compositions, and the conditions under which these processes can take place (i.e., temperature and time, etc.).

Hallet (1978) discussed some of the processes that are involved during the freezing of fine-grained soils. He suggested that, in fine or silty soils where there is a significant freezing point depression, constitutional supercooling may not occur at the ice lens surface, but at a characteristic distance away from this surface where the equilibrium temperature gradient and the actual temperature gradient allows constitutional supercooling. This should lead to a characteristic ice lens spacing.

Chamberlain (1983) examined ice segregation and frost heave processes during laboratory soil column freeze tests in the downward freezing direction. One of the soils tested was a saturated Dartmouth sand containing 18 percent fines (fines being defined as those particles with size less than 0.02 mm). The use of seawater as the soil solution resulted in the formation of a thick freezing zone with many ice lens growth sites, each with its own unfrozen soil solution concentration. This process repeated itself and resulted in multiple layers of alternating ice and unfrozen soil solution. These results suggest that under conditions with very small freezing temperature gradients, such as under the Beaufort Sea, thick zones with alternating layers

of ice-bonded and non-ice bonded (high unfrozen soil solution content) material could form. The non-ice bonded layers are potential failure planes and must be considered by engineers in the design of offshore artificial islands and pipelines.

Kay and Groenevelt (1983) conducted a field study and laboratory sand column freezing tests. The results of the field study showed that solute redistribution occurred during the natural downward freezing. It was believed that convective transport of solutes caused by water being drawn to the freezing zone was a significant mechanism of solute redistribution. Solute redistribution by solute exclusion by the advancing freeze front could not be confirmed.

A non-frost susceptible coarse sand was used in their laboratory sand column freezing tests. The columns were saturated with a KCl solution with a salinity of about 0.776 ppt (0.369 ppt Cl). An upward moving unidirectional freezing isotherm was established by lowering the bottom temperature about 4 °C (to -3.5 °C). Their results indicated that there was no evidence of effective solute exclusion from the frozen zone. However, the 0 °C isotherm appeared to move in leaps and it was believed that solute exclusion occurred on the local scale. This should have resulted in an increased solute concentration and, consequently, a decrease in the soil solution freezing point just ahead of

the freezing front. As the 0 °C isotherm advanced, the temperature at some characteristic distance ahead of the ice-containing zone (partially frozen zone) was thought to have dropped below its freezing point and a second ice-forming site developed. This process should result in banding with alternating ice and unfrozen soil solution containing zones. They noted that their sampling procedure, which provided averaged concentrations across the microregions of salt rejection and accumulation, was not capable of detecting the individual unfrozen soil solution layers.

Wilson (1983) conducted laboratory freezing tests to study salt redistribution in a saturated column of granular soil. The soil columns measured about 46 cm in diameter and about 71 cm in length. Artificial seawater solutions were used as the soil solution. The initial soil solution salinities varied from 0 to 80 ppt. Various step changes in temperature were applied for the surface thermal condition. The soil used was a gravelly sand obtained from a gravel pit near Prudhoe Bay, Alaska and was the same as that used for artificial island construction in that area.

A downward moving freezing isotherm was established by applying a constant sub-freezing temperature to the soil surface. With saline soil solutions, no clearly distinguishable freeze front could be found. Freezing

occurred over a wide range of temperatures and depths due to a changing solute concentration in the unfrozen soil solution as a consequence of salt exclusion. During the phase change, latent heat was released gradually over the entire depth of the partially frozen region, and not at a well defined interface, as temperatures were lowered. For this reason, the freezing front in a saline soil may be better described as a freezing zone. The soil strength was visually weaker in the freezing zone than in the upper more frozen zone.

Wilson (1983) concluded that:

1) There was solute redistribution as the soil freezes such that the soil solution salinity just below the freeze front is greater than its initial average salinity.

2) The degree of solute redistribution decreased with increasing soil solution salinity.

3) The degree of solute redistribution increased with colder surface temperatures.

Additional interpretations of the work by Wilson (1983) were made by Mahar et al. (1983), and indicate that the effect of salt transport due to diffusion or natural convection downward through the column could cause the freezing process described by Hallet (1978) to occur more readily. A solute concentration gradient in the unfrozen soil solution could occur above the freeze front where the

larger solute concentrations and soil solution densities exist at colder temperatures (near the top of the soil column). This condition should result in solute transport downward toward the lower concentrations due to convection associated with the density gradient and diffusion associated with the concentration gradient.

As solute transport occurs, the salinity at a given point should decrease which stimulates more ice growth. Mahar et al. (1983) believe that given enough time and a sustained thermal gradient, solute transport should continue until nearly all the solutes are drained out of the soil.

Their conclusions included the following:

1) The salinity of the unfrozen soil solution increased toward the colder temperatures (at the top) in the partially frozen zone.

2) The unfrozen water content in the partially frozen soil above the freezing front decreased with decreasing temperature. Unfrozen water contents as high as 20 percent were observed at the top (cold end) of the column at which the soil temperature was measured at -8 °C.

3) Salt transport should occur in the partially frozen zone if a thermal, and hence, density gradient (density decreasing with depth) is maintained.

In summary, for fine-grained soils, Hallet (1978) suggested that constitutional supercooling may not occur at

the growing ice lens surface but at a characteristic distance away from this surface. This should result in a zone of ice lenses with a characteristic spacing.

Chamberlain (1983) reported multiple layers of alternating ice and unfrozen soil solution when freezing downward in Dartmouth sand with seawater as the soil solution. Banding was also thought to occur during the experiments by Kay and Groenevelt (1983) involving upward freezing of Dartmouth sand columns saturated with a KCl solution of relatively low concentration.

Wilson (1983), and Mahar et al. (1983) studied salt redistribution during freezing in gravelly sand from the Prudhoe Bay area. They concluded that the degree of solute redistribution depends on the salinity and thermal gradient. Also, solute transport should occur in the freezing zone, if a thermal gradient is maintained.

In the above investigations, the relationship between solute redistribution and freezing rate, and salt transport through the thawed region have not been well defined.

3.3 BPS Theory

The BPS theory (Burton, Prim, and Slichter, 1953) which describes the unidirectional freezing of a solid from its melt containing impurities has been applied to the laboratory freezing of NaCl solutions to determine or

predict salt redistribution (Weeks and Lofgren, 1967, Cox and Weeks, 1975). Although the simplifying assumptions of the original authors are sometimes not observed, the BPS theory has been useful for describing solute distribution for a freezing liquid. This theory will be applied to the freezing sand column tests and is briefly reviewed here.

There appear to be several factors that contribute to determining the salinity profile in a unidirectional freezing experiment at any given time. These include:

1. The initial amount of salt entrapped in the partially frozen region containing sand, ice, and brine.

2. Brine expulsion or the squeezing of brine out of the partially frozen region as the result of differential volume changes during the freezing of ice from the brine.

3. Brine drainage from the partially frozen region.

The first factor, initial salt entrapment, may be investigated with the BPS theory. When saline water freezes, salt is rejected at the ice-brine interface. Depending on the mixing conditions in the brine, a build-up of salt near the interface may result as freezing continues. It is assumed that, near the interface, salt and heat transfer is by diffusion. The thermal diffusivity is much greater than the diffusivity of the salt and, consequently, the thermal changes are much more rapid than the compositional changes. This situation causes a region near

the interface to be supercooled which is referred to as constitutional supercooling because it is caused more by compositional changes as opposed to thermal changes (Rutter and Chalmers, 1952).

The BPS equation used to predict the salinity profile of NaCl ice (Weeks and Lofgren, 1967, and Cox and Weeks, 1975) and sea ice (Nakawo and Sinha, 1981) is

$$k = \frac{k^*}{k^* + (1 - k^*) \exp [- (\delta/D)v]} \qquad (3.1)$$

where:

k = effective distribution coefficient

k^* = k at $v = 0$ (assuming a cellular interface to remain stable)

δ = thickness of the diffuse layer (heat and mass transport is by diffusion only)

D = diffusion coefficient

v = velocity of freezing interface.

Also,

$$k = \frac{S_s}{S_o} \qquad (3.2)$$

where:

S_s = salinity of the ice (solid)

and,

S_o = salinity of the liquid or initial concentration in the liquid.

Equation 3.1 can be written as

$$\ln[(1/k)-1] = \ln[(1/k^*) - 1] - (\delta/D)v \qquad (3.3)$$

which is a straight line on a graph of $\ln[(1/k)-1)]$ versus v with a slope of $-(\delta/D)$ and a $v = 0$ intercept of $\ln[(1/k^*)-1)]$.

For NaCl ice formation, Weeks and Lofgren (1967) found for freezing velocities ranging from 10^{-5} to 3×10^{-3} cm/s (0.86 to 259.2 cm/day) that $k^* = 0.26$ and $\delta/D = 5.090 \times 10^3$ s/cm. For NaCl solutions, $D \simeq 1.5 \times 10^{-5}$ cm^2/s which indicates the thickness of the diffusive layer, δ, to be about 0.08 cm.

Cox and Weeks (1975) obtained $k^* = 0.26$ and $\delta/D = 7.243 \times 10^3$ s/cm for growth velocities ranging from about 2×10^{-5} to 28×10^{-5} cm/s (1.73 to 24.2 cm/day). Substitution of these values for k^* and δ/D into Eq. 3.1 gives

$$k = \frac{0.26}{0.26 + (0.74)\exp(-7.243 \times 10^3 v^*)} \qquad (3.4)$$

where v^* (cm/s) was defined as the growth velocity of the bridging layer which is about 3 cm above the freezing front of the cellular interface. v^* was assumed to be equal to the interface velocity, v.

For growth rates less than 2 X 10^{-5} cm/sec, k values decreased (salt rejection increased) rapidly with decreasing v^* and may have been due to the solid/liquid interface changing from cellular to a more planar one. For growth velocities less than 2 X 10^{-5} cm/s, k can be estimated by (Cox and Weeks, 1975)

$$k = 0.8439 + 0.0529 \ln(v^*). \qquad (3.5)$$

Nakawa and Sinha (1981) obtained $k^* = 0.12$ and $\delta/D = 4.2 \text{ X } 10^{4}$ s/cm for sea ice formation. Substitution of these values into Eq. 3.1 gives

$$k = \frac{0.12}{0.12 + (0.88) \exp(-4.2 \text{ X } 10^{4} v)}. \qquad (3.6)$$

Equation 3.6 predicts slightly lower values for k than Eq. 3.4. This is thought to be caused by the natural brine drainage that commonly occurs during the sampling process of sea ice. Cox and Weeks (1975) used a nondestructive, in-situ method of brine measurement.

In summary, since $k = S_s/S_o$, k is determined by obtaining values for S_s and S_o for a growth velocity v. Values for k^* and δ/D are obtained from a graph of $\ln[(1/k)-1]$ versus v. A straight line graph of $\ln[(1/k)-1]$ versus v suggests that BPS theory can be applied.

3.4 Hydraulic Conductivity

The hydraulic conductivity, K (cm/s) is an indication of a material's ability to conduct water. It is defined by Bear (1972) as

$$K = k\,(g/\nu) \tag{3.7}$$

where g (cm/s^2) is the gravitational acceleration, ν (cm^2/s) is the kinematic viscosity and k (cm^2) is the permeability of the porous matrix. k depends solely on the properties of the soil matrix and is related to the mean (or effective) grain diameter, d (microns), by

$$k = 0.617 \times 10^{-11} d^2. \tag{3.8}$$

The flow of water in frozen soils is not as well understood as in unfrozen soils. Campbell (1974) showed that for unsaturated, frozen soil when the soil release curve can be represented as

$$\psi = \psi_m\,(\theta/\theta_s)^{-b} \tag{3.9}$$

and the hydraulic conductivity can be represented by

$$K = K_s\,(\theta/\theta_s)^{(2b+2)} \tag{3.10}$$

where:

ψ = soil water matric potential in cm water

ψ_m = air entry value, cm water

K_s = saturated hydraulic conductivity, cm/day

θ_s = saturated volumetric water content, cm^3 of water/cm^3 of soil

θ = unsaturated volumetric liquid water content, cm^3 of water/cm^3 of soil

b = a constant determined for a particular soil.

For unsaturated, unfrozen Botany sand, Campbell (1974) determined b = 0.14 where

$$K = K_s (\theta/\theta_s)^{(2b + 3)}. \qquad (3.11)$$

This is the same as Eq. 3.10 except the exponent has been increased by 1.

Both Eq. 3.10 and Eq. 3.11 indicate that K is a power function of the unsaturated liquid water content. This might suggest that K of saturated, frozen soils may be a power function of the unfrozen water content, the air, for purposes of K determinations, being replaced by ice.

Horiguchi and Miller (1983) measured the hydraulic conductivity of several saturated, frozen silts and clays. They determined that, with the unfrozen water content, w_u (cm^3 unfrozen water/cm^3 soil), represented by

$$w_u = A\ T^B, \qquad (3.12)$$

K (m/s) could be predicted by

$$K = C\ T^D \qquad (3.13)$$

where A, B, C, D are empirically determined soil parameters. Solving Eq. 3.12 for T and substituting into Eq. 3.13 gives

$$K = A' w_U^{B'} \tag{3.14}$$

which has the same form as Eq. 3.10 where A' is the unfrozen saturated hydraulic conductivity ($\theta = \theta_s$), K_s, and B' is a constant determined for a particular soil. Since

$$w_U = V_{AU}\, \epsilon \tag{3.15}$$

where V_{AU} is the absolute unfrozen soil solution content (cm^3 of unfrozen soil solution/cm^3 unfrozen soil solution and ice) and ϵ is the porosity, then substitution of Eq. 3.15 into Eq. 3.14 gives

$$K = K_s\, (V_{AU}\, \epsilon)^{B'}. \tag{3.16}$$

This suggests further that K for saturated frozen sands may be represented as a power function of w_U or V_{AU}. K_s and ϵ can be determined experimentally. For the determination of B', K may be measured experimentally at a freezing temperature T_F for which V_{AU} may also be determined by the method described in Section 2.3.10. B' can then be calculated by substitution of values for K, K_s, ϵ, and V_{AU} into Eq. 3.16 and solving for B'.

In summary, the hydraulic conductivity, K, of

saturated frozen soils may be represented by an expression of the form

$$K = K_s (w_u)^{B'} \qquad (3.17)$$

where B' is a constant determined for a particular soil.

3.5 Laboratory Methods and Procedures

3.5.1 Introduction

Several different experiments were conducted to determine specific characteristics of the salt redistribution process during freezing in saline sand soils, somewhat similar to those found at Prudhoe Bay, Alaska. A 35 ppt NaCl solution was used as the soil solution. This concentration and type of solution was chosen since it closely represents the concentration and major ion constituents in normal seawater.

The laboratory tests were conducted to determine:

1) Whether or not the effective distribution coefficient, k, is an appropriate parameter to describe the redistribution of solutes during the freezing of saline sands.

2) k for freezing sand soils saturated with a 35 ppt NaCl solution for different constant rates of freezing.

3) The effect of freezing rate on k.

4) The thickness and concentration of a highly saline

layer that may exist ahead of the freezing interface.

5) The effect of freezing direction, upward or downward, on salt redistribution.

6) The velocities of salt movement.

3.5.2 Freezing Column Tests

The columns used in the freezing test were constructed of tenite butyrate tubing. Figure 3.1 shows a diagram of one of the columns. They measured 2 1/2-inches O.D., 2 3/8-inch I.D., and were 42 cm long. The bottom end of the column was sealed with a polyethylene cap attached with Devcon 5-minute epoxy. A pipe fitting was fastened to the center of the cap to which one end of a latex tube was attached with a hose clamp and the other end was pinched closed. The tube measured 3/8-inch I.D., 1/2-inch O.D. and was about 20 cm in length. To assure a good seal, a 1/8-inch layer of Dow Corning 734 RTV self-leveling silicone sealant was placed in the bottom of the column.

The latex tube served two purposes. One was to act as the wetting port which allowed the upward wetting of the sand columns and avoided air entrainment or cavitation that could have occurred by wetting downward. The second purpose was to act as an expansion chamber. As the column was frozen downward, the excess soil solution from the volumetric ice expansion in the frozen region could

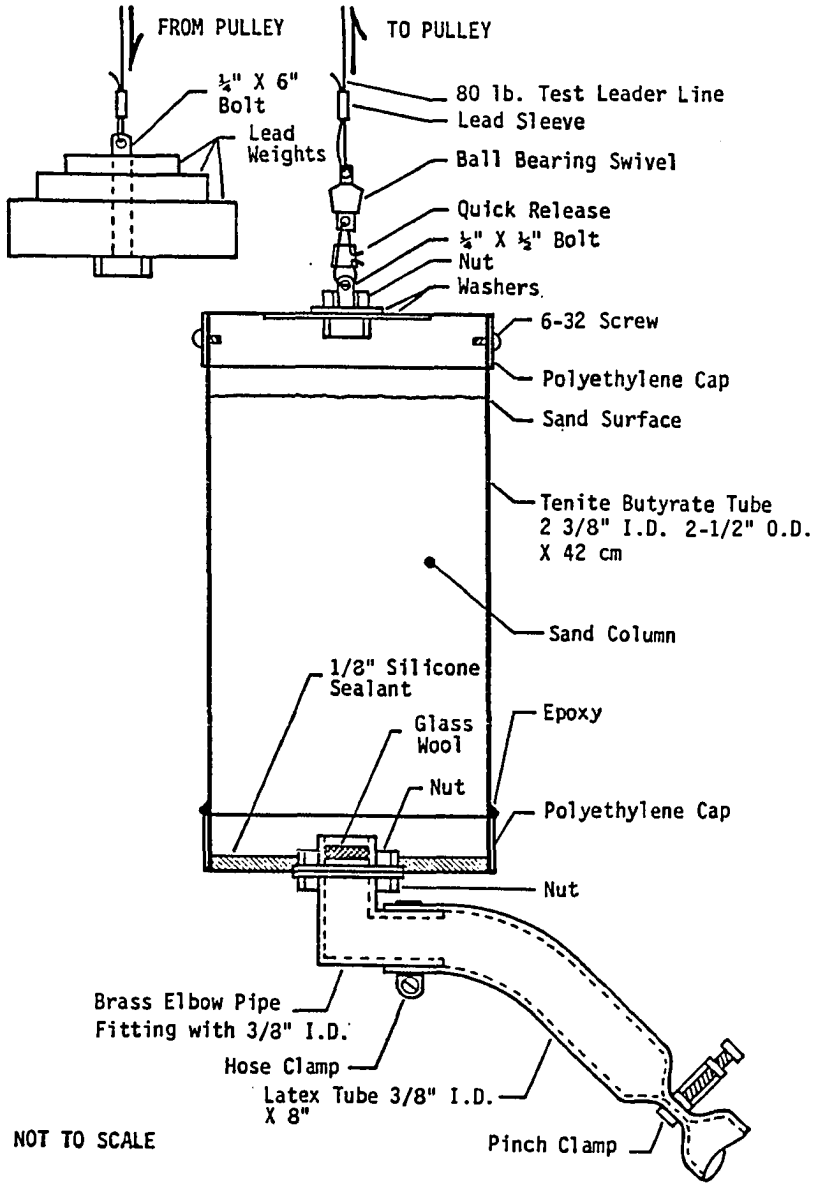

Fig. 3.1: Diagram of the sand columns used in the laboratory freezing experiments.

accumulate in the tube and expand it. It took approximately 20 psi to expand the latex tube which was designed to act like a safety valve to protect the column (tenite butyrate tube) from bursting (since the bursting pressure of the column was greater than 20 psi).

A polyethylene cap was attached on top of the column by three brass screws. A 1-inch long 1/4-inch diameter bolt was modified and fastened to the center of the cap from which the column was suspended.

A suspension apparatus was constructed that would allow the simultaneous freezing of six columns. A photograph of this apparatus is shown in Figure 3.2 with details schematically illustrated in Figure 3.3. This apparatus was made to suspend and freeze the columns at a constant rate. The framework of the structure was made of 3/4-inch steel angle iron supporting two horizontal and parallel, 1-inch diameter solid steel rods. These rods were supported at each end by radial anti-friction ball bearings and rotated very easily.

A Synchron™ constant speed motor was used to rotate the steel rods. Different speeds were obtained by using motors with different speed ratings which were between 1 and 10 revolutions per hour (rph). These speeds were greater than desired so the Synchron™ motors were incorporated into a speed reducing gear box and mounted on the end of one of

Fig. 3.2: Photograph of apparatus used in the freezing sand column experiments.

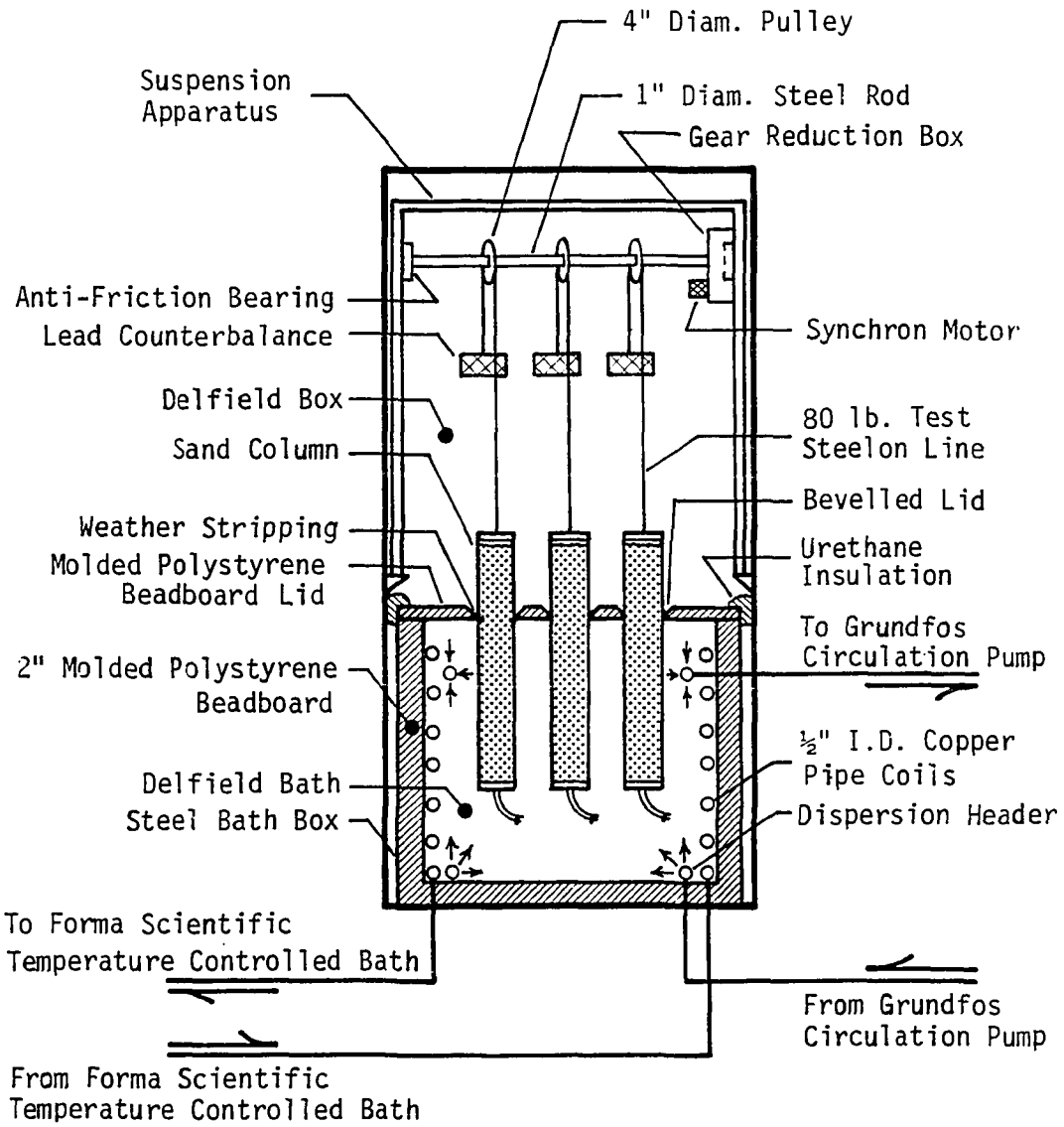

Fig. 3.3: Diagram of apparatus used in the laboratory freezing column experiments.

the rods. A flexible chain drive connected both steel rods and allowed both rods to be driven with one motor.

The suspension apparatus was placed in a Delfield model 6125 refrigerator/freezer. A temperature controlled bath was constructed and placed below the suspending apparatus and will be referred to as the bath. The area in the Delfield refrigerator/freezer above the Delfield bath will be referred to as the box.

The bath was constructed from 1/16-inch thick plate steel. It was insulated with 2-inch thick molded polystyrene beadboard and lined with 1/2-inch I.D. copper pipe coils. Anti-freeze was circulated through the coils with a temperature-controlling Forma Scientific Bath (model number 2161). The bath was also filled with anti-freeze which was circulated with a Grundfos circulating pump (type UPS 15-42F) to prevent temperature gradients.

A 1-inch thick, snugly-fitting, molded polystyrene beadboard lid was made to seal the bath and to insulate it from the box. Holes in the lid for the columns were lined with a fur type weather stripping to minimize any convective air movement between the box and bath. The top edge of the molded polystyrene beadboard lid around the holes was bevelled so that the thickness of the lid that was in contact with the columns was reduced to about 1/4-inch. The weather stripping was about 1/4-inch wide with a mat

thickness of about 1/4-inch and was attached to the molded polystyrene beadboard lid with Devcon 5-minute epoxy.

Steelon™ leader line (80 lb. test) was used to suspend the columns. The column end was attached to the line with the use of a ball bearing swivel (common fishing gear) to assure vertical positioning of the columns. A 1/4-inch diameter by 6-inch bolt was fastened to the other end of the Steelon™ line. All Steelon™ line connections were made with Berkley™ lead connector sleeves.

The Steelon™ line was fed over pulleys which were constructed out of 1/8-inch plate steel. The 4-inch diameter pulleys had a small V-notch groove milled into them to fit the Steelon™ line. Three pulleys were fastened to each of the two steel drive rods.

Lead weights were used to counterbalance the columns in the suspension apparatus so that the load on the Synchron™ motor could be regulated. Counterbalancing of the columns was used to keep the rotational rate constant no matter how many columns were placed on the suspension apparatus. Usually, the columns were counterbalanced so that there was about a 100 gram load in the direction of column movement which made the motor work in a braking mode. The columns were counterbalanced after about every 10 cm or so of column movement to adjust for the buoyancy of the displaced bath fluid.

A 15-inch x 22-inch triple pane window with an R-factor of about 5 was placed in the door of the Delfield refrigerator/freezer to allow the columns to be observed without disturbing the thermal environment (without opening the door).

3.5.3 In-Situ Electrical Conductivity Columns

An in-situ electrical conductivity column was constructed and used to obtain non-destructive measurements of the electrical conductivity profiles at any time. The column is shown in Figure 3.4 and is an altered version of one of the columns described above.

Sintered bronze filters (type F-60) from Pacific Sintered Metals Company (PSM) were used for the conductivity cell sensors. The filters measured 3/8-inch in diameter and were 1/8-inch thick with a particle removal size of 15 to 25 microns.

The filters were glued to the wall of the tenite butyrate tube with a combination of two different epoxies. Devcon 5-minute epoxy was used on the face of the sintered bronze filter to be fastened to the column. Epoxylite #3402 was used on the tenite butylrate tube side. This was done because the Devcon 5-minute epoxy had a much higher viscosity and faster drying time than the Epoxylite #3402 epoxy which minimized the seepage of the epoxy into the

Fig. 3.4: Photograph of column used to measure in-situ electrical conductivity with temperature probe positioned in center of column.

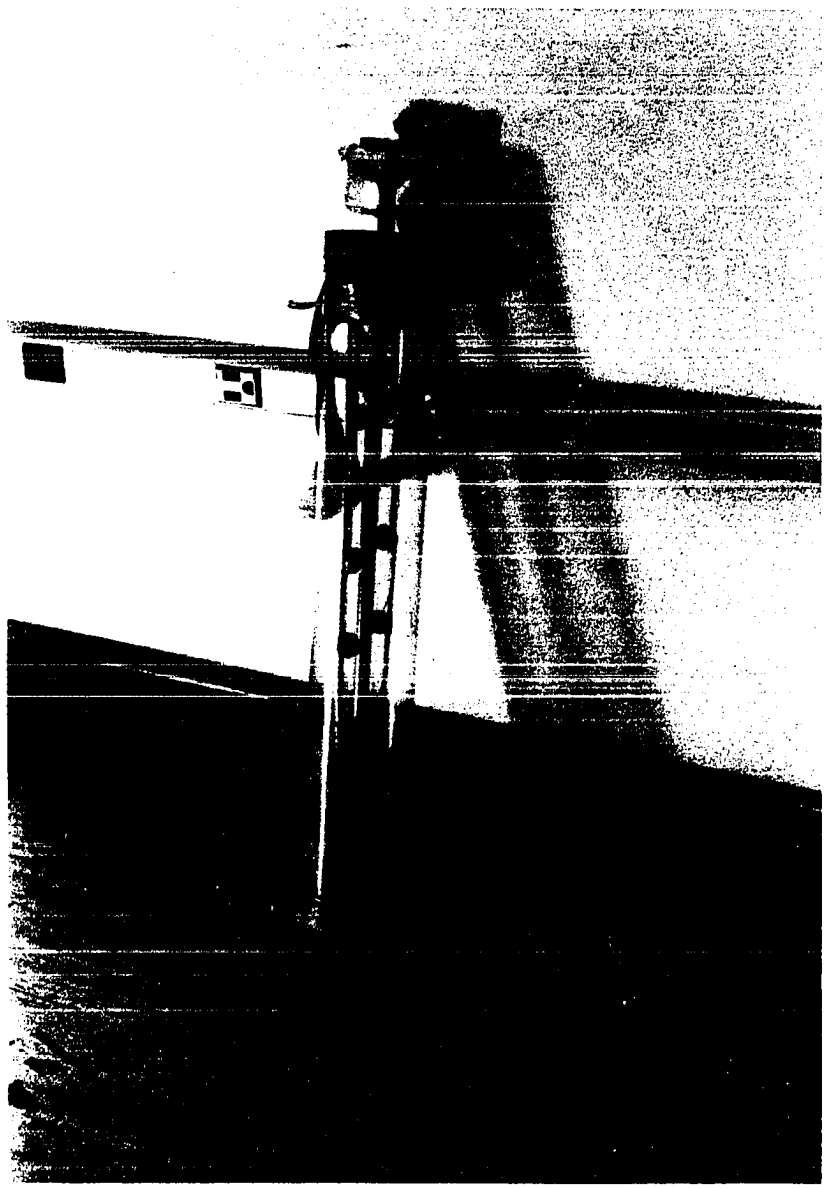

filter pores before it set-up. However, the Epoxylite #3402 epoxy adhered much better to the tenite butyrate than the Devcon 5-minute epoxy and so it was used on the column side. The two epoxies apparently adhered to each other since a good bond resulted.

It is important to note that Devcon 5-minute epoxy is not considered waterproof and may decay when exposed to moisture over a long time period. Some decay was observed in these experiments, but it was not sufficient for any of the bonds or seals to fail.

The sensors were fastened to the column so that two sensors faced each other at a specific depth. Ten complete cells (twenty sensors) were placed at ten different depths in the column.

Multi-stranded flat wire cable was placed down the outer side of the column and fastened to the individual sensors with lead solder through a small 1/16-inch hole that was drilled through the column wall. A drop of Devcon 5-minute epoxy was applied to the solder joint between the flat wire cable and the sensor to insulate it and to aid in the bonding of the flat sensor to the curved column wall. A RS-232 type female connector was connected at the top of the flat wire cable which eventually led to the electrical conductivity measuring equipment.

A temperature probe which will be described later was

also constructed and installed in this column so that both the in-situ electrical conductivity measurements and centerline temperature profiles could be taken on the same column.

A second in-situ electrical conductivity column was constructed specifically to detect the high saline layer that possibly existed ahead of the freezing interface. This column is an altered version of one of the columns shown schematically in Figure 3.1. An effort was made to design the electrical conductivity cells so that the salinity and thickness of this layer could be detected.

Several different designs for conductivity cells were tested. The following requirements were placed on the design of the conductivity cells:

1) The cell must be small enough to detect a layer of different salinity with a thickness of about 1 mm. This was the order of magnitude of the thickness of the interface layer detected in the freezing of NaCl, seawater, and soil solutions as described by Osterkamp (1968), Terwilliger and Dizio (1970), Weeks and Ackley (1982), and Hallet (1978).

2) The cell must be able to detect salinities in the range from the initial 35 ppt to about 85 ppt. This is a rough approximation of the expected range for the salinity of the saline layer.

3) The cell should be able to detect a salinity

difference of about 2 to 3 ppt. The salinity of the soil solution in the layer ahead of the freezing interface may not be much different from that of the bulk soil solution of the thawed layer.

Several cell designs were tested, but only one satisfied the criteria listed above. It consisted of sintered bronze filter material as the conductivity cell plates. These small thin plates were made from PSM (Pacific Sintered Metals Company) sintered bronze filters (type F-60) that were cut with a jewelers saw. The thin plates of sintered bronze filter material were soldered to an electronic circuit board which had a thin layer of copper sheathing on one side. A small cut, about 0.5 mm wide, was made through the sintered bronze filter plate in the middle, but did not go all the way through the circuit board. This cut served as the sensor gap of the conductivity cell. Small copper wires were soldered at each end of the cell and served as leads.

The cell measured 4 mm long by 2 mm wide by about 0.5 mm thick (the dimension along the longitudinal axis of the column). This cell was able to detect a layer with a minimum thickness of about 0.5 mm., a 3 ppt salinity difference, and was good for the salinity range from about 10 to 90 ppt NaCl.

Nine of these cells were constructed. The cells were

installed in the column so that three cells were at each of three different depths. At each level, two cells were on opposite sides of the column and about 1 cm from the wall. The third cell was placed in the center of the column. The cells were strung across the column between two holes which were drilled through the wall of the column. A multi-stranded flat wire cable was placed along the outer side of the column and was soldered to the conductivity cell leads. A drop of Devcon 5-minute epoxy was placed on the solder joint to insulate it and fasten the wire leads to the column. The flat wire cable was attached to a RS-232 female connector which eventually led to the conductivity measuring equipment.

The problem with most of the experimental cell designs that proved unsatisfactory was that a cell constant could not be determined. The electrical conductivity readings during cell constant calibrations were erratic and non-repeatable. This was probably due to the irregular packing of the sand near the cell. Since the cell constant is a reflection of the cell design and geometry, it depends strongly upon the plate spacing and effective plate area of the cell. This means that any changes in the geometry of sand matrix within the cell could effect the electrical conductivity reading.

It should be noted that all electrical conductivity

measurements in this study were made balancing both resistance and capacitance of the conductivity cell. As the frequency of the source voltage increases, capacitance effects become important (Jackson, 1958). Since a 1000 Hz source was used, the capacitance of the cells was balanced.

3.5.4 Temperature Probe

A temperature probe was designed and constructed to measure temperature profiles in the electrical conductivity column and is shown above with the large-celled electrical conductivity column in Figure 3.4. The probe consisted of an acrylic plastic tube with a 3/8-inch O.D. and a 5/16-inch I.D. The probe was approximately 45 cm long so that it reached the full length of the column (42 cm) and extended past the column about 3 cm.

Seventeen YSI thermistors (type 44007) were attached at different positions along a multi-stranded flat wire cable. A RS-232 female connector was attached to the thermistor string at the top of the probe. The wire ends of the thermistors were dipped in Plasti Dip™ to insulate them before they were soldered on to the flat wire cable. The solder joints were also coated with Plasti Dip™ to insulate them.

After the thermistors were attached to the flat wire cable the entire thermistor string assembly was slid into

position within the probe tube. A special plexiglass harness was made to hold the RS-232 connector and fix the position of the thermistors with respect to the probe tube.

A 1/2-inch long by 3/8-inch O.D. copper tubing cap sealed the end of the probe and was made to fit into the pipe fitting at the bottom of the column. This allowed the position of the lower probe end to be fixed every time the probe was installed. A 3/8-inch hole was cut in the center of the top polyethylene end cap to align the top end of the probe.

The probe was filled with Dow Corning 200 Silicone Fluid (5-cs. viscosity) to assure a good thermal contact between the thermistors and the probe wall. It also acted as a good electrical insulator and did not harm the integrity of the Plasti Dip™ or flat cable coating. Sand was eventually placed inside the temperature probe to assure that there was no convection of the silicone fluid within the probe due to temperature gradients.

The thermistors were calibrated simultaneously as a probe unit by a method similar to that described in Section 2.3.3.

3.5.5 Sand Type

Thirty-grit, silica sand manufactured by Granusil™ was used as the soil type. This is a common type of silica sand and is commercially available. The sand was sieved on a Gilson™ automatic sieving machine so that it would pass the 30, but not the 60 sieve size.

The sand was received in a washed form so that the electrical conductivity of the soil solution of the sand when saturated with distilled water was about 0.2 mmhos/cm at 25 °C or about 0.1 ppt (assuming a NaCl electrical conductivity and salinity relation for the soil solution). Additional washing was not considered necessary since the salinity of the soil solution used in the experiments was much higher (35 ppt NaCl) and any error induced by residual sand solutes was considered negligible.

3.5.6 Saline Sand Column Preparation

For each test, the column with the temperature probe and in-situ electrical conductivity cells and five other columns were used. The five columns were cut up for analyses at various times during the test. The small-celled, in-situ electrical conductivity column was only used in a special freeze test and the procedure for its use will be described in Section 3.5.9.

First, the in-situ electrical conductivity column with

temperature probe was prepared. Dry sand was slowly poured into the column. The sides of the column were tapped as the sand was poured in to help pack the sand.

The sand was slowly wetted upwards by connecting a 3/8-inch I.D. Tygon tube from the soil solution source (35 ppt NaCl), located about 1 meter above the column, to the latex tubing at the column bottom. After about 5 minutes, the column had been saturated and the wetting process was complete.

The sand was packed by tapping the column walls. Electrical conductivity readings were periodically made during tapping and would change as additional rearrangement of the soil matrix occurred. After a relatively short period of time the readings would remain unchanged indicating rearrangement of the soil matrix had ceased and tapping was then stopped. The amount of tapping was noted. The depth of the sand was usually about 39 cm.

In the same manner, the other five columns were prepared with the same amount of sand in each column. They were packed by giving them the same amount of tapping as the in-situ electrical conductivity column since the electrical conductivity profiles of these columns could not be taken. The porosity of the soil matrix was determined to be about 39.8 $\pm$ 0.5 percent when using this type of packing method.

3.5.7 Procedure for Downward Freezing

Initially, the columns were placed in the bath so that the sand surface in the column was flush with the bottom of the lid. The columns were allowed to equilibrate for about 24 hours before turning the Synchron™ motor on which marked the start of the test. The tests were stopped after about 30 cm of column movement. Five rates of freezing, similar to those associated with seabed freezing, were conducted: 0.1, 0.2, 0.5, 0.97, and 1.93 cm/day.

The box temperature (cold end of the columns) was kept at approximately -14 °C ± 2 °C. The bath temperature (warm end of the columns) was kept at about -0.6 °C ± 0.1 °C.

3.5.8 Procedure for Upward Freezing

The procedure was similar to that used for downward freezing except that the columns were placed in the bath so that the column bottoms were approximately 2 cm below the lid. The bath was made the cold end with a temperature of about -15 °C ± 0.1 °C and the box became the warm end with a temperature of about 1.0 °C ± 0.5 °C.

After the columns were installed in the starting positions they were allowed to equilibrate for about 24 hours before starting the Synchron™ motor which marked the start of the test. The test was stopped after about 30 cm of column movement. Only one freezing rate of 0.97 cm/day was

used for this study.

3.5.9 Interface Salinity Test

A test was conducted to detect the salinity distribution at the interface. Of particular interest was the highly saline layer that possibly existed ahead of the freezing interface.

The procedure was the same as in the downward freezing tests except the small celled in-situ electrical conductivity column was used instead of one of the regular columns. A freezing rate of 0.97 cm/day was used.

3.5.10 In-Situ Electrical Conductivity Measurements

A flat wire cable connected the RS-232 female connector from the in-situ electrical conductivity column to a switch box located on the outside of the Delfield refrigerator/freezer. In-situ electrical conductivity measurements were taken with a Beckman conductivity bridge type RC-19 connected to the switch box.

The capacitance balancing capability of the bridge was exceeded and additional capacitance boxes were needed. One was a General Radio Type 1419-k decade capacitance box and was rated up to 1 micro farad. A second capacitance box was constructed using non-electrolytic capacitors to provide up to 500 microfarads capacitance.

3.5.11 Calibration of In-Situ Electrical Conductivity Column Cells

Calibration of the cells in the in-situ electrical conductivity column was conducted in the following manner. First, the column was filled with sand and saturated with a NaCl solution. Three different concentrations were used in the calibrations: 3.5 ppt, 35 ppt, and 60 ppt. The electrical conductivity was measured and the electrical conductivity cell constants for each cell at each concentration were determined using the following equation,

$$CC = \frac{C(S,1)}{BR} \tag{3.18}$$

where CC (cm^{-1}) is the cell constant, BR (mmhos) is the bridge reading, and C(S,1) (mmhos/cm) is the electrical conductivity at 1 °C (near the warm end temperature) of the calibration salt solution of salinity S. The electrical conductivity of each calibration salt solution was determined from the electrical conductivity and salinity relation for NaCl discussed in Section 3.5.18.

3.5.12 Temperature Measurement

A flat multi-conductor wire cable connected the temperature probe to the switch box mounted on the outside of the Delfield refrigerator/freezer. The resistances of

the temperature probe thermistors were measured using a HP3465B Multimeter connected to the switch box. This enabled precision resistance measurements to be made allowing a sensitivity of about $\pm$0.005 °C and an accuracy of a few hundredths of a degree or less.

3.5.13 Data Reduction

All temperature and electrical conductivity data were hand recorded and transferred to the University of Alaska VAX 4400 computer system for data reduction.

3.5.14 Sampling

At various times throughout the tests one of the five columns was sectioned on a Craftsman™ bandsaw mounted in a 90 degree rotated position which allowed the columns to be cut up while being held vertically (the same orientation as during the test) so as to not disturb the salt distribution. Wood cutting, 4 teeth/inch skip-tooth blades were used.

The sectioning process usually required approximately 5 minutes to cut the 39 cm long sand columns into about 25 sample segments. The segments were 2 cm long except near the freezing interface where, for about 5 cm above and below the freezing interface, the column was cut up into 1 cm segments.

3.5.15 Sample Preparation

After the columns were segmented, the samples were prepared for gravimetric water content and soil solution electrical conductivity measurements. The method used was the same as that described for the field samples in Section 2.3.5 except that instead of using about 100 grams of sample, the entire segmented sample was used.

3.5.16 Electrical Conductivity Determination

The procedure used for measuring the electrical conductivity (non in-situ) of the soil solutions was the same as that for the field samples and is described in Section 2.3.6.

3.5.17 Calculation of Soil Properties

The methods used for the calculation of the soil properties S_B , S_U, W_B, W_U, and V_U are the same as those described in Section 2.3.9 for the field samples.

3.5.18 Electrical Conductivity and Salinity Relation

The electrical conductivity and salinity relation for NaCl solutions needed to be defined in order to determine the soil solution salinity of the samples. Solutions of NaCl were prepared and their electrical conductivities measured for the salinity range from 0 to about 247 ppt.

Algorithms were developed converting electrical conductivity to salinity (and vice-versa). The procedure and algorithms are given in Baker (1987).

3.5.19 Salinity and Freezing Temperature Relation

Algorithms for the conversion of the freezing temperature, T_F, to the brine salinity, S_b, were developed for sodium chloride solutions for the T_F range of 0 to -20.667 °C (S_b = 0 to 230 ppt) and have the form

$$S_b = a_0 + a_1 T_F + a_2 T_F^2 + ... + a_n T_F^n. \qquad (3.19)$$

Values for the freezing point depression (FPD) and S_b were given by Wolf and Brown (1965). Values for T_F were assumed to be equal to -FPD. Table 3.1 gives the coefficients of the algorithms for the conversion of T_F to S_b.

3.6 Laboratory Results and Discussion

3.6.1 Introduction

Since this study is one of the first of its kind, many questions arose that could not be foreseen. These questions were addressed with the available data and it is felt that the conclusions and implications will be useful, especially in the design of future experiments of salt redistribution during freezing.

In-situ electrical conductivity and thermistor

Table 3.1

Algorithms for the conversion of the freezing temperature, T_F, to the brine salinity, S_b, for NaCl solutions for the T_F range of 0 to -20.667 °C (salinity range from 0 to 230 ppt)

Form: $S_b = a_0 + a_1T_F + a_2T_F^2 + ... + a_nT_F^n$

	T_F Interval, °C (S_b Interval, ppt)	
	0 to -1.79 (0 - 30)	-1.79 to -20.667 (30 - 230)
	Residual Mean Square	
	0.00013	0.00167
	Multiple R-Square	
	1.00000	1.00000
n	a_n	
0	-0.35922089E-01	-0.73124826E+00
1	-0.16830587E+02	-0.17889927E+02
2	0.22433665E+00	-0.41168058E+00
3	0.14280893E+00	-0.32115794E-02
4	----------	0.46955195E-04

resistance measurements were made. Values for S_B, S_U, W_B, W_U, V_U, $\partial S/\partial t$, and temperature were calculated. The distribution coefficient, k, was determined for these tests and was investigated as a method for predicting salt redistribution during freezing. Special freeze tests were conducted to examine salt redistribution during upward freezing and at the freezing interface.

Table 3.2 gives a summary of the laboratory tests including the test name, freezing rates, sampling time from the start of the test, and column number.

3.6.2 Salt Redistribution

Figure 3.5 shows the bulk soil solution salinity, S_B, profile for Freeze Test FT-2. This test was conducted at a downward freeze rate of 0.5 cm/day. These profiles are typical of those for other downward freezing rates and show that:

1) There is a substantial amount of salt redistribution during freezing.

2) The thawed zone, defined as that region below the mechanically ice-bonded interface (IBI), has very smooth S_B profiles. The IBI was detected visually and is shown by the dash-dot lines to the right of the profiles. Values for S_B are nearly constant, but usually increased slightly with depth. This indicates that the salt rejected from the ice

Table 3.2

Summary of laboratory freezing tests

Test Name	Freezing Rate (cm/day)	Sampling Time (days)	Column Number
[1]FT-1	0.97	4.2736	11
		9.1764	12
		14.0757	13
		21.2285	14
		30.1625	15
[1]FT-2	0.50	12.0903	17
		21.1146	18
		32.0903	19
		43.2292	20
		62.1132	21
[1]FT-3	1.93	3.5243	24
		6.5104	25
		9.5069	26
		12.6097	27
		15.5417	28
[1]FT-4	0.20	33.0313	58
		77.0556	57
		128.1944	56
[1]FT-5	0.10	57.4271	60
		133.1111	59
[2]SFT-1	0.97	6.2625	30
		12.2451	31
		16.9986	32
[1]SFT-2	0.97	16.5368	44
		28.0090	45

Notes:

1) The Freeze Tests FT-1 to 5 and Special Freeze Test SFT-2 were conducted with downward freezing.
2) Special Freeze Test SFT-1 was conducted with upward freezing.

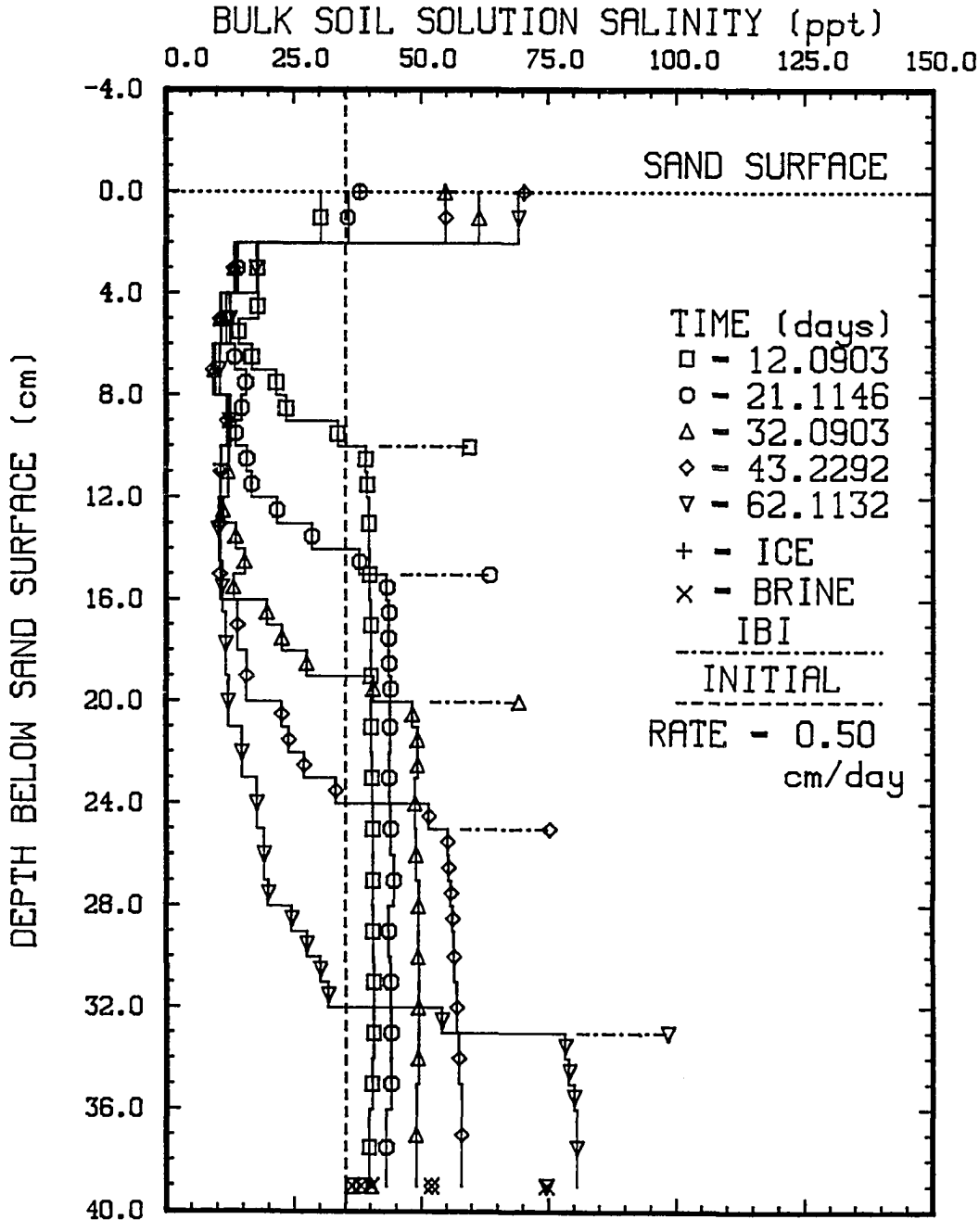

Fig. 3.5: Bulk soil solution salinity vs. depth for test FT-2.

phase and draining from the partially frozen zone has been thoroughly mixed in the thawed layer. Since diffusion alone cannot account for this rapid rate of salt transport and mixing, the profile suggests that there must be some type of convective mechanism responsible.

3) The salinity in the thawed section increases with time as more salt is drained or rejected from the frozen zone to the thawed zone. At all times, the S_B profiles in the thawed region are very similar in that they are relatively smooth and gradually increase in salinity with depth and, consequently, reflect density stable profiles.

4) At the top of the columns, the salinity increases with time to relatively high values. There are several possible explanations for this which include an upward expulsion of the unfrozen soil solution caused by freezing pressures and subsequent sublimation or evaporation occurring at the sand surface. Observations of the latex tubes revealed that they were not expanding as freezing progressed and suggests that the excess soil solution due to ice formation was expelled upward. This was also indicated by a comparison of the calculations for the expected volume of excess solution due to ice formation with that observed at the sand surface.

Ice crystal formation was visible between the top of the sand column and the top lid. The amount of ice that

formed was usually very small, about 5 to 10 grams. This suggests that sublimation and/or evaporation at the top of the columns may have been partially responsible for a concentration of salt there. The bulk salinity of this ice was measured, when present, and is also shown in Figure 3.5 as a singular point. The high salinity of some of these ice samples is just a reflection of the sampling method that was used. Ice crystals were simply scraped off the column surface and lid before sectioning the columns and so inclusion of some of the saline soil solution resting on top of the sand column was unavoidable.

5) The solution in the latex expansion tubes attached to the bottom of the columns was also analyzed for salinity and these values are shown as singular points at a depth of 39 cm in Figure 3.5. The solution salinity in the latex tube was usually less than that of the soil solution immediately above. Salt transport into the latex tube, could have been restricted by the small opening (about 1 cm diameter) of the pipe fitting at the bottom of the column and by a glass wool filter inside the pipe fitting.

6) The IBI was observed to be generally slightly bell shaped and was easily identified during sampling. The bottom of the IBI zone is clearly identified as the top portion of the smooth S_B profiles. Salinities calculated for the zone containing the IBI were averages of the frozen and

thawed parts. This appears as a rapid change in values of S_B for a couple of centimeters above the top of the smooth S_B profiles of the thawed region.

7) Salt banding was not observed or indicated by the S_B profiles on the scale of sectional sampling which was either 1 or 2 cm. If banding was present, it occurred on a much smaller scale than that of the sectional sampling.

8) The smooth S_B profiles suggest that the rejected salt from the partially frozen zone is transported through the thawed zone at velocities of at least the freezing velocity. If this were not so, there would be a substantial build-up of salt just below the IBI which was not observed. This implies salt movement at velocities of at least 2 cm/day (the fastest freezing rate).

The bulk gravimetric water content, W_B, profiles for Freeze Test FT-2 are shown in Figure 3.6. They were generally not significantly changed by freezing. For all the freezing rates, except for 0.1 cm/day, there was a slightly higher water content just above the freezing interface of about 5 to 10 percent greater than the initial content.

Freeze Test FT-5 was conducted at a freeze rate of 0.1 cm/day (the slowest rate used in these studies) and displayed some differences in the W_B profiles. A low moisture content of about 13 percent existed at the top of

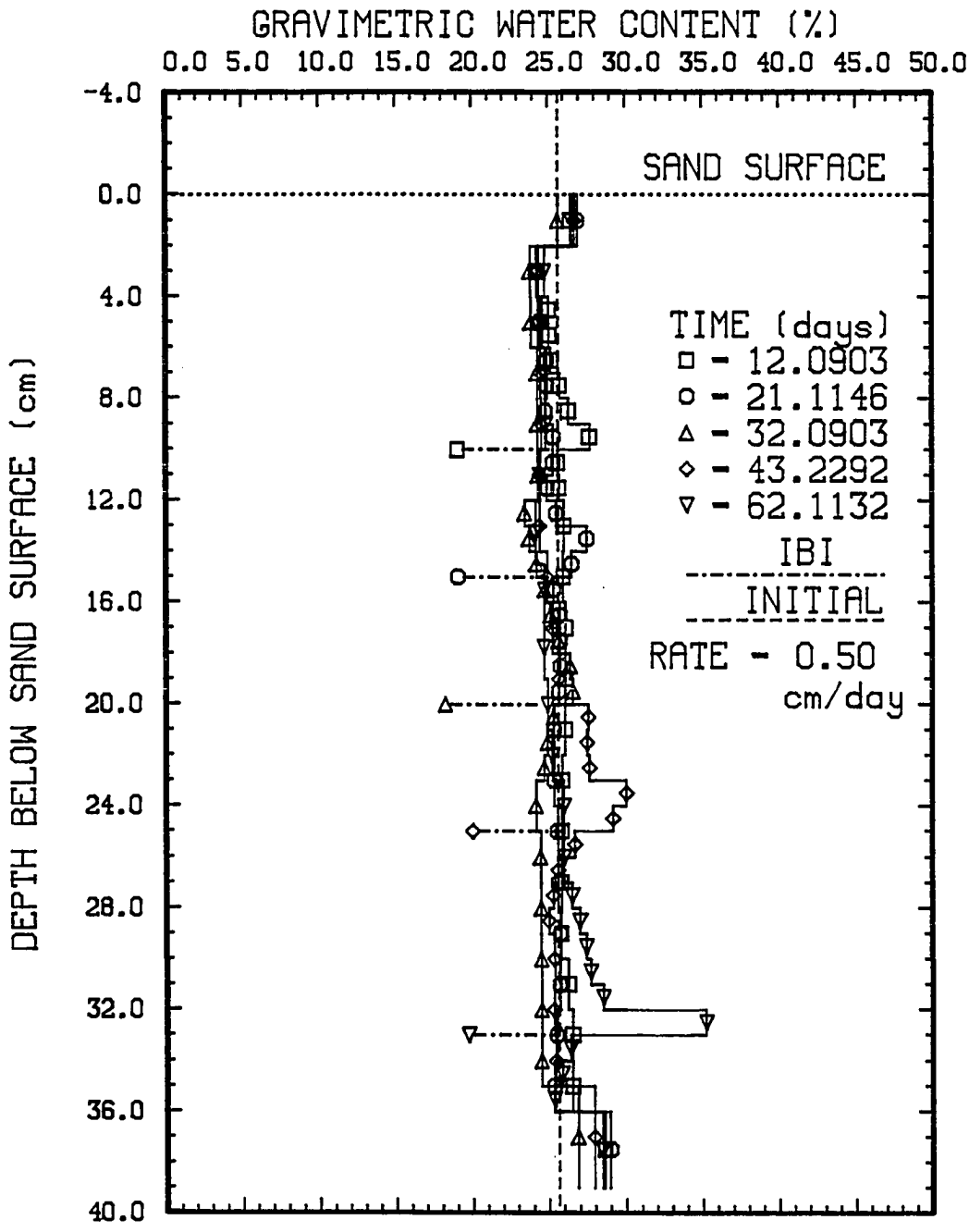

Fig. 3.6: Gravimetric water content vs. depth for test FT-2.

the column. It is believed that sublimation and/or evaporation at the sand surface (during the long testing period of 133 days) may be partially responsible for this. There was also a low moisture content of about 17 percent at the mechanically Ice-Bonded Interface (IBI). The reason for this is not fully understood.

The temperature profiles for Freeze Test FT-2 are shown in Figure 3.7. The most apparent feature on these profiles is that there is a gradual change of the temperature from the box temperature (cold end) to the bath temperature (warm end).

There is a gradual increase in temperature from several centimeters above the IBI (marked at the same locations as on the S_B profiles) to a few centimeters below the IBI. Temperatures in the thawed region become warmer, rapidly, with depth until nearly reaching the bath temperature at about 4 to 5 cm below the IBI. The temperatures near the bottom become slightly colder with increasing depth of the freezing interface (or time). It should be noted that the bottom thermistor is not at the bottom of the column which was at a depth of 39 cm.

Much of the curvature in the temperature profiles near the bath-box interface may have been the result of the bath temperature (about -0.6 °C) being kept warmer than the freezing temperature of the soil solution in the thawed

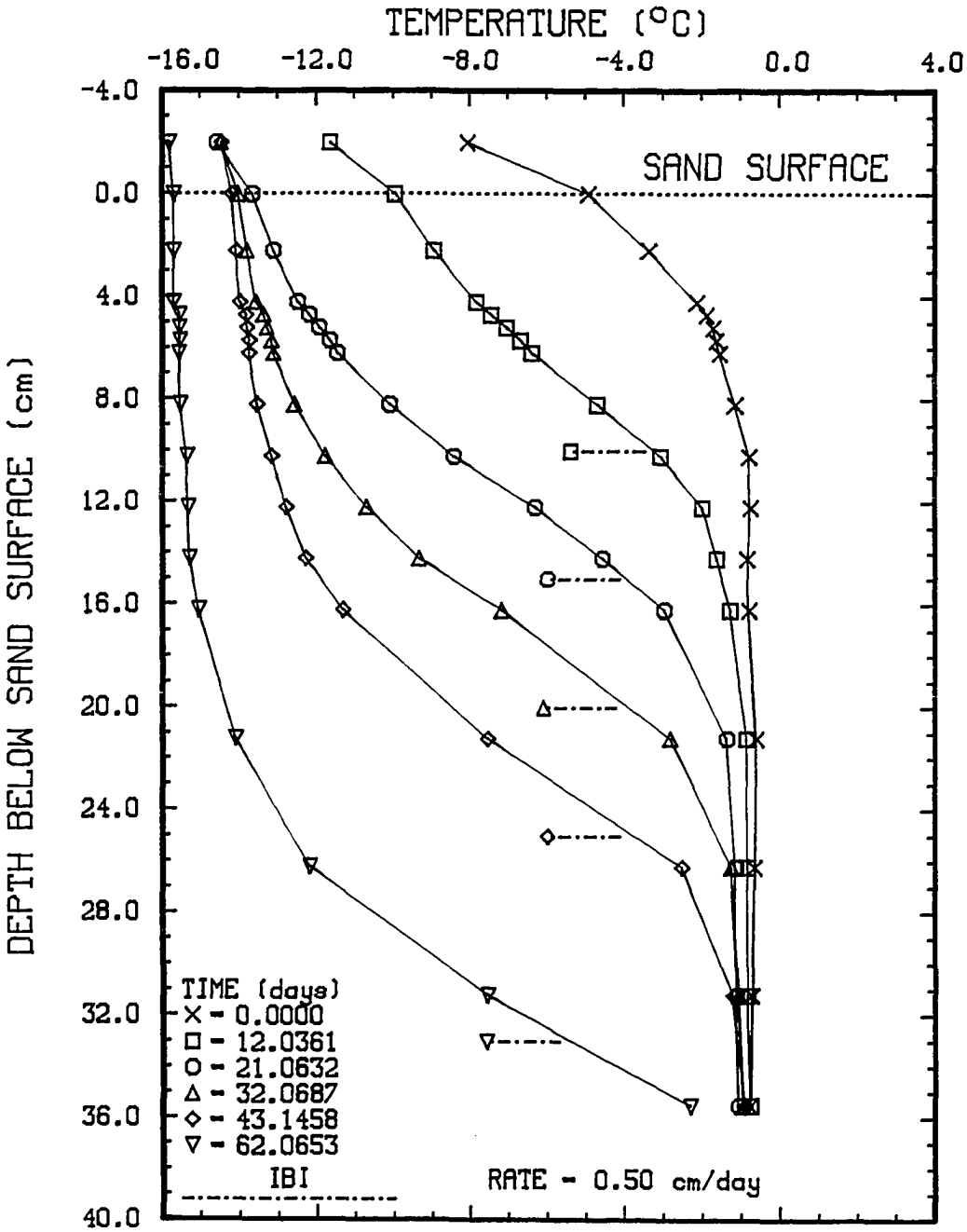

Fig. 3.7: Temperature vs. depth for test FT-2.

zone. This difference was about 1 °C initially and became greater, about 4 °C, at later test times as the soil solution salinity in the thawed zone increased to about 80 ppt (freezing temperature decreased to about -5.08 °C). If the bath temperature had been kept closer to the freezing temperature of the soil solution in the thawed section, the temperature change near the bath-box interface may have been significantly reduced. In addition, some of the curvature may be attributed to latent heat effects as described by Johansen (1977), Wilson (1983), and Osterkamp (personal communication).

Radial, or non-vertical, heat flow near the interface between the box and the bath is indicated by the bell shaped IBI. This may have caused the temperature profiles to have a greater slope near the interface than if all heat flow was vertical.

The temperature at 2 cm above the sand surface was noticeably warmer, at early test times, than the box temperature (kept at about -15 °C). This suggests that the air circulation in the box near the column just above the bath may have been somewhat less than farther away.

Figure 3.8 shows the unfrozen soil solution salinity, S_u, profiles for Freeze Test FT-2. The temperature at the midpoint of each sample was determined by a linear interpolation between the closest upper and lower

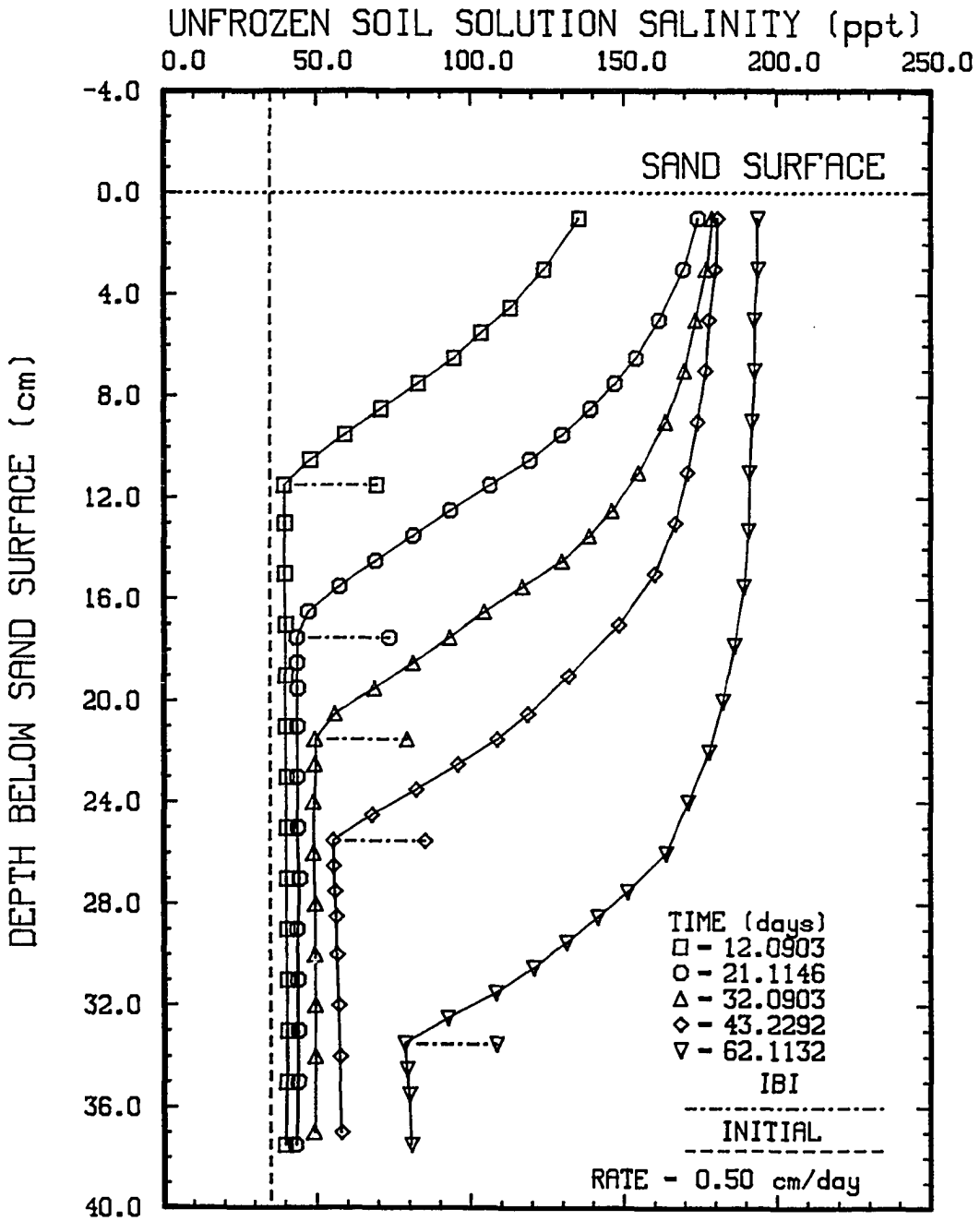

Fig. 3.8: Unfrozen soil solution salinity vs. depth for test FT-2.

thermistors. The method for determining S_U from temperature, W_B, and S_B values is described in Section 3.5.17.

The location of the IBI (the top of the thawed region) was identified by comparing S_B and S_U values. Above the IBI, the column is partially frozen and, so, S_B is less than S_U. Below the IBI, the column is thawed and $S_B = S_U$. The location of the IBI determined in this manner appears at the top of the smooth and nearly vertical portion of the S_U profile. Values of S_U increase almost linearly in the frozen region for about 5 cm to 10 cm above the thawed region and then become nearly constant above this level at later times. In the thawed region, the S_U profiles are the same as the S_B profiles.

The S_U profiles in the zone above the thawed region are density unstable (i.e. the salinity decreases with depth) and suggest that the soil solution may be draining downward due to gravitational forces. This implies that if the column's position were fixed, and given enough time, the denser and more saline soil solution would eventually move downward being replaced by fresher soil solution from below. This would result in additional freezing and eventually the salt concentration should decrease in the partially frozen section.

A test was conducted to study changes in the

temperature and salinity profiles with time with the column's position fixed. The test consisted of freezing the column with the electrical conductivity cells and thermistor probe for about 28 cm at a rate of 0.97 cm/day; the column movement was then stopped and electrical conductivity and temperature measurements were made for a period of about 5 days. The results indicated no detectable change in the electrical conductivity or temperature profiles. This suggests that salt transport occurring within the partially frozen zone due to density gradients in the unfrozen soil solution does not occur or is slower than what could be detected by the measurements for the time period of the test. This was consistent with values determined for the change in salinity with time, $\partial S/\partial t$, discussed in Section 3.6.5 for a constant freezing rate.

It should be noted that the position of the top of the thawed region indicated by the S_u profiles is usually 1 or 2 cm lower than that indicated visually and by the S_B profiles. The cause for this was most likely due to the differences between the columns used for temperature measurement and sampling. The temperatures used to determine the S_u profiles are from the temperature probe column. Temperature distributions within the temperature probe column were probably affected by the presence of the probe and were probably slightly different than for the

sampled columns. However, these effects are believed to be minor and the general nature of the temperature profile is assumed to be nearly the same for both the probe column and for those used for sampling.

Figure 3.9 shows the unfrozen gravimetric water content, W_u, profile for Freeze Test FT-2. The method for determining these profiles is given in Section 3.5.17.

As expected, there was an increase in W_u values near the top because the S_s values were much greater in this region, probably due to upward expulsion of unfrozen soil solution and concentration via sublimation and/or evaporation at the sand surface (discussed above). Consequently, this resulted in greater W_u values.

Both Freeze Test FT-4 (v = 0.2 cm/day) and FT-5 (v = 0.1 cm/day) were run concurrently. Three columns were sampled for test FT-4 and two for test FT-5. The in-situ conductivity column (with temperature probe) was part of test FT-5 and was run with the other two sampling columns at 0.1 cm/day. Therefore, temperature profiles were not obtained for test FT-4 and, consequently, S_u and W_u profiles could not be determined.

3.6.3 Effective Distribution Coefficients

The effective distribution coefficient, k, was determined for the downward freezing saline sand columns. k

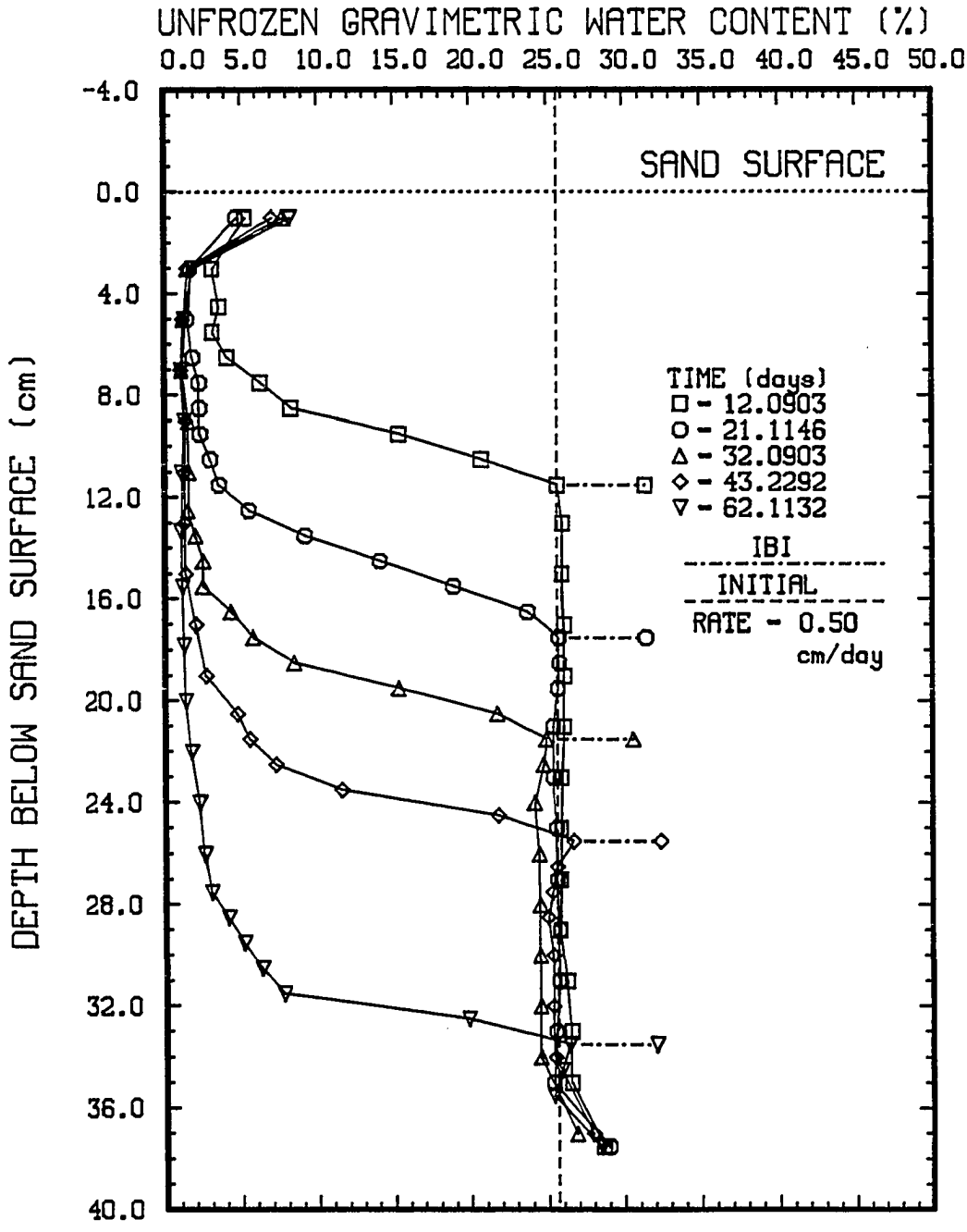

Fig. 3.9: Unfrozen gravimetric water content vs. depth for test FT-2.

is defined as the ratio of the bulk soil solution salinity of the frozen material, S_F, to that of the underlying thawed material, S_T, and is given by

$$k = S_F/S_T. \qquad (3.20)$$

Calculations of the effective distribution coefficients were based on the salinities above and below the interface so as to not include the bell shaped IBI. During sampling, the shape and position of the IBI, which was fairly sharp and easily identified, was recorded. The interface zone appears on the S_B profiles as a zone of rapid change in S_F values for a couple of centimeters above the thawed zone.

Values for S_F are less affected by gravity drainage and unfrozen soil solution expulsion just above the IBI because there has been the minimum time for drainage to occur and the least amount of freezing has transpired. Therefore, to accurately determine k, the value used for S_F was of the freezing zone just above the IBI (about 2 to 3 cm above the thawed region) where unfrozen soil solution expulsion and gravity drainage effects have not had time to significantly change S_F. Using values for S_F at greater distances above the IBI, where additional freezing and time for gravity drainage have occurred, resulted in k values being lower by as much as a factor of two or so. The values used for S_T

were those of the top 1 to 2 cm of the thawed zone. The interface velocity, v, was assumed to be the rate at which the columns were frozen.

Table 3.3 gives a summary of values for k and ln[(1/k)-1] determined for the freezing tests. Table 3.4 gives the average values of k and ln[(1/k) - 1] computed for each freezing rate. Values for k for the first columns to be sampled at the rates 0.1, 0.97, and 1.93 cm/day were not used in computing the average k values or in the linear regression curve fitting of this data. This was done because it was believed that column freezing during the equilibration period prior to the start of the tests had significantly affected salt redistribution. Consequently, the calculated k values for these columns, taken at early sampling times, were not reflective of the actual k values calculated for later times with greater depth of freezing.

Figure 3.10 is a graph of ln[(1/k)-1] versus v. By a method of least squares, a curve fitted to this data gave

$$\ln[(1/k)-1] = 0.6641 - 0.7586\ v \qquad (3.21)$$

where the slope = $-\delta/D = -0.7586$ day/cm (6.5543×10^{4} s/cm) and $k^{*} = 0.34$ (assuming $k^{*} = k$ at $v = 0$). The correlation coefficient and residual mean square were 0.83651 and 0.04747, respectively.

The best fit of the data was achieved with k as a

Table 3.3

Summary of salt redistribution parameters for freezing tests

v (cm/day)	TIME (days)	COL #	S_F (ppt)	S_T (ppt)	$k(S_F/S_T)$	$\ln[(1/k)-1]$
0.10	57.4271	60	18.02	41.11	0.44	0.2485
0.10	133.1111	59	14.80	46.95	0.32	0.7763
0.20	33.0313	58	16.47	39.91	0.41	0.3535
0.20	77.0556	57	16.33	49.10	0.33	0.6964
0.20	128.1944	56	18.50	75.15	0.25	1.1188
0.50	12.0903	17	16.79	39.22	0.43	0.2896
0.50	21.1146	18	21.74	43.37	0.50	-0.0045
0.50	32.0903	19	22.63	48.36	0.47	0.1288
0.50	43.2292	20	27.00	55.27	0.49	0.0463
0.50	62.1132	21	31.72	78.34	0.40	0.3850
0.97	4.2736	11	26.18	35.81	0.73	-1.0001
0.97	9.1764	12	20.37	36.77	0.55	-0.2171
0.97	14.0757	13	23.35	41.22	0.57	-0.2679
0.97	21.2285	14	24.78	47.17	0.53	-0.1015
0.97	30.1625	15	32.74	62.38	0.52	-0.0999
0.97	16.5368	44	24.11	43.46	0.55	-0.2200
0.97	28.0090	45	31.68	58.72	0.54	-0.1581
1.93	3.5243	24	29.61	37.26	0.79	-1.3539
1.93	6.5104	25	25.70	37.44	0.69	-0.7834
1.93	9.5069	26	25.91	39.55	0.65	-0.6410
1.93	12.6097	27	32.65	47.14	0.69	-0.8129
1.93	15.5417	28	34.67	54.29	0.64	-0.5688

Table 3.4

Summary of average salt redistribution parameters for freezing tests

v (cm/day)	AVERAGE k	STANDARD DEVIATION	$\ln[(1/k)-1]$
0.10	0.32	0.00	0.7763
0.20	0.33	0.08	0.7052
0.50	0.46	0.04	0.1690
0.97	0.54	0.02	-0.1771
1.93	0.67	0.03	-0.7015

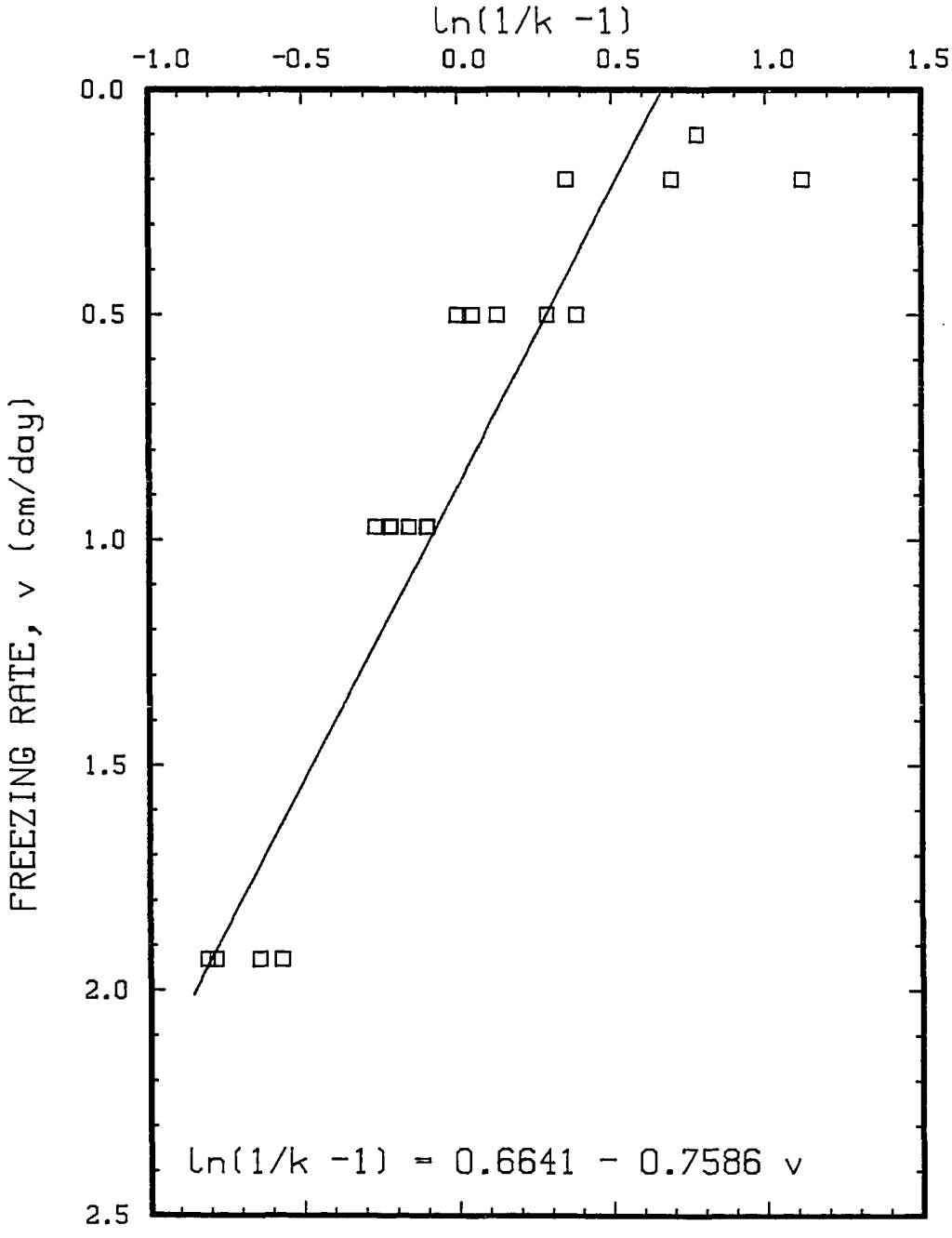

Fig. 3.10: Graph of ln[(1/k)-1] vs. freezing rate where k is the effective distribution coefficient.

linear function of ln(v) as described by

$$k = 0.5593 + 0.1341 \ln(v) \qquad (3.22)$$

The correlation coefficient and residual mean square were 0.88720 and 0.00184, respectively. Figure 3.11 is a graph of k versus v and the fitted curve. This result is similar to that reported by Cox and Weeks (1975). They suggested for low freezing velocities, such as those of this study, that values for k could be predicted better by an equation with the form of Eq. 3.22 than with the BPS equation with the form of Eq. 3.21. This may be partially due to a change in the morphology of the ice/water interface, but may also be a reflection of the mechanism(s) by which rejected salt is being removed from the region of the interface, perhaps by gravity drainage.

The freezing tests indicated the following important results:

1) k is dependent upon the freezing rate as a linear function of ln(v) according to Eq. 3.22.

2) Salt redistribution can be predicted by BPS theory, but not quite as well as by Eq. 3.22 for the freezing velocities studied.

3) Gravity drainage and/or expulsion of the soil solution significantly reduces the salinity of the partially frozen region (S_F values) and, consequently, increases the

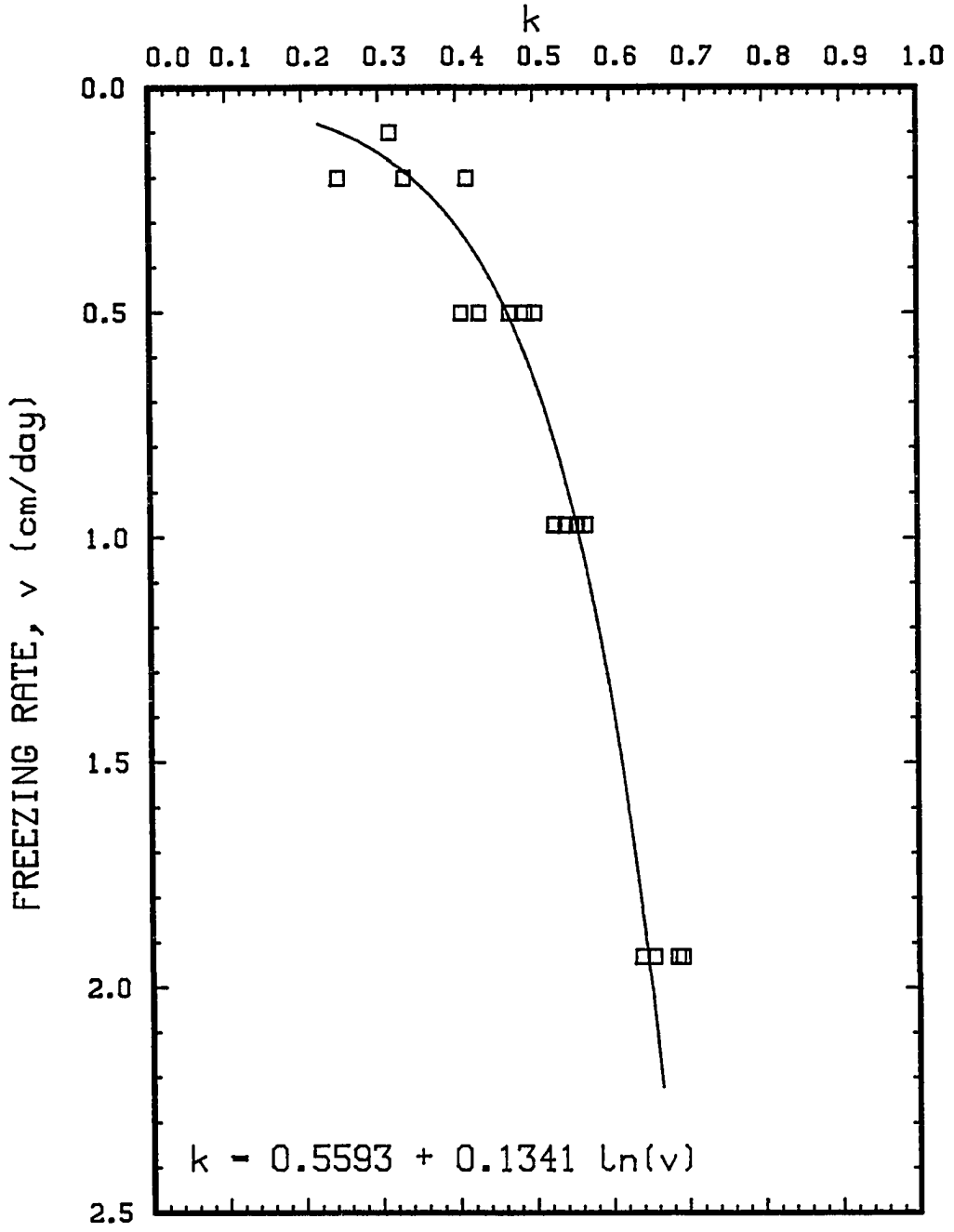

Fig. 3.11: Effective distribution coefficient, k, vs. freezing rate.

salinity of the thawed region (S_T values).

4) Velocities of the rejected salt from the partially frozen zone through the thawed zone are at least 2 cm/day.

3.6.4 In-Situ Electrical Conductivity

The in-situ method for measuring the electrical conductivity of the soil solution allowed electrical conductivity profiles to be made at any time during the test. It is a non-destructive sampling method and enabled a profile to be obtained very rapidly from which a S_m profile was determined.

A comparison was made between the S_m profiles determined from in-situ measurements of electrical conductivity and by the sampling method for Freeze Tests FT-1, FT-2, and FT-3. Table 3.5 gives a summary of the results for Freeze Test FT-2. These data indicate that in-situ electrical conductivity measurements were in reasonable agreement with direct measurements in the thawed regions, but, as expected, not for the partially frozen regions. The S_m values in the thawed region agreed to within about $\pm$ 10 percent of each other for all the measurements and for most measurements the agreement was significantly better. This implies that the effects of the sampling procedure on salt redistribution (in particular, the cutting of the columns) were small.

Table 3.5

Difference in percent between the bulk soil solution salinities determined from in-situ measurements and sampling methods for test FT-2

CELL NO.	DEPTH (cm)	TIME (days) 12.0361	21.0632	32.0687	43.1458	62.0653
		SOIL SOLUTION SALINITY DIFFERENCE (PERCENT)				
1	2.0	-705.9	-1145.2	-1859.1	-1659.7	-2363.8
2	4.0	-738.1	-1343.6	-1559.5	-1528.6	-2127.8
3	6.0	-465.7	-1702.7	-1980.4	-1995.1	-2576.4
4	8.0	-195.5	-740.1	-1080.3	-1283.5	-1742.4
5	12.0	5.0	-363.0	-1115.0	-1751.3	-2526.2
6	16.0	2.7	-2.4	-377.7	-918.2	-1714.9
7	21.1	2.7	4.2	0.5	-419.9	-1118.2
8	25.9	-9.3	1.7	3.2	1.8	-693.4
9	31.0	-5.2	-5.6	6.8	7.5	-29.9
10	35.8	-4.5	1.8	4.4	4.9	8.2

Notes:
1. Depth is given in centimeters below sand surface
2. Time is given in days from beginning of test
3. Freezing rate = 0.50 cm/day.

In the partially frozen region, comparison of S_w values determined by the two methods differ dramatically by as much as a factor of about 24. Apparently, as expected, the cell constants calculated for the thawed region could not be used for the frozen region. Cell constants for the frozen material were not determined and, therefore, accurate S_w values could not be determined from in-situ electrical conductivity measurements.

3.6.5 Expulsion and Gravity Drainage of the Unfrozen Soil Solution

A finite difference numerical model for determining unfrozen soil solution expulsion was applied to the freezing column tests. This model was similar to that described by Cox and Weeks (1975) for determining brine expulsion during the freezing of pure NaCl solutions. For application of this model to freezing saline sands, the following additional assumptions were made:

1) The soil porosity remains constant. There is no rearrangement of the soil matrix during freezing so as to change the porosity.

2) The soil is assumed to be saturated with unfrozen soil solution and/or ice within the pore spaces at all times.

A description of the continuity equations that apply

and the general procedure are given by Cox and Weeks (1975). The method as applied to freezing in soils is outlined in Appendix A. Briefly, given the initial and final temperature profiles and the initial S_B profile of the frozen portion of the column, the final S_B profile can be determined assuming salinity changes are due solely to unfrozen soil solution expulsion. The difference between the actual S_B profile and that calculated with only unfrozen soil solution expulsion occurring is the contribution to S_B changes by gravity drainage of the unfrozen soil solution.

Figure 3.12 shows the measured and predicted (only unfrozen soil solution expulsion occurring) salinity profiles for Freeze Test FT-2. The model was applied using each two adjacent (in time) S_B profiles for a total of four runs at each rate of freezing. Each expulsion profile (dashed line) is located just to the left of the initial S_B profile. This shows that expulsion alone cannot account for the large salinity changes from one profile to the next. If changes in the S_B values were solely caused by expulsion, the expulsion profile would be the same as the final measured S_B profile which is generally the next S_B profile to the left of the initial S_B profile. It is very apparent that salinity changes due to unfrozen soil solution expulsion are quite small in comparison to those associated with unfrozen soil solution drainage. Table 3.6 gives the

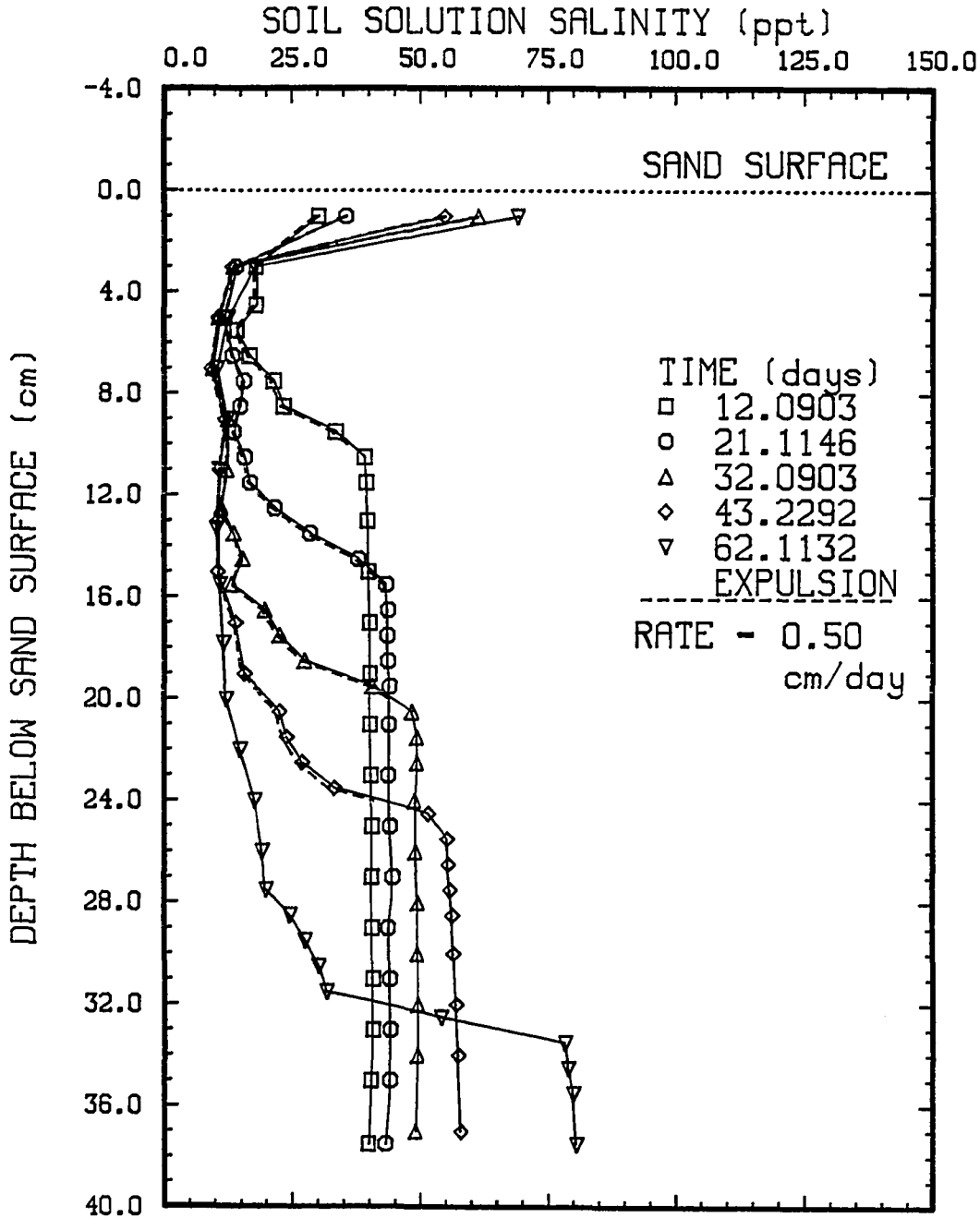

Fig. 3.12: Effect of unfrozen soil solution expulsion on experimental salinity profiles for test FT-2.

Table 3.6

Effect of brine expulsion on experimental salinity profiles for test FT-2 from 32.0903 to 43.2292 days

DEPTH (cm)	INITIAL SALINITY	FINAL SALINITY	PERCENT EXPULSION
1.0	61.51	61.46	0.77
2.0	37.50	37.45	1.40
3.0	13.48	13.46	12.94
4.0	12.10	12.07	17.53
5.0	10.71	10.68	24.51
6.0	10.09	10.05	18.53
7.0	9.46	9.42	15.49
8.0	11.01	10.95	12.82
9.0	12.56	12.48	12.52
10.0	12.39	12.30	9.12
11.0	12.23	12.11	7.81
12.0	11.54	11.40	15.34
13.0	12.46	12.28	9.53
14.0	14.56	14.32	6.01
15.0	14.31	14.03	7.44
16.0	16.47	16.10	8.81
17.0	21.18	20.61	7.86
18.0	25.05	24.40	6.33
19.0	34.12	33.31	4.36
20.0	44.56	43.86	2.89

values for percent of salinity change due to unfrozen soil solution expulsion, $(\Delta S)_m$, defined as (Cox and Weeks, 1975)

$$(\Delta S)_m = \left[\frac{S_c - S_1}{S_2 - S_1}\right] 100 \qquad (3.23)$$

where:

S_c = salinity calculated assuming only expulsion occurring

S_1 = initial salinity

S_2 = final salinity

These values agree very closely with those predicted by Cox and Weeks (1975) for the freezing of pure NaCl solutions. They indicate that salt redistribution in the partially frozen region during downward freezing is not primarily due to unfrozen soil solution expulsion, but to gravity drainage.

Values for the change in salinity with time, $\partial S/\partial t$, between each sampled column were calculated for Freeze Tests FT-1, FT-2, and FT-3. Table 3.7 gives the values for $\partial S/\partial t$, average V_u, and the temperature gradient, $\partial T/\partial z$ for Freeze Test FT-2 between the times 32.0903 days and 43.2292 days. These are typical values calculated between any two consecutive sampling times for the three freeze tests. If gravity drainage is a major mechanism for salt transport, then values for $-\partial S/\partial t$ should increase with increasing permeability. The permeability of the frozen soil was not

Table 3.7

Rate of change of salinity due to gravity drainage for test FT-2 from 32.0903 to 43.2292 days

DEPTH (cm)	∂S/∂t X 10 E6 (ppt/sec)	AVERAGE BRINE VOLUME (ppt)	AVERAGE TEMPERATURE GRADIENT (°C/cm)
1.0	-6.85	276.02	0.08
2.0	-3.50	166.11	0.08
3.0	-0.17	60.82	0.12
4.0	-0.13	55.02	0.16
5.0	-0.09	49.13	0.15
6.0	-0.16	46.42	0.14
7.0	-0.23	43.67	0.18
8.0	-0.41	51.30	0.23
9.0	-0.59	59.21	0.28
10.0	-1.02	58.66	0.32
11.0	-1.45	58.14	0.36
12.0	-0.78	57.81	0.39
13.0	-1.75	62.42	0.48
14.0	-3.92	72.09	0.57
15.0	-3.65	76.17	0.78
16.0	-4.02	96.88	0.81
17.0	-6.92	133.39	0.77
18.0	-9.96	172.95	0.81
19.0	-18.31	260.10	0.81
20.0	-24.48	413.91	0.81

measured and, since the microstructure of the frozen soil system was not known, the permeability could not be determined. However, with increasing V_u values, the permeability should increase and, consequently, so should values for $-\partial S/\partial t$ (note that increasing rates of salt removal indicate increasing $-\partial S/\partial t$ values). Also, salt removal by gravity drainage should increase with an increase in the density gradient in the unfrozen soil solution. Because of the dependency of the unfrozen soil solution salinity and, therefore, density on temperature there should be an increase in values for $-\partial S/\partial t$ with $\partial T/\partial z$.

Figure 3.13 is a graph of $-\partial S/\partial t$ versus V_u and $\partial T/\partial z$ for the test FT-2 for which there were no points where $V_u \geq$ 500 ppt. The negative $-\partial S/\partial t$ values shown were generally a reflection of the increased salt concentration just near the surface of the column and are not considered representative of the partially frozen zone.

As expected, values for $-\partial S/\partial t$ increased with increases in V_u or $\partial T/\partial z$. For test FT-2, values for $-\partial S/\partial t$ appear to increase almost linearly with V_u for $\partial T/\partial z > 0.5$ °C/cm. A least squares curve fit of this data gave

$$\partial S/\partial t = 2.36 - 7.07 \times 10^{-2} V_u \qquad (3.24)$$

where $\partial S/\partial t$ has units of (ppt/s) X 10^6. The residual mean square is 5.57 and the correlation coefficient is 0.92480.

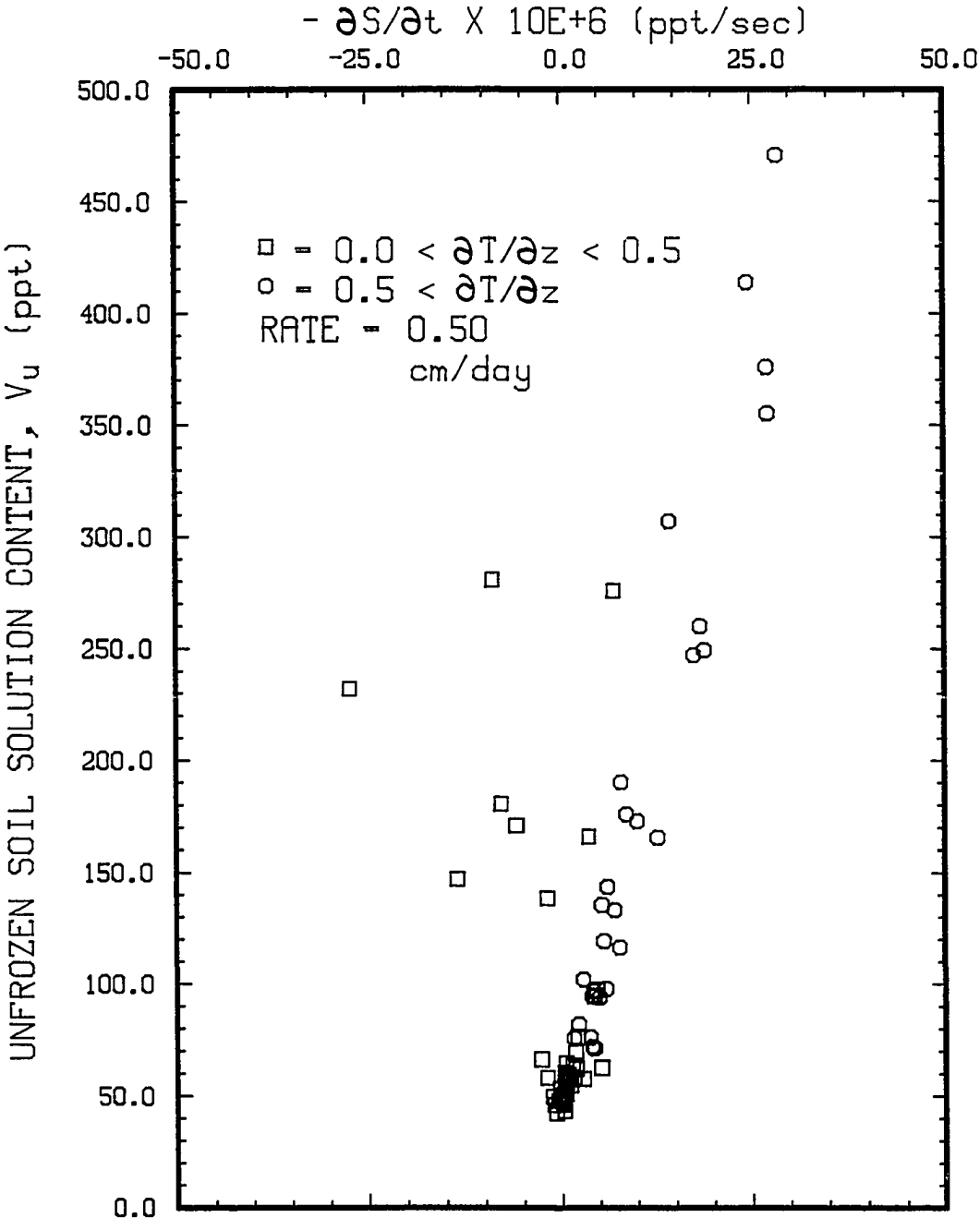

Fig. 3.13: Graph of rate of change of salinity due to gravity drainage vs. unfrozen soil solution content for test FT-2.

The linear dependence between $\partial S/\partial t$ and V_u was not nearly as well defined for tests FT-1, and FT-3, or for any of the tests for $\partial T/\partial z < 0.5$ °C/cm. However, all tests clearly showed increasing values for $-\partial S/\partial t$ with increases in V_u and $\partial T/\partial z$. This result gives support for gravity drainage as being the major mechanism for salt transport.

3.6.6 Special Freeze Tests

Special Freeze Test SFT-1 was conducted to determine salt redistribution during upward freezing. A comparison of these test results with those of downward freezing tests gave information on the effect of gravitational forces on salt redistribution.

Test SFT-1 was run at a freezing rate of 1 cm/day. The run was stopped after about 17 days because of a malfunction of the Delfield refrigerator/freezer. Only 3 of the 5 sampling columns had been analyzed prior to the malfunction.

Figure 3.14 shows the S_s profiles for test SFT-1. They are remarkably smooth and constant at about the initial salinity of 35 ppt throughout the entire column. A comparison of the S_s profiles for the different columns show that they all are very smooth and undisturbed in the thawed region. These very constant S_s profiles indicate that the rejected salt from ice formation remains in place. Salt redistribution due to freezing was not detected.

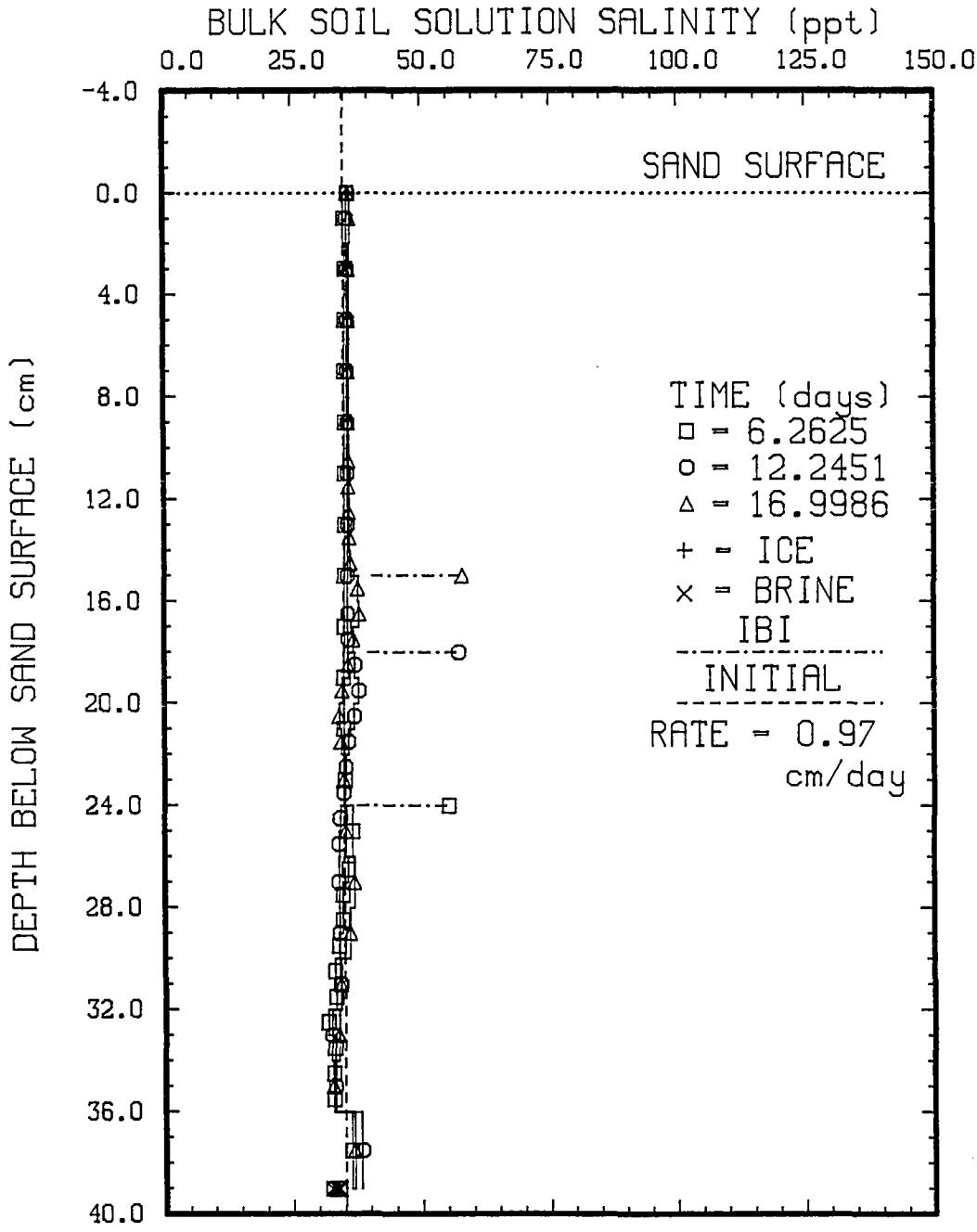

Fig. 3.14: Bulk soil solution salinity vs. depth for test SFT-1.

Although banding was not observed, it may have occurred on a scale smaller than that of the sample interval, which was either 1 or 2 cm.

The bulk gravimetric water content, W_B, profile is shown in Figure 3.15. These profiles are essentially constant at the initial W_B value of about 26.4 percent. There is a slight, but noticeable increase near the bottom of the column. It is believed that this is probably caused by the expansion of the pore space as a result of excess ice formation (possibly ice lenses) during the rapid freezing of the bottom few centimeters during the equilibration period prior to the start of the test.

Figure 3.16 shows the temperature profiles for SFT-1. Figure 3.17 shows the unfrozen soil solution salinity, S_U, and Figure 3.18 shows the W_U profiles for SFT-1. The S_U profiles display very density stable forms.

A comparison of the S_B profiles for downward and upward freezing shows a distinct difference in the extent of salt redistribution. Freezing downward clearly resulted in significant salt redistribution while upward freezing produces no noticeable salt redistribution. This suggests that gravity driven salt transport has a significant effect on salt redistribution for downward freezing.

Special Freeze Test SFT-2 was conducted to determine whether or not a very saline layer existed ahead of the

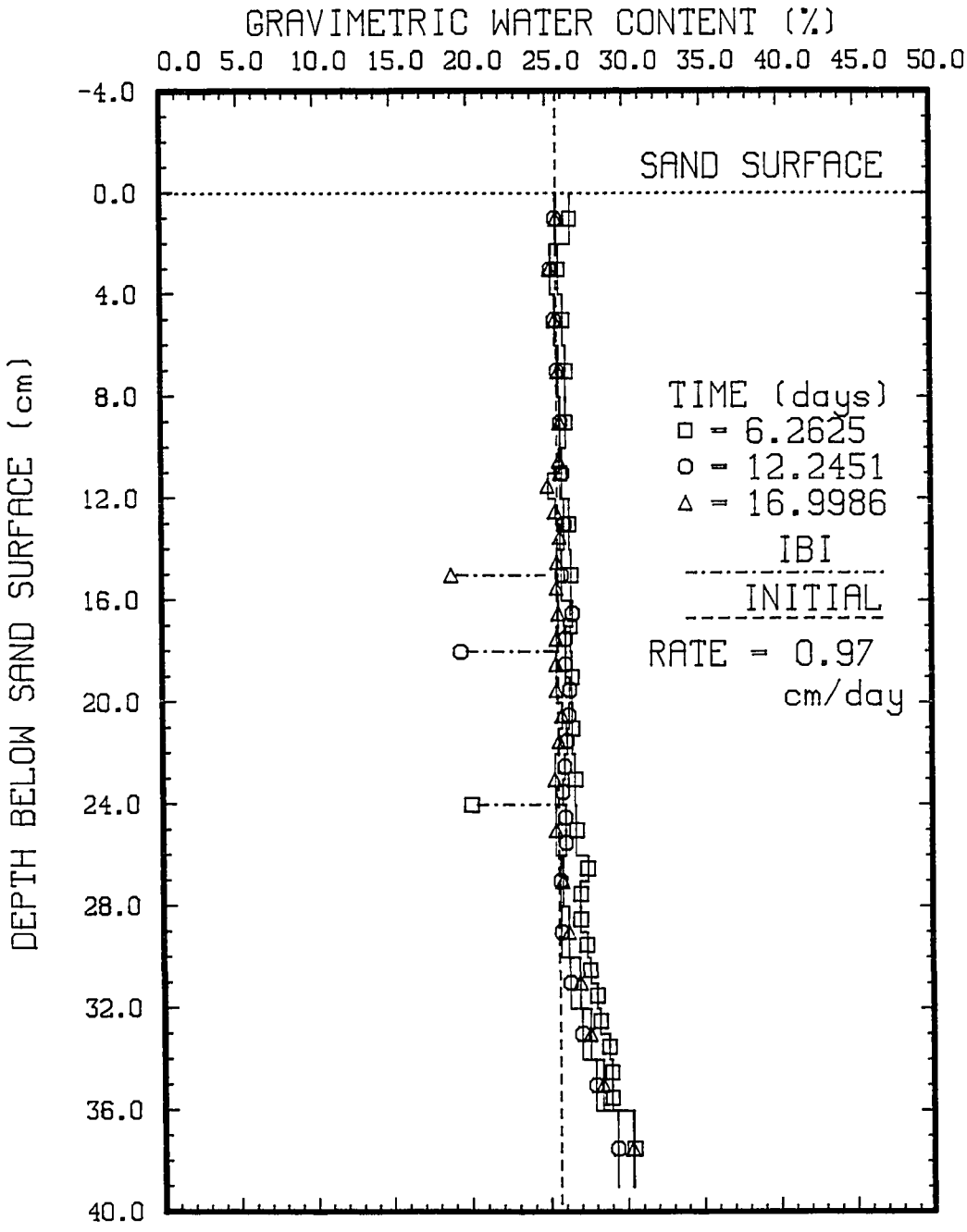

Fig. 3.15: Gravimetric water content vs. depth for test SFT-1.

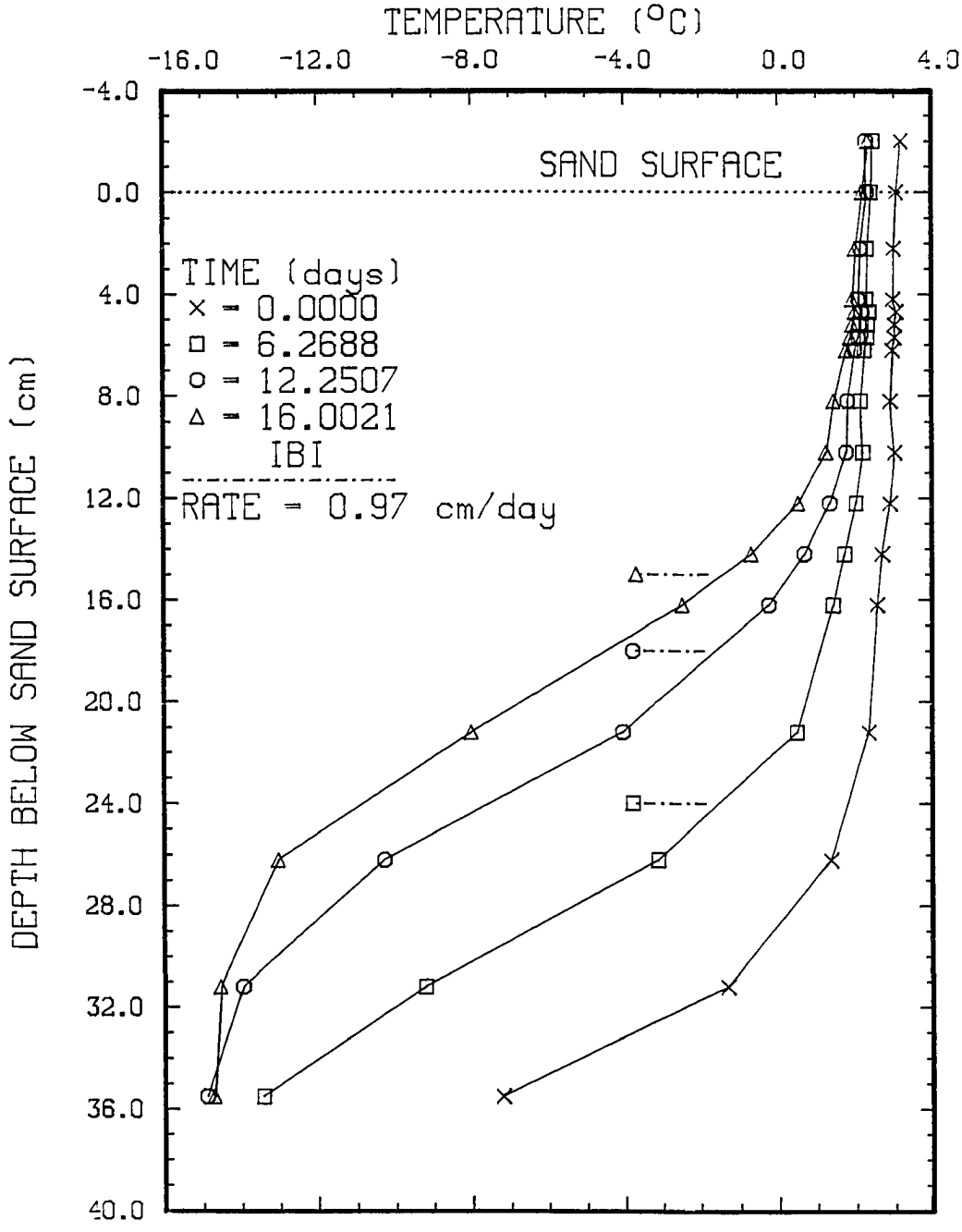

Fig. 3.16: Temperature vs. depth for test SFT-1.

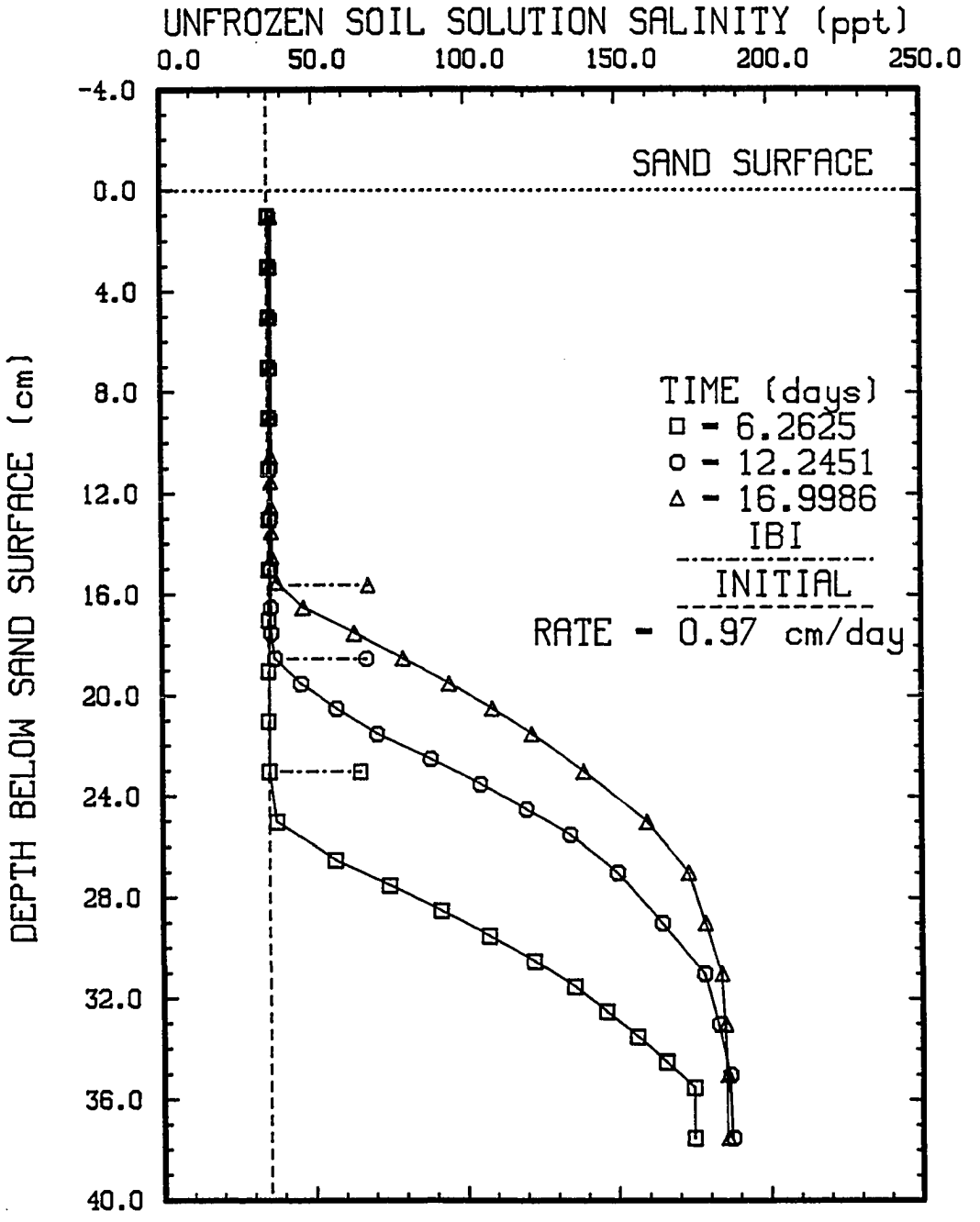

Fig. 3.17: Unfrozen soil solution salinity vs. depth for test SFT-1.

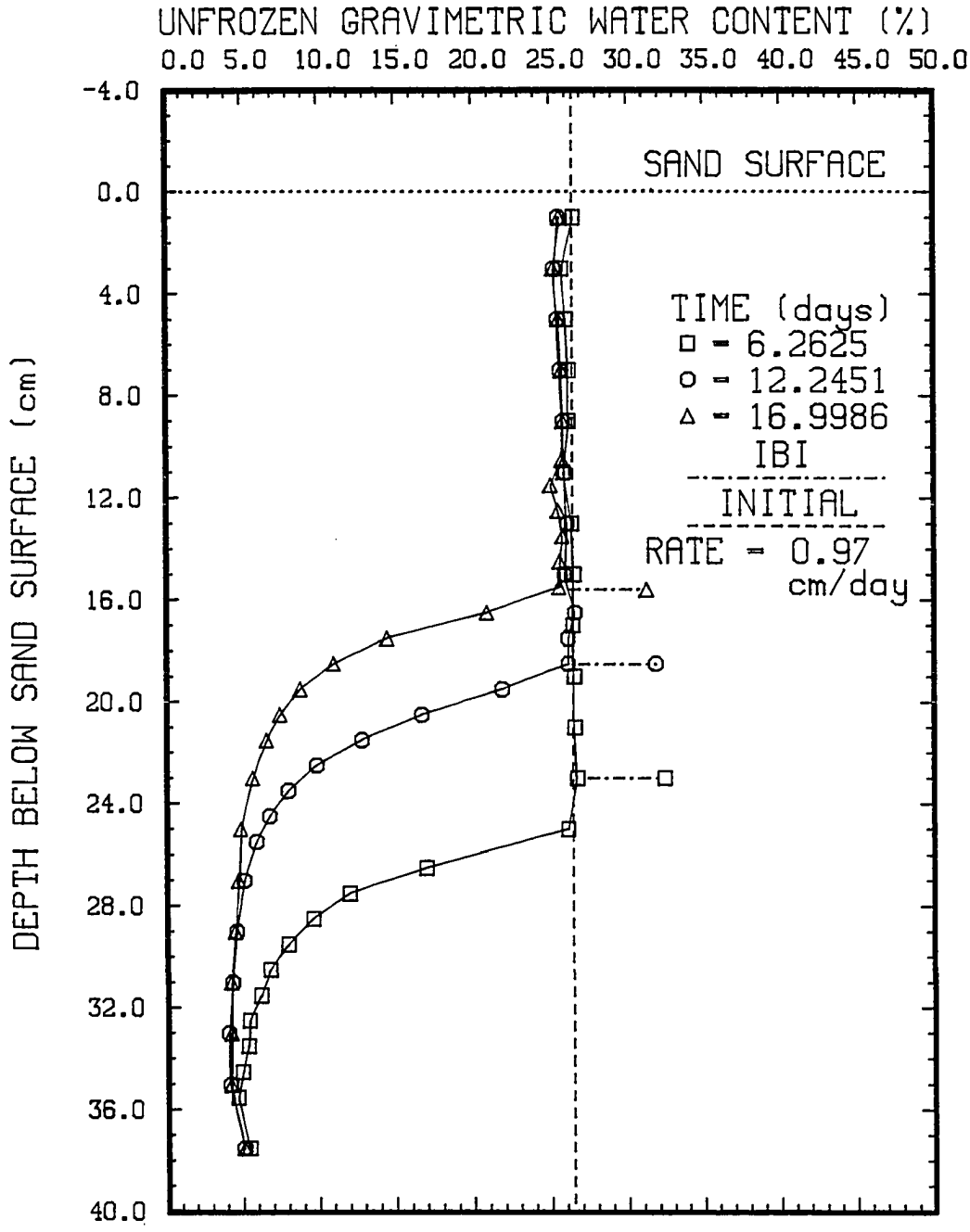

Fig. 3.18: Unfrozen gravimetric water content vs. depth for test SFT-1.

freezing interface during downward freezing. Small electrical conductivity cells designed for this test did not indicate such a layer. It is possible that if such a layer did exist its thickness may be somewhat less than about 0.5 mm and/or the salinity of the layer is not much different from the salinity of the thawed zone next to the freezing interface.

3.7 Conclusions

The conclusions are:

1) Significant salt redistribution occurred during downward freezing of saline sand columns with constant freezing rates which were between about 0.1 and 2 cm/day.

2) The salinity of the partially frozen zone decreases with decreasing freezing rate, v (i.e. greater salt redistribution with decreasing v) for the freezing rates studied.

3) Salt redistribution during freezing can be described by the distribution coefficient, k, as defined in BPS theory according to Eq. 3.21, or somewhat better by a linear function of ln(v), as described by Eq. 3.22, for the freezing rates investigated.

4) Rejected salts during freezing are transported into the thawed region by a convective mechanism. This produced very smooth and density stable S_s profiles.

5) Velocities of the rejected salt from the partially frozen zone through the thaw zone were at least 2 cm/day.

6) The main mechanism for salt transport in the partially frozen region appears to be gravity drainage with expulsion accounting for only a few percent of the total salinity change.

7) If a highly saline layer ahead of the freezing interface exists, it is very thin (< 0.5 mm) or has a salinity that is not significantly different (a few ppt) from the thawed soil solution near the freezing interface.

8) Salt redistribution does not occur during upward freezing on a large scale. Banding could not be detected on the scale of sectional sampling which was 1 cm.

Chapter 4

SALT FINGERING

4.1 Introduction

In a saturated soil, an unstable accelerating interface between two fluids of different density moving vertically develops into long linear fingers (amplitude greater than wavelength) (Saffman and Taylor, 1958). This phenomenon has been termed fingering or linear fingering. Salt fingering in the present context will refer to the formation of these linear fingers in miscible soil solutions containing salt. Fingering is commonly encountered in groundwater movement and petroleum reservoir engineering. In groundwater movement, the fluids are usually miscible, such as saltwater intrusion into coastal aquifers. In reservoir engineering, the fluids are usually immiscible, such as water flooding where water is injected into the oil reservoir (Gupta et al., 1973). However, miscible displacement can occur if solvent is injected. Most studies of fingering have been made with immiscible fluid systems, but fingering between miscible fluids in a porous medium has been investigated by Wooding (1959, 1960, 1969), Heller (1966), and Paterson (1984).

Heat and salt flow in subsea permafrost may involve several different physical settings under which convection can occur, each with its own boundary conditions,

dimensionless numbers, and criterion for stability. The primary driving forces that cause convection are differences in temperature and salinity, which result in density instabilities. Heat and salt flow can be greatly enhanced with the onset of convection (as compared to a diffusive process).

Salt rejection from growing sea ice in shallow water may result in a concentrated brine layer beneath the sea ice (Page and Iskandar, 1978). These salts are thought to infiltrate the sediments (Osterkamp, 1975; Page and Iskandar, 1978). Also, sediment freezing near the seabed may cause salts to be rejected to lower levels in the sediments. The processes by which these salts move through the sediments have not been investigated but would appear to involve convection with density instabilities.

Convection may also occur at the IBPT where melting of the relatively fresh soil ice may cause a fresher, less dense, buoyant soil solution to be released. The density differences between the newly released soil solution and the more dense overlaying soil solution may be enough to cause relatively rapid soil solution movement or convection (Harrison and Osterkamp, 1978).

Gravity-driven convective solute transport processes in subsea permafrost (Osterkamp, 1975; Harrison and Osterkamp, 1978), including a type of large scale salt fingering model

(Swift et al., 1983; Swift and Harrison, 1984), have been previously considered to explain the transport of salt to the IBPT, but have not been consistent with both theory and field observations. It was suggested that an unidentified process may be occurring.

Small scale salt fingering is a gravity driven process not yet considered for salt transport in subsea permafrost. A review of the previous literature on salt fingers in a porous medium is given. Laboratory experiments were performed to investigate salt fingering as a salt transport process in subsea permafrost and the results of these tests are presented and discussed in this chapter.

4.2 Literature Review

A Hele-Shaw cell is a device for investigating two-dimensional flow in porous medium. It is based on the similarity between the differential equations governing saturated flow in a porous medium and those describing the flow of a viscous fluid in the narrow space between two parallel planes (Paterson, 1984). The spacing is analogous to a grain size and in this way the Hele-Shaw cells can simulate a soil with a representative grain size. Wooding (1969) examined linear fingering in Hele-Shaw cells for the miscible system consisting of potassium permanganate solutions and distilled water. The more dense potassium

permanganate solution was placed on top of the distilled water. Vertically moving waves at the unstable horizontal interface developed into fingers. This system is analogous to the saline soil solution overlaying fresher soil solution in the sediments near the seabed along the WDL.

Using the continuity and mass transport equations and Darcy's Law, a characteristic velocity, V_c, for miscible fluids can be written as (Wooding, 1969)

$$V_c = \left[\frac{\rho_s - \rho_w}{2}\right]\left[\frac{k\ g\ \sin(\beta)}{\mu}\right] \qquad (4.1)$$

where:

ρ_s = solution density

ρ_w = water density

k = equivalent cell permeability

μ = dynamic viscosity of water (the change in viscosity due to solute is considered negligible)

g = gravitational acceleration

β = angle from the horizontal.

Fluid motion was observed in different gravitational fields by tilting the Hele-Shaw cell. Therefore, the gravity component in the plane of the cell is g[sin(β)].

It was determined that the mean amplitude (length) of the fingers initially increased as $(\text{time})^2$ which was followed by a transition to a growth rate proportional to time. The mean wavelength (width) increased as $(\text{time})^{1/2}$

and suggests a tendency for adjacent fingers to coalesce by mutual entrainment with time (Elder, 1968). Finger velocities of several cm/hr were observed with density differences between soil solutions of only about 0.004 g/cm^3. The shape of the fingers observed in the experiments of Wooding (1969) with miscible fluids resembled those described by Saffman and Taylor (1958), and Chuoke et al. (1958) for immiscible fluid systems.

Salt fingers were also observed to develop between two miscible fluids of different densities in a vertical tube filled with a porous material (Wooding, 1959). The denser fluid may overlie the less dense fluid and be stable as long as the density gradient, dp/dz, does not anywhere exceed (Wooding, 1959)

$$dp/dz = \frac{3.390\ \mu\ \kappa_s}{g\ k\ b^2} \qquad (4.2)$$

where b is a characteristic horizontal dimension, the radius of the tube, and κ_s is the salt diffusivity through the soil matrix.

In summary, the phenomenon of linear fingering involves the development of long linear fingers between two fluids of different density. It describes a gravity driven convective process that can greatly enhance salt transport. Finger velocities on the order of several cm/hr have been observed between two miscible fluids differing in density by

only about 0.004 g/cm^3 in a simulated porous medium. Fingers have also been observed between two fluids of different density in a vertical tube filled with a porous material when the density gradient exceeds that described by Eq. 4.2.

4.3 Laboratory Methods and Procedures

4.3.1 General

Several columns and boxes were constructed to determine the nature and rate of salt transport in unstable two-layered, saturated sand systems. Two plexiglass boxes were constructed. The larger box had inside dimensions of approximately 17 X 5 X 28 cm and the smaller box had inside dimensions of approximately 19 X 1 X 29 cm. Both boxes had a 1/4-inch wall thickness.

In addition, a segmented plexiglass column was constructed with dimensions of 2 1/2-inches I.D., 2 3/4-inch O.D., and a length of 56 cm. The column was segmented into 14 sections with lengths of 4 cm each. Plexiglass rings with a diameter of 2 3/4-inches I.D., and 3-inch O.D., and about 1/2-inch long were fit tightly over the joints of the column sections. Application of Dow Corning 4 Compound on these rings helped make a water tight seal and also enabled the rings to slide downwards for cross-sectional viewing of the segments and sampling.

A special harness was constructed to enable the column to be hung vertically and also acted as a clamp to ensure that the segments remained together during the test.

4.3.2 Salt Fingering Tests

Silica sand was used as the porous medium in all fingering tests and was the same as that used in the freezing experiments described in Section 3.5.5.

Two different tests were performed with the larger box. In the first test, the bottom of the box was filled with about 10 cm of sand saturated with 35 ppt NaCl solution colored with Indigo Rhodamine dye. The sand was packed by tapping on the sides of the box and vibrating on the bottom with a Craftsman™ orbital sander for a short period of time (about 10 seconds). The excess dyed solution was removed with a hand vacuum pump so that the dyed sand was not oversaturated.

The remaining space in the box was then filled with dry silica sand and saturated by slowly pouring distilled water from the top. This was done in a manner so that there was a smooth interface at the fresh and saline soil solution boundary.

A layer of 3/8-inch thick closed cell foam was placed on top of the sand. A water tight lid was bolted on top of the box and compressed the foam slightly so that there was

no free air trapped in the box.

The box was allowed to equilibrate overnight for about 12 hours. The box was then quickly rotated 180° so that the sand, saturated with salt solution, overlaid the sand saturated with distilled water. This marked the start of the test. The development and movement of the salt fingers were recorded by manual measurements with a ruler, watch, and photographs.

A second test was performed by filling the bottom of the box with about 10 cm of sand saturated with dyed distilled water which was then placed in a freezer overnight and frozen. The top of the frozen sand surface was slightly convex, upward in the middle, due to the volumetric expansion during freezing. This top surface was leveled using a heat gun and the box was replaced in the freezer for about one hour to refreeze the very top layer melted by the heating. The box was then placed in a Forma Scientific temperature controlled bath kept at about -2.0 °C so that about the bottom 4 centimeters of the box (dyed and frozen end) was submerged in the bath. The top portion of the box was exposed to the room temperature.

The box was filled with sand and saturated with 35 ppt NaCl solution by slowly pouring the solution on top of the sand. This marked the start of the test. The development and movement of the fingers (freshwater) were recorded as

before. All fingering tests were terminated when the fingers extended the full length of the box. An experiment similar to the first described for the large box was also performed using the small box to test for scale effects.

The segmented column was used in one experiment and was prepared using a procedure similar to that explained above for the large box tests. The column was filled with about 15 cm of sand saturated with a dyed 35 ppt NaCl solution. After settling, all excess salt solution was removed. The column was then filled with dry sand, saturated with distilled water, sealed, and placed in the suspending harness. After the column was harnessed, it was placed in the Delfield box and allowed to equilibrate for about 12 hours at +1.0 °C. The column was then quickly rotated so that the dyed saline sand overlaid the sand saturated with distilled water. This marked the start of the test. Salt finger movement was recorded as before. When the fingers had extended the full length of the column, the test was stopped and the column was segmented. Photographs were taken of the cross-section of each segment which allowed a three dimensional description of the fingers to be made. The individual segments were analyzed for gravimetric moisture content, and salinity of the soil solution.

Two additional tests for determining the salt movements by salt fingers were conducted in the two in-situ electrical

conductivity columns used in the freezing column tests. The first test involved the filling of both columns to a depth of about 31 cm with sand. This layer was saturated by wetting with 35 ppt NaCl solution through the bottom latex access tube. The columns were then placed in the Delfield box set at about +1.0 °C and allowed to equilibrate for about 12 hours. The columns were filled an additional 7 cm with sand and saturated by slowly pouring a dyed 70 ppt NaCl solution on top of the sand surface so that a flat interface existed between the fresh and saline layers. This marked the start of the test.

In-situ electrical conductivity measurements were made on both columns to determine the salt movement. Temperature profiles were also obtained on the column with large conductivity cells. Photographs were taken to describe the geometry of the convection fingers and to monitor their movement.

For the second test, the columns were filled with about 10 cm of dry sand and then saturated with dyed distilled water. The columns were then placed in the Delfield box so that the portion containing the dyed sand was submerged in the Delfield bath which was kept at about -5.0 °C. The remaining portion of the column was exposed to the temperature in the Delfield box which was kept at about +1.0 °C. The bottom portion was allowed to freeze overnight.

The column was then filled with sand (about 28 cm more) and saturated with 35 ppt NaCl solution and raised so that only the bottom 3 cm of the column was exposed to the -5.0 °C temperature of the Delfield bath. This marked the start of the test. In-situ electrical conductivity and temperature measurements were made as before.

4.4 Results and Discussion

Table 4.1 gives a summary of the salt fingering experiments. Box Test BT-2 was conducted with 35 ppt dyed NaCl solution over distilled water as the soil solutions in the large box. Box Test BT-3 was the same, but was conducted in the small box. Box Test BT-4 was conducted with 35 ppt NaCl solution over frozen dyed distilled water as the soil solutions in the large box.

Tables 4.2, 4.3, and 4.4 give a summary of values for time, t, since the start of the test, the parameter, V_{ct}, finger amplitude, A, and average vertical finger growth rate, v_A, for tests BT-2, BT-3, and BT-4, respectively. The horizontal finger width at the initial interface between the two solutions was defined as finger wavelength and the finger amplitude was the vertical finger length from the interface. Average finger growth rates were observed to be as high as about 3 cm/hr in tests BT-2 and BT-3. In test BT-4, finger growth rates at a thawing, fresh-ice boundary

Table 4.1

Summary of salt fingering tests

Test Name	Description
[1]BT-2	Conducted in large box with 35 ppt dyed NaCl solution overlaying distilled water.
[1]BT-3	Conducted in small box with 35 ppt dyed NaCl solution overlaying distilled water.
[1]BT-4	Conducted in large box with 35 ppt NaCl solution overlaying frozen dyed distilled water.
[2]SCT-1	Conducted in both in-situ electrical conductivity measuring columns with 70 ppt dyed NaCl solution overlaying 35 ppt NaCl solution.
[2]SCT-2	Conducted in both in-situ electrical conductivity measuring columns with 35 ppt NaCl solution overlaying frozen dyed distilled water.
[2]SCT-3	Conducted in segmented column with 35 ppt dyed NaCl solution overlaying distilled water.

Notes:

1. BT = Box Test
2. SCT = Special Column Test

Table 4.2

Values for time (from start of test), the parameter, $V_c t$, finger amplitude, and average finger growth rate for test BT-2

TIME (t) (hrs)	$V_c t$ (cm) (1)	FINGER AMPLITUDE (cm)	AVERAGE FINGER GROWTH RATE (cm/hr)
1.133	5.19	0.50	0.44
1.483	6.80	1.50	2.86
1.783	8.17	2.40	3.00
2.200	10.08	3.50	2.64
3.150	14.43	5.00	1.58
4.333	19.86	8.20	2.70
5.767	26.42	10.50	1.60
6.333	29.02	11.70	2.12
7.550	34.60	13.70	1.64
10.983	50.32	15.20	0.44

Notes:
1. V_c = 4.582 cm/hr

Table 4.3

Values for time (from start of test), the parameter, $V_c t$, finger amplitude, and average finger growth rate for test BT-3

TIME (t) (hrs)	$V_c t$ (cm) (1)	FINGER AMPLITUDE (cm)	AVERAGE FINGER GROWTH RATE (cm/hr)
0.450	2.06	0.50	1.11
0.900	4.12	1.70	2.67
1.100	5.04	2.20	2.50
1.517	6.95	3.40	2.88
2.750	12.60	5.70	1.86
3.933	18.02	8.00	1.94
4.967	22.78	9.50	1.45
6.117	28.03	11.10	1.39

Notes:
1. V_c = 4.582 cm/hr

Table 4.4

Values for time (from start of test), the parameter, $V_c t$, finger amplitude, and average finger growth rate for test BT-4

TIME (t) (hrs)	$V_c t$ (cm) (1)	FINGER AMPLITUDE (cm)	AVERAGE FINGER GROWTH RATE (cm/hr)
0.333	1.53	0.70	2.10
0.833	3.82	3.50	5.60
1.583	7.25	4.50	1.33
3.983	18.25	6.50	0.83
6.050	27.72	7.00	0.24

Notes:
1. V_c = 4.582 cm/hr

were observed to be as high as about 5.6 cm/hr.

Figure 4.1 shows a graph of the mean finger amplitude versus the parameter $V_{ct}t$ for the box tests. Figure 4.2 shows a graph of finger wavelength, L, versus time, t. For BT-2, A initially increased proportionally to $t^{2.94}$ followed by a transition period to an amplitude proportional to $t^{0.98}$. The wavelength was proportional to $t^{0.99}$. The results of these box tests were similar to those of Wooding, (1969).

For BT-3, A initially increased proportionally with $t^{1.59}$ followed by a transition period where A was proportional to $t^{0.86}$. The wavelength was proportional to $t^{0.6}$ and developed at a slightly lower growth rate than observed for test BT-2 which was conducted in the large box. This suggests that the narrower wall spacing in test BT-3 may have restricted wavelength development while not significantly affecting the finger growth rate. Photographs of the initial and final finger development for test BT-3 are shown in Figures 4.3 and 4.4, respectively.

Box test BT-4 displayed a noticeably different behavior in final finger growth from that in test BT-2 or BT-3. Initially, A increased proportionally to $t^{1.76}$ similar to test BT-2 and BT-3, but was followed by a transition to where A was proportional to $t^{0.36}$. The wavelength was proportional to $t^{0.95}$ which was similar to

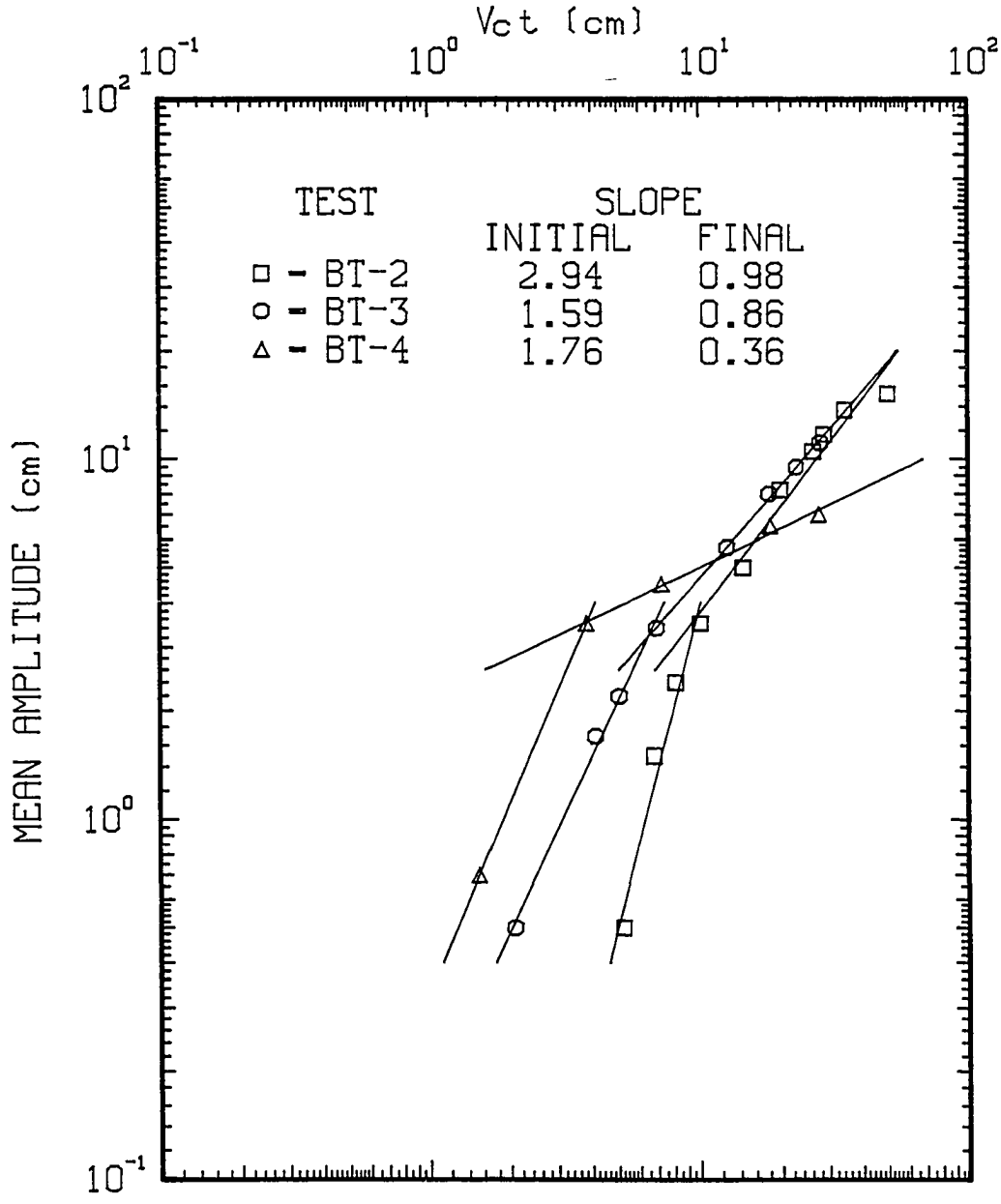

Fig. 4.1: Amplitude, A, vs. the parameter, V_{ct}, for the salt fingering tests performed in boxes.

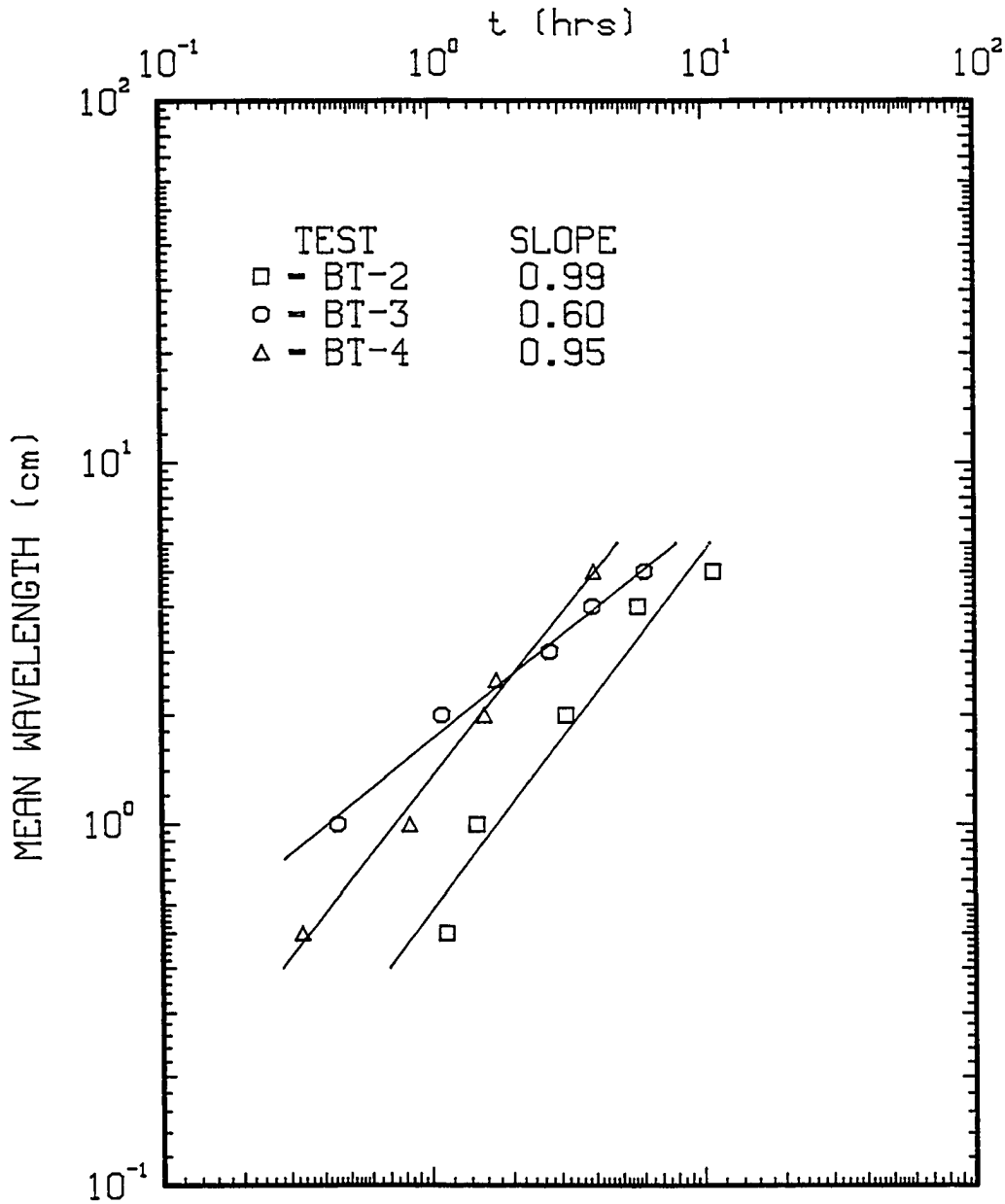

Fig. 4.2: Wavelength, L, vs. time, t, for the salt fingering tests performed in boxes.

Fig. 4.3: Photograph of initial salt finger development for test BT-3 after 1 hour 6 minutes.

Fig. 4.4: Photograph of final salt finger development for test BT-3 after 22 hours 53 minutes.

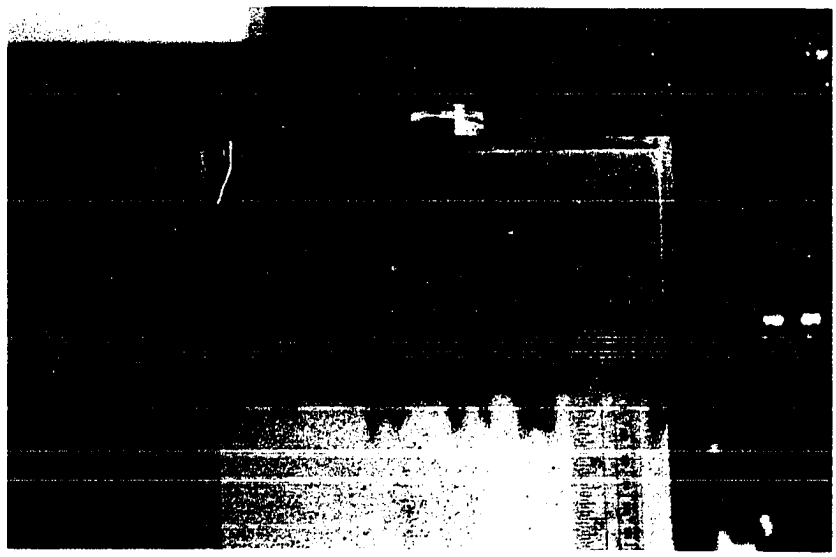

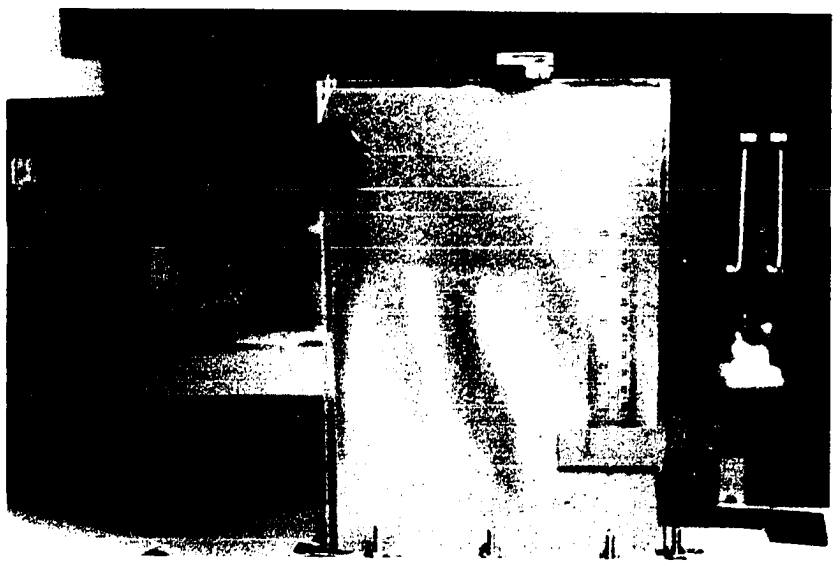

test BT-2 and BT-3. Photographs of initial and final finger development for test BT-4 are shown in Figures 4.5 and 4.6, respectively.

The fingering behavior of test BT-4 appears to be dependent upon the rate at which the frozen soil solution thaws and becomes mobile. The key point shown by this test is that thawing at the frozen boundary released fresher more buoyant soil solution that moved rapidly upward through the soil matrix in the form of fingers.

Salinity profiles with time for Special Column Tests SCT-1 and SCT-2 are shown in Figures 4.7 and 4.8, respectively. These data were obtained from in-situ electrical conductivity measurements made on the large celled conductivity column. Test SCT-1 had dyed 70 ppt NaCl soil solution overlaying 35 ppt NaCl soil solution. Test SCT-2 had 35 ppt NaCl soil solution overlaying frozen, dyed, distilled water soil solution. The initial salinity profiles are indicated on the graphs by dashed lines. The low initial salinity values for the top saline region are probably a reflection of the method used for column preparation. After the sand and dyed 70 ppt NaCl solution were added, minimal packing of the sand by tapping of the column sides was done to avoid disturbing the smooth interface between the 35 and 70 ppt NaCl soil solutions. This probably resulted in poor packing around the electrical

Fig. 4.5: Photograph of initial finger (freshwater) development for test BT-4 after 33 minutes.

Fig. 4.6: Photograph of final finger (freshwater) development for test BT-4 after 22 hours 33 minutes.

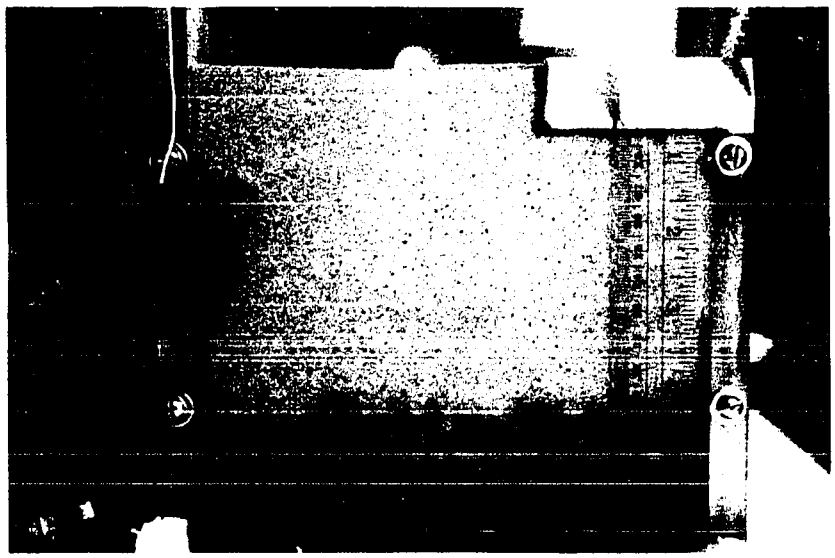

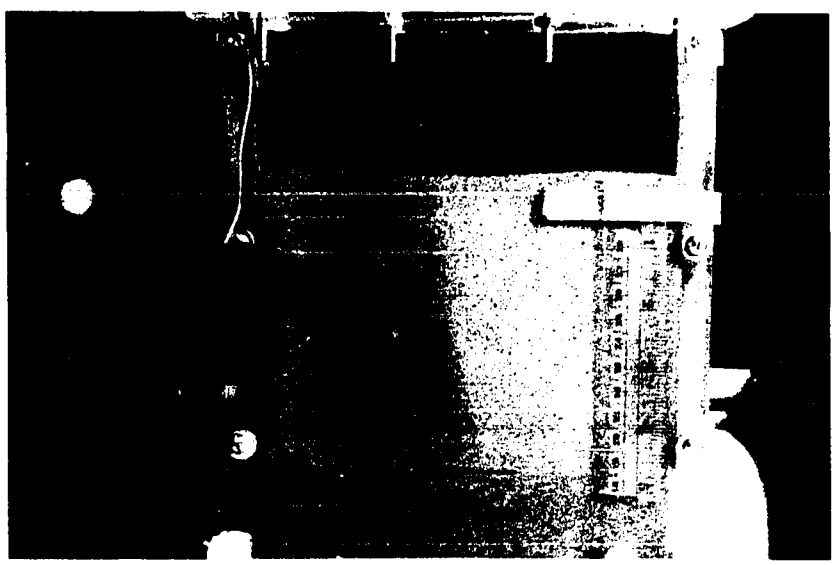

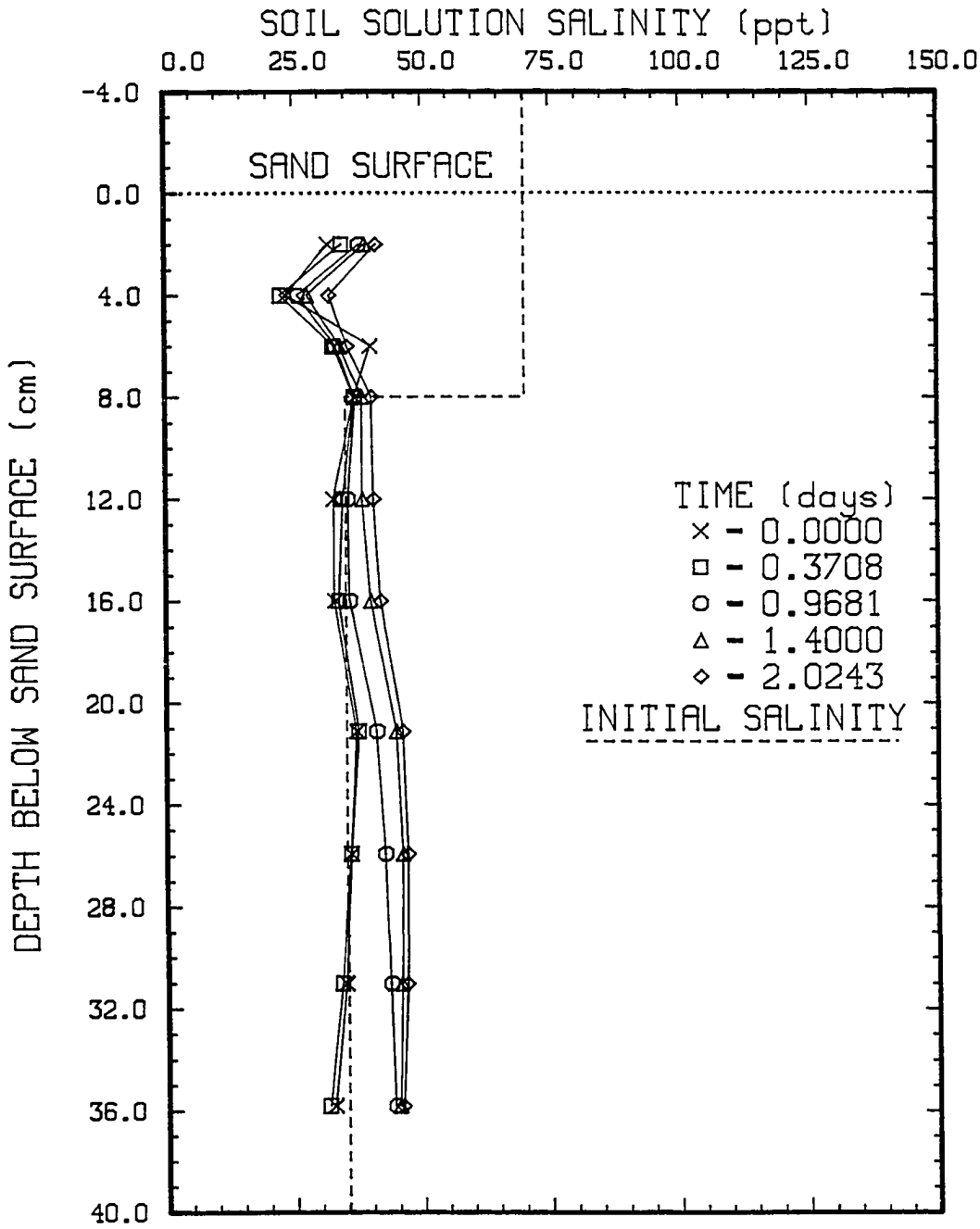

Fig. 4.7: Soil solution salinity profiles for test SCT-1 determined from in-situ electrical conductivity measurements.

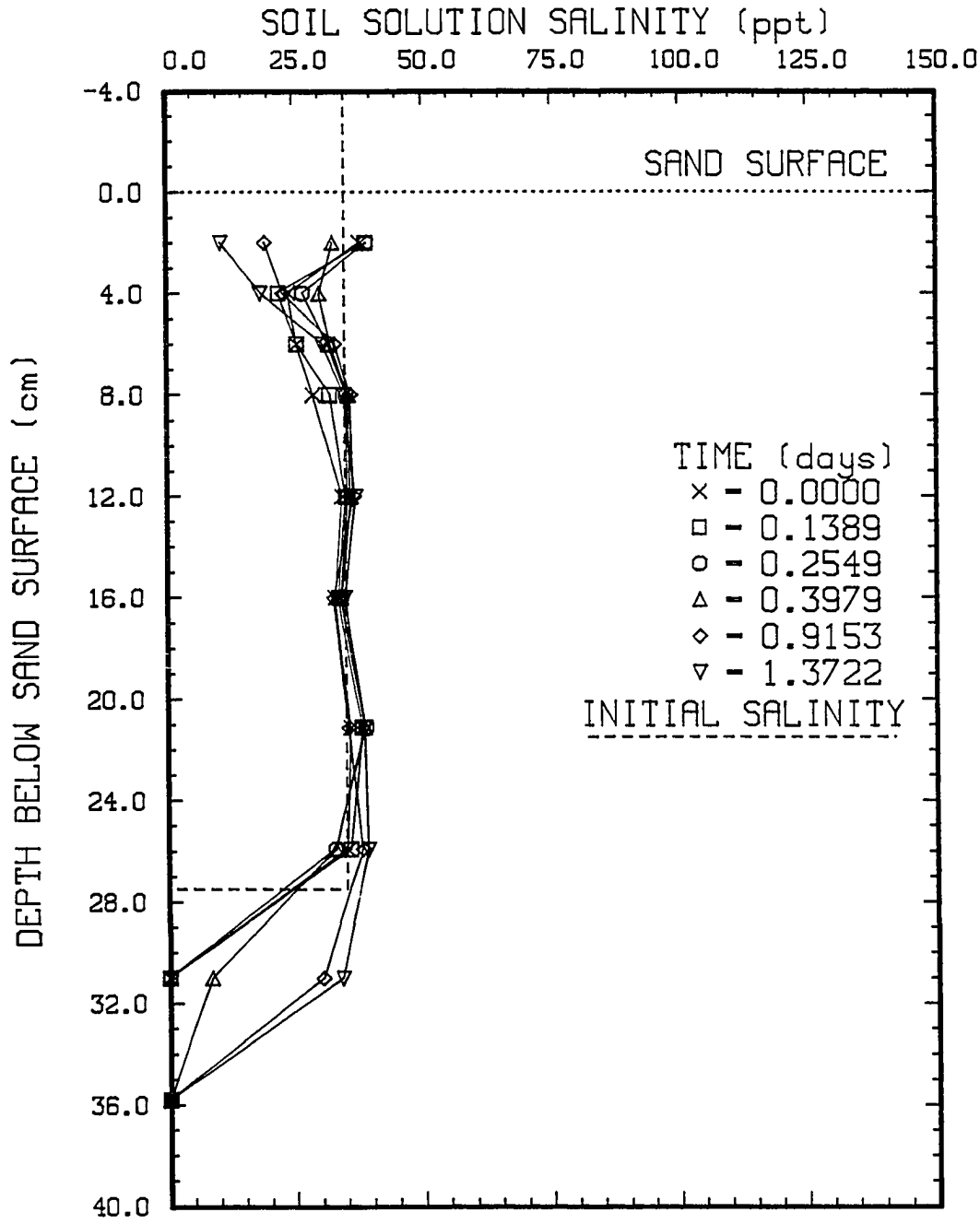

Fig. 4.8: Soil solution salinity profiles for test SCT-2 determined from in-situ electrical conductivity measurements.

conductivity sensors and, hence, low salinity values for this region. However, the salinity values for the lower, fresher region clearly increase in salinity with time.

Tables 4.5 and 4.6 give values for the change of salinity with time, $\partial S/\partial t$, for Test SCT-1 and SCT-2, respectively. The values of $\partial S/\partial t$ are based on differences in S and t values between two successive profiles with respect to time. They clearly show substantial salt redistribution during the time of the test. The less than expected change of the salinity profiles in the initial saline section of the column in test SCT-1 is probably due to poor packing of the sand near the electrical conductivity cell sensors in this region as mentioned above.

It was especially difficult to get a three dimensional view of the fingers formed in the column tests. Therefore, the relation between wavelength and time was not determined for these tests.

It was assumed that the wall effects did not significantly change the final conclusions of the tests. Both the box and column tests seem to give results in agreement with those of Wooding (1969). The contribution of the dye to the electrical conductivity measurements was determined to be negligible.

Special Column Test SCT-3 was conducted in the segmented column with dyed 35 ppt NaCl soil solution

Table 4.5

Rate of change of soil solution salinity based on conductivity cell data from columns vs. depth for test SCT-1

		TIME (days)			
		0.3708	0.9681	1.4000	2.0243
CELL NO.	DEPTH (cm)	∂S/∂t X 10E+6 (ppt/sec)			
1	2.0	86.01	65.86	28.05	40.64
2	4.0	-32.46	64.76	48.78	79.81
3	6.0	-224.67	7.97	19.23	28.19
4	8.0	0.86	1.54	39.86	34.38
5	12.0	56.22	20.81	77.24	40.69
6	16.0	24.59	43.00	109.96	35.73
7	21.1	14.81	68.61	102.16	23.74
8	25.9	-0.54	132.47	91.27	18.45
9	31.0	-22.72	186.62	54.41	19.79
10	35.8	-30.45	251.06	21.19	11.36

Notes:
1. Depth is given in centimeters below sand surface.
2. Time is given in days from beginning of test.

Table 4.6

Rate of change of soil solution salinity based on conductivity cell data from columns vs. depth for test SCT-2

		TIME (days)				
		0.1389	0.2549	0.3979	0.9153	1.3722
CELL NO.	DEPTH (cm)	∂S/∂t X 10E+6 (ppt/sec)				
1	2.0	93.22	8.06	-522.94	-297.93	-218.53
2	4.0	-162.92	483.13	258.47	-158.38	-113.23
3	6.0	8.80	599.25	38.76	19.78	-61.26
4	8.0	276.12	325.99	25.58	9.97	-29.67
5	12.0	63.90	42.27	45.68	12.99	7.51
6	16.0	56.86	49.26	14.96	-34.62	55.69
7	21.1	182.69	63.51	-14.06	-66.08	76.02
8	25.9	55.50	-299.99	10.17	117.83	25.58
9	31.0	0.49	2.06	672.02	488.31	98.47
10	35.8	0.26	0.10	-0.11	-0.03	0.12

Notes:
1. Depth is given in centimeters below sand surface.
2. Time is given in days from beginning of test.

overlaying distilled water soil solution. The initial (dashed line) and final salinity profiles are shown in Figure 4.9. At the end of the test (1.0694 days), salt redistribution resulted in a density stable salinity profile. The bottom section shows a dramatic increase in salinity from 0 to about 17 ppt. This confirms that the salt has moved downward with an average velocity of 1 to 2 cm/hr to the column bottom.

It is important to note that the dye seemed to have a small affinity for the sand particles. This resulted in the leading interface of the dyed finger moving somewhat slower than the actual finger. This was detected from increased salt concentrations in sand samples taken ahead of the dyed fingers. Consequently, actual amplitudes of the salt fingers were estimated to be as much as about 20 percent greater than that indicated by the dyed fingers. However, this difference was not considered significant enough to change the conclusions of these tests.

Investigative salt fingering tests were also conducted using reconstituted subsea permafrost soil samples prepared in a similar manner as that described in Section 2.4.2. A procedure was used similar to that used for test SCT-1, except a dyed 35 ppt NaCl soil solution was placed over distilled water as the soil solution. Fingering velocities of about 1 cm/hr were observed over a 24 hour period. This

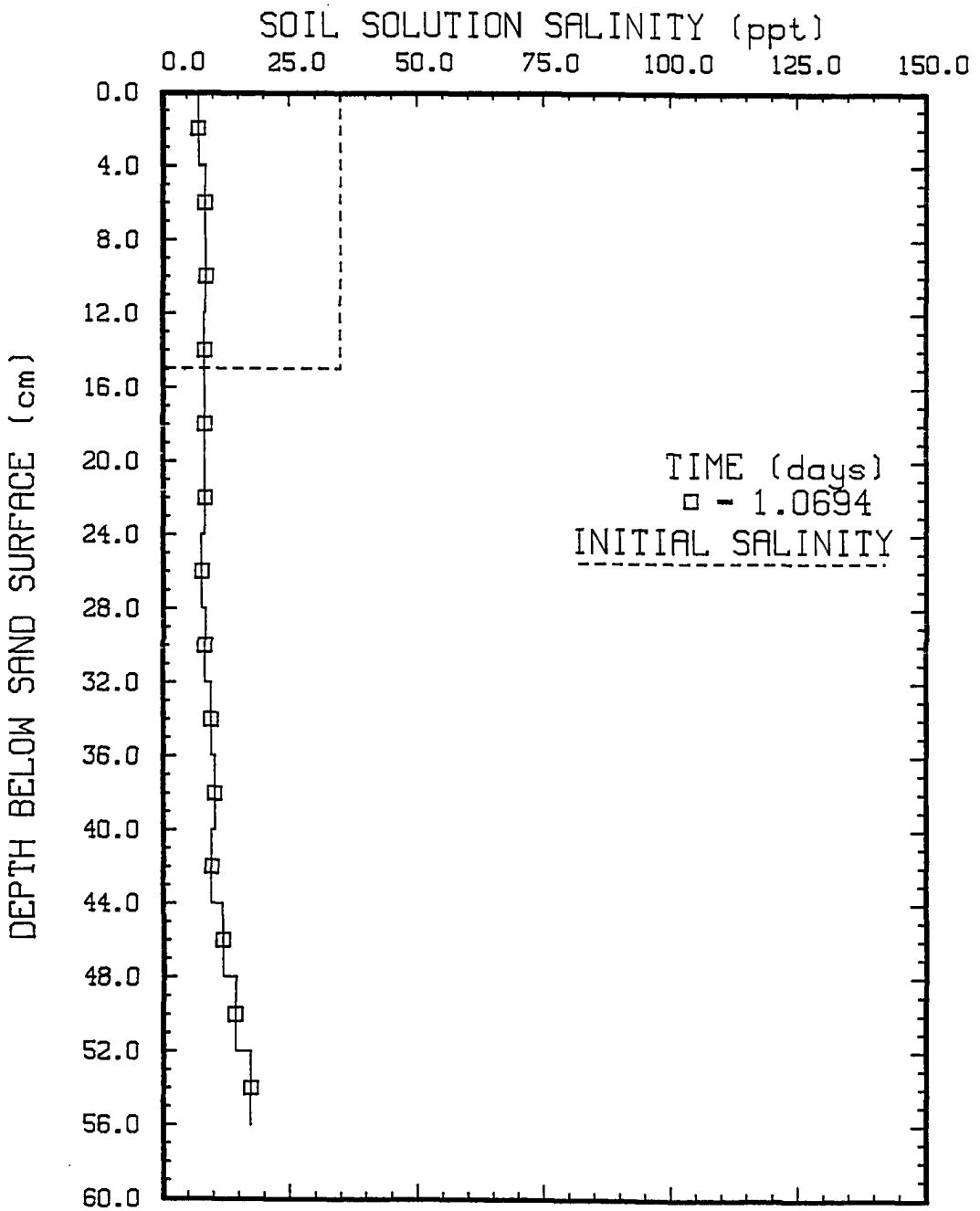

Fig. 4.9: Soil solution salinity vs. depth for test SCT-3.

shows that salt fingering exists in subsea permafrost samples; however, the sediments were dark and it was difficult to see the dyed salt fingers. Consequently, the lighter colored silica sand was used in the above experiments.

4.5 Conclusions

The following conclusions were made.

1) Salt fingering is a gravity driven mechanism for rapid salt transport in sands and subsea permafrost sediments.

2) Finger velocities of several cm/hr were observed with salinity differences of 35 ppt between soil solutions.

3) Initial finger growth rates were proportional to t^A where A (a constant) was between about 1 and 3. This was followed by a transition to where the finger growth rates were proportional to t^b where b was a constant between about 0.36 and 1.

4) Finger wavelength is proportional to t^c where c is a constant between about 0.6 and 1. This is an indication of mutual entrainment between fingers as they develop.

5) Fingers (freshwater) that develop as a result of thawing at the boundary between a fresh, frozen sand overlain by thawed saline sand move rapidly upward through the thawed sand at velocities of several cm/hr.

6) Instabilities in the soil solution salinity profile are stabilized rapidly by salt redistribution due to fingering.

7) The narrow (1 cm) width box test, BT-3, appeared to restrict finger wavelength development without reducing the finger growth rate.

8) Salt fingering tests using reconstituted subsea permafrost soil samples showed salt finger growth rates of about 1 cm/hr.

Chapter 5

MEASUREMENTS OF HYDRAULIC CONDUCTIVITY AND APPLICATION OF LABORATORY RESULTS TO SUBSEA PERMAFROST

5.1 Introduction

Preliminary interpretation of the field data indicated salt was infiltrating the sediments as a result of sediment freezing and/or infiltration of a concentrated layer of brine overlaying the sediments. Laboratory freezing tests in columns of sand indicated that gravity driven convection of salt was occurring with velocities of at least 2 cm/day. Salt fingering was shown to be a gravity-driven convection mechanism for rapid salt transport in sandy soils with observed velocities up to several cm/hr. The above results suggest that the hydraulic conductivity should be larger than suggested by previous field measurements in the coarse-grained subsea permafrost along the WDL. This would be important for the interpretation of field observations because the governing equations for fluid flow through a porous medium, and therefore the salt transport regime, are dependent upon the hydraulic conductivity. In the present chapter, results of hydraulic conductivity measurements of the sediments are reported. The stability criterion for salt fingering and some of the implications of the laboratory results for subsea permafrost are discussed.

5.2 Hydraulic Conductivity of the Sediments Near the Seabed

Both laboratory and field measurements of the hydraulic conductivity, K, of thawed subsea permafrost sediments have been made. Osterkamp and Harrison (1976) reported an average value of 4 X 10^{-7} m/s (13 m/y) for K for a sample obtained in a Shelby tube at site 3370 m offshore along the WDL at a depth of 6.7 m. The sediments were 22 percent gravel, 20 percent sand, and 49 percent silt with less than 10 percent clay. This value for K is thought to have been affected by compression of the sample during driving of the Shelby tube and is therefore probably too low.

Harrison and Osterkamp (1982) report values of K to be appoximately 1 to 10 m/y based on in-situ measurements using a pore water collection probe. These values have been questioned by Swift et al. (1983) on the basis of a measurement problem. The problem is due to the possibility that clogging of the filters in the probe used to measure hydraulic conductivity may have occurred. This may have restricted fluid flow during collection of the pore water and, consequently, resulted in low calculated values for K. Also, the fact that the incoming flow rarely obeys Darcy's law may have affected measured values for K.

Matava (1986) reported in-situ values based on measurements of transient pore pressure decay after driving a probe to measure the pore water pressure. However, a

somewhat similar apparatus as that of Harrison and Osterkamp (1982) was used so that these measurements may be subject to the same problems resulting from the possible clogging of the probe filters.

These evaluations of previous measurements of K suggest that values for K might be larger than the results of the measurements indicate. Therefore, laboratory measurements of K were conducted.

Hydraulic conductivity measurements were made on reconstituted samples taken between 0.2 and 2 m below the seabed. Sediment sample cores from sites located at 100 m and farther from shore were combined, washed with distilled water, and oven dried at 105 °C. The dried sediments were then sieved, separating the silt (defined as those particles with size less than 105 microns) from the remaining sediments. The effect of silt content on K was determined by measuring K of the sediments prepared with various silt contents.

The results (Table 5.1) indicated that the hydraulic conductivity decreased with increasing silt content and ranged from 0.02 cm/sec with no silt to about 0.0007 cm/sec with about 15 percent silt. These values are typical of those reported by Bear (1972) and Bowles (1984) for similar soils.

Table 5.1

Measurements of hydraulic conductivity, K, versus silt content for subsea permafrost sediments

silt content (percent by dry weight)	K (cm/sec)
0	0.02
3	0.01
10	0.001
15	0.0007

These values of K are greater than those previously reported for subsea permafrost along the WDL at Prudhoe Bay by a factor of about 10^2 to 10^3 (Osterkamp and Harrison, 1976; Harrison and Osterkamp, 1982; Matava, 1986). The differences between the previously reported values for K and those of this study may be due to the reasons discussed above or to possible variations of lithology between the sampling sites. If these values of K are truly characteristic of in-situ conditions in subsea permafrost then a reassessment of current interpretations and modeling studies will be required.

The measured value of K for the silica sand used in the laboratory salt fingering experiments was about 0.1 cm/s and is, as expected, similar to the K value measured for the subsea permafrost sample containing no silt. If these

laboratory measurements of K are characteristic of the in-situ values in the thawed subsea permafrost, then pore fluid velocities may be expected to be much larger than previously estimated (Harrison and Osterkamp, 1982).

5.3 Stability Criterion for Salt Fingering

Wooding (1959) investigated the stability of viscous liquids with variable density in a long vertical tube containing a porous medium, such as sand. He defined the Rayleigh number, Ra, as

$$Ra = \frac{d\rho}{dz} \frac{g\ k\ b^2}{\kappa_s\ \mu} \qquad (5.1)$$

where:

$d\rho/dz$ = density gradient

k = permeability of the porous medium

μ = viscosity of the solution

b = typical linear dimension, the radius in the case of a circular tube

g = gravitational acceleration.

κ_s is the diffusivity of the solute through the saturated porous medium and is defined as the quantity of the solute diffusing across the unit area within the porous medium per unit time under unit density gradient. The boundary conditions are such that a no-slip condition is not observed at the tube wall, but the velocity component normal to the

wall vanishes as do the gradients of small disturbances in density and pressure normal to the wall. Wooding (1959) found that

$$\kappa_s = 0.633\ D\ \varepsilon \tag{5.2}$$

where:

D = molecular diffusivity of the solute when the porous medium is absent

ε = porosity.

The ratio $\kappa_s/D\varepsilon$ was found to be relatively unaffected by the packing or porosity and was determined as 0.633 for a number of different particle sizes by Penman (1940), van Bavel (1952) and Wooding (1959). It was also determined that the lowest value for Ra for marginal stability is 3.390 and arises when potential fluid movement is antisymmetric about a plane through the axis of the column with upward motion on one side and downward motion on the other.

Solving Eq. 5.1 for the density gradient, $d\rho/dz$, gives (noting Ra = 3.390)

$$d\rho/dz = \frac{3.390\ \mu\ \kappa_s}{g\ k\ b^2}. \tag{5.3}$$

This is the stability criterion by Wooding (1959) for a denser fluid overlaying a less dense fluid in a vertical tube containing a porous material.

5.4 Application of Laboratory Results to Subsea Permafrost

The possible mechanism(s) for salt transport through the sediments at the ARCO West Dock, Prudhoe Bay, Alaska, has been investigated by several previous studies. These studies were conducted to investigate and account for the different field observations of the subsea permafrost regime at the ARCO West Dock. These include the thaw rate, smoothness, and temperature at the IBPT which is lower than the freezing point of normal seawater, and the uniform salinity (typically about 43 ppt) of the thawed layer overlaying the IBPT and the uniform temperature at the IBPT (about -2.4 °C) from about 440 m to 3.5 km offshore.

Harrison and Osterkamp (1978) analyzed the diffusion of salt as a possible mechanism for salt transport in the development of the thawed layer overlaying the IBPT. Their results suggested that such a diffusive regime should be unstable to convection of the interstitial porewater and did not account for the necessary velocities of salt movement. Swift et al. (1983) concluded that the salt transport mechanism is probably convection of the pore water, but the driving force for the motion was not determined. Driving by the release of relatively fresh, buoyant water by thawing should occur, but it may not provide enough energy to explain the observations. Swift and Harrison (1984) conducted a numerical simulation to investigate the

circulation of brine in the thawed sediments overlaying the IBPT. These simulations showed the development of large convection cells, similar in shape to salt fingers, but they were not consistent with observations of the uniform salt distribution at the IBPT and in the thawed layer above it. The results of these simulations were strongly dependent upon the values used for the hydraulic conductivity. It was suggested that a not yet identified process may be acting to transport salt to the IBPT.

In the following discussion, the stability criterion of Wooding (1959) was used to evaluate the potential for gravity-driven convection, by salt fingering, in the subsea permafrost. Convective salt transport by fingering may be occurring if the density gradient for stability exceeds that predicted by Eq. 5.3.

The characteristic linear dimension b, as defined by Wooding (1959), was taken as the tube radius. The tube contained one complete cell which included one downward moving salt finger and one upward moving fresh finger. In this work, the characteristic dimension was taken as the approximate radius of an imaginary column containing one complete cell, and it was assumed that a similar value would exist in the field. From the laboratory results, this was observed to be about 3.2 cm for the column tests and was also the approximate cell size in the box tests. Although

the dimension of the cell size was shown to increase with time, it does so relatively slowly compared to vertical finger growth and its selection was not thought to affect the final conclusions significantly.

Comparison of fall and spring soil solution salinity profiles of the sediments near the seabed indicated that salt, rejected from sea ice formation and sediment freezing, is infiltrating the sediments. Analysis of the top two meters of the sediments (excluding the top 0.2 m) indicated that the silt content was quite low at about 3 percent. A measured value of K of 0.01 cm/s corresponds to this silt content. Also, the following values were used for the soil solution at about 0 °C (assuming soil solution properties similar to a 40 ppt NaCl solution, from Kaufmann, 1960)

$$\mu \simeq 0.0181 \text{ g/cm-s}$$

and,

$$D \simeq 7.1 \times 10^{-6} \text{ cm}^2/\text{s}.$$

In addition, it was assumed that

$$K = 0.01 \text{ cm/s (3 percent silt)}$$

$$g = 980 \text{ cm/s}^2$$

and,

$$\varepsilon \simeq 0.40.$$

Substitution of known values into Eq. 5.2 gives

$$\kappa_s = 1.80 \times 10^{-6} \text{ cm}^2/\text{s}.$$

Also, since

$$k = K \nu/g \tag{5.4}$$

$$\nu = \mu/\rho$$

and,

$$\rho \simeq 1.030 \text{ g/cm}^3$$

then,

$$\nu \simeq 0.0175 \text{ cm}^2/\text{s}$$

and so,

$$k = 1.8 \times 10^{-7} \text{ cm}^2.$$

Substitution of known values into Eq. 5.3 gives the stability criterion for convection to be

$$d\rho/dz = 6.2 \times 10^{-5} \text{ g/cm}^4. \tag{5.5}$$

At site PB450.8, a thawed layer with very high S_s values of up to 182 ppt at a depth of about 0.8 m overlies a partially frozen zone with much lower S_s values of about 43 ppt about 5 cm below. This gives a density gradient of about 2.2×10^{-2} g/cm^4 which is almost three orders of magnitude greater than that required for stability as predicted by Eq. 5.3 (6.2×10^{-5} g/cm^4). This suggests that as the sediments thaw during the summer and the ice content decreases, the hydraulic conductivity will increase

and allow the highly saline soil solution to move rapidly downward. In this manner, it may be possible for the salt to be transported to the IBPT where it would account for the depressed freezing temperature at the IBPT of about -2.4 °C.

The laboratory results revealed that velocities of salt transport through the thawed sands by fingering can be quite high. Typical velocities reached 1 to 2 cm/hr with a salinity difference of about 35 ppt. The laboratory freezing tests revealed very density-stable, bulk soil solution salinity profiles in the thawed region also indicating rapid transport of the rejected salt from the freezing zone.

The laboratory results also showed that gravity drainage of the unfrozen soil solution, probably by fingering, is mainly responsible for salinity changes in the freezing zone. It was suggested by Mahar (1983) that gravity drainage of the unfrozen soil solution in the freezing (partially frozen) zone would eventually cause the bulk salinity of the frozen zone to become very fresh, given enough time.

Application of the stability criterion of Eq. 5.3 to the partially frozen sediments near the seabed can be used to evaluate the potential for gravity-driven convection by salt fingering. The stability criterion depends on the hydraulic conductivity which is dependent upon the unfrozen

soil solution content as described by Eq. 3.15 (see Section 3.4)

$$K = K_s (V_{AU} \varepsilon)^{B'}. \qquad (3.15)$$

At site PB554.1, the unfrozen soil solution salinity profile shows a nearly linear decrease in salinity from about 79 ppt at 0.32 m to about 53 ppt at 1.33 m. This gives a measured value for $d\rho/dz$ of about 2.1×10^{-4} g/cm^4 (recalling $dp/dS = 0.0008$ g/cm^3 ppt). The absolute unfrozen soil solution content, V_{AU}, is about 0.6. If $K_s = 0.01$, and $B' = 3.28$, then $K = 9.27 \times 10^{-5}$ cm/s from Eq. 3.15 ($k = 1.65 \times 10^{-9}$ cm^2). Substitution of these values into Eq. 5.3 gives the density gradient for stability as (using $b = 3.175$)

$$d\rho/dz = 0.0068 \text{ g/cm}^4$$

which is larger than the measured density gradient by a factor of about thirty, suggesting that, under the above assumptions, convection was not occurring in the partially frozen sediments near the seabed. However, this conclusion is tentative since the values of critical parameters, especially B' and K, are not well established. It is clear that a strong density gradient, which would normally result in convection in ice-free soil, was found in the sediments near the seabed. Presumably, convection could occur until

the unfrozen water content decreased (see Eq. 3.15) sufficiently to reduce K and preclude gravity drainage.

The formation of freshwater fingers at a thawing, relatively fresh frozen boundary overlain by a saline soil were observed in the laboratory fingering tests. This suggests that convective motion, by freshwater fingers, at the IBPT may be occurring, the driving force being the release of fresher buoyant soil solution of the thawing ice-bonded subsea permafrost. However, the results of laboratory fingering tests do not obviously account for the observed uniform temperature of -2.4 °C observed at the IBPT and it is suggested that additional research be conducted addressing this problem.

The stability criterion of Wooding (1959) described by Eq. 5.3 can also be used to investigate the thickness of the concentrated brine layer ahead of a freezing interface (if one exists). If a layer of sufficient salinity forms due to solute rejection it will only remain stable until $d\rho/dz$ exceeds the criterion of Eq. 5.3. The hydraulic conductivity of the quartz sands used in the laboratory test was determined to be about 0.1 cm/s ($k = 1.79 \times 10^{-6}$ cm^2). Substitution of values as given above for K_s, g, μ, and b into Eq. 5.3 gives $d\rho/dz = 6.26 \times 10^{-6}$ g/cm^4.

If the thickness of the concentrated brine layer is assumed to be about 0.1 cm (a typical value for freezing

saline solutions, e.g., Osterkamp and Weber, 1970) then $\Delta\rho$ = 6.26 X 10^{-7} g/cm^3. This corresponds to a very small salinity difference of about 7.83 X 10^{-4} ppt between that of the brine layer and of the thawed layer below. Any significant increase in salinity ahead of the freezing zone above that of the thawed layer should result in very efficient mixing of the layer with the underlying thawed solution. This result explains why the concentrated brine layer ahead of the frozen zone could not be detected during downward freezing. The sensitivity of the in-situ electrical conductivity cells was not sufficient to detect such small salinity differences. When freezing upwards, the build-up of salt ahead of the freezing zone should produce a stable density gradient above the frozen zone. If a high brine layer does exist ahead of a downward freezing zone, it is either very thin or has a salinity not much greater than that of the underlying soil solution of the thawed zone. Also, any gravity drainage of the unfrozen soil solution from the partially frozen zone will probably mask any solute build-up by exclusion ahead of the interface.

5.5 Conclusions

The application of laboratory measurements of hydraulic conductivity and salt finger velocities to the problem of salt movement in subsea permafrost is not

simplistic. Among the difficulties are the variations in soil type, soil solution salinity, temperature, and ice content. In consideration of this, the following tentative conclusions are suggested:

1) Salts rejected during sediment freezing appear to be infiltrating the underlying thawed or partially frozen sediments near the seabed by gravity-convection, probably by fingering, which may be occurring in the top layer of the seabed that annually freezes. The stability criterion is given by Eq. 5.3 (Wooding, 1959).

2) It is suggested that gravity-driven convection of the unfrozen soil solution in the partially frozen sediments near the seabed continues until the hydraulic conductivity is reduced by additional freezing so as to satisfy the stability criterion.

3) Velocities of salt fingers measured in the laboratory experiments are much greater than the thawing velocity of the IBPT. This suggests that salt may be transported at a sufficient rate to the IBPT and may account for the depressed freezing temperatures at the IBPT.

4) The stability criterion suggests that if a high brine layer exists ahead of a downward freezing interface, the salinity build-up at the interface is probably only slightly greater than that of the underlying thawed soil.

5) Laboratory measurements of the hydraulic

conductivity of subsea permafrost sediments indicate that it is much greater than previous measurements would suggest. If these laboratory measurements are characteristic of in-situ conditions in subsea permafrost then pore fluid velocities may be expected to be much larger than previously estimated and a reassessment of current interpretations and modeling studies will be required.

Chapter 6

SUMMARY

Salt redistribution during freezing is an important subject in subsea permafrost studies. Both field investigations and laboratory experiments were performed to obtain new data and to develop new insights into the posssible mechanism of salt transport in subsea permafrost.

The field work determined the sediment characteristics, S_B, W_B, and temperature profiles which were used to calculate the unfrozen sediment properties, such as, S_U, W_U, V_U, and $\partial S/\partial t$. Interpretation of these data indicates significant amounts of salts are infiltrating the sediments during the freezing season, as shown by positive $\partial S/\partial t$ values for this period. Near zero or negative $\partial S/\partial t$ values for the thawing season suggests salt is being transported to lower regions in the sediments during this period. The spring salinity profiles are generally more erratic than in the fall and are a reflection of the rejected salt by sea ice formation infiltrating the sediments, sediment freezing, and of gravity drainage of the unfrozen soil solution in the partially frozen zones. A comparison of the spring and fall S_B profiles implies minimum salt transport velocities of 2 m/year in the top 2 m of the sediments.

The top 0.20 m or so of the near-shore sediments are frozen in the early fall and contains small ice lenses

angled from about 0 to 30 degrees from the vertical which shows that it is frost susceptible.

Temperature profiles confirm earlier results by Osterkamp and Harrison (1982) that there is a nearly constant IBPT temperature of about -2.4 °C beyond about 413 m to about 3.5 km offshore.

The depth to the IBPT can be predicted, approximately, by the Stefan equation along the WDL out to about 400 m offshore. Previous work by others (Harrison and Osterkamp, 1976, Osterkamp and Harrison, 1985) showed that the depth of the IBPT could be approximated by a simple Stefan solution from about 450 m to 3 km offshore.

The laboratory freezing tests indicated that significant salt redistribution occurred during downward freezing of saline sand columns with constant freezing rates which were between about 0.1 and 2 cm/day. The salinity of the partially frozen zone decreases with decreasing freezing rate, v.

Salt redistribution during freezing can be described by the distribution coefficient, k, as defined in BPS theory according to Eq. 3.21, or somewhat better by a linear function of ln(v), as described by Eq. 3.22, for the freezing rates investigated. Rejected salts during freezing are transported into the thawed region by a convective mechanism which is probably gravity-driven convection by

salt fingering. Velocities of the rejected salt from the partially frozen zone through the thaw zone were at least 2 cm/day.

The main mechanism for salt transport in the partially frozen region appears to be gravity drainage with expulsion accounting for only a few percent of the total salinity change. If a concentrated saline layer ahead of the freezing interface exists, it is very thin (< 1.0 mm) or has a salinity that is not significantly different (a few ppt) from the thawed soil solution near the freezing interface. Salt redistribution does not occur during upward freezing. Banding could not be detected on the scale of sampling which was 1 cm.

The laboratory freezing tests indicated that salt movement through a sandy soil could attain velocities of at least 2 cm/day. Salt finger experiments showed that velocities of several cm/hr could be obtained with salinity differences of 35 ppt between soil solutions. Initial finger growth rates were proportional to t^{A} where A (a constant) was between about 1 and 3. This was followed by a transition to where the finger growth rates were proportional to t^{b} where b was a constant between about 0.36 and 1. Finger wavelength is proportional to t^{c} where c is a constant between about 0.6 and 1. This is an indication of mutual entrainment of the soil solution between fingers as

they develop.

Freshwater fingers develop as a result of thawing at the boundary between frozen sand containing freshwater ice overlain by thawed saline sand. These fingers moved rapidly upward through the thawed sand at velocities of several cm/hr. Salt fingering tests using reconstituted subsea permafrost soil samples showed salt finger growth rates of about 1 cm/hr.

Application of the laboratory results to subsea permafrost is not simplistic. Difficulties are encountered when accounting for the effects of variations in soil type, soil solution salinity, temperature, ice content, and freezing and thawing of the sediments. These applications suggest that gravity-driven convection, probably by salt fingering, may be occurring in the top layer of the sediments that annually freezes. The stability criterion for the density gradient is given by Eq. 5.3 (Wooding, 1959). Gravity-driven convection of the unfrozen soil solution in the freezing zone continues until the hydraulic conductivity is reduced by additional freezing so as to satisfy Eq. 5.3.

Salt transport velocities by convective fingering are several orders of magnitude greater than the thawing velocity of the IBPT. This enables salt to be transported at a sufficient rate to the IBPT and accounts for the

depressed freezing temperatures at the IBPT.

The stability criterion of Eq. 5.3 predicts that if a concentrated brine layer exists ahead of a downward freezing interface, the salinity build-up at the interface is not much greater than that of the underlying thawed soil or is very thin. Gravity drainage of the unfrozen soil solution from the partially frozen zone probably masks any solute build-up by exclusion ahead of it.

REFERENCES CITED

Adams, C.M., French, D.N., and Kingery, W.D., 1963, Solidification of Sea Ice, in Ice and Snow; Properties, Processes and Applications, edited by Kingery, W.D., MIT Press, Cambridge, Mass., 745-762.

Alexander, V., and others, 1975, Environmental Studies of an Arctic Estuarine System, Corvallis, Oregon, U.S. Environmental Protection Agency, Final Report, Grant R081124-03, ROAP/Task 21 ARY/002, Program Element 1BA0SS.

Assur, A., 1960, Composition of Sea Ice and Its Tensile Strength, CRREL Research Report 44.

Banin, A., and Anderson, D.M., 1974, Effects of Salt Concentration Changes During Freezing on the Unfrozen Water Content of Porous Materials, Water Resources Research, 10(1), 124-128.

Baker, G.C., 1987, Electrical Conductivity, Freezing Temperature, and Salinity Relationships for Seawater and Sodium Chloride Solutions for the Salinity Range From 0 to Over 200 ppt (in preparation).

Baker, G.C., Matava, T., Osterkamp, T.E., and Harrison, W.D., 1987, Subsea Permafrost: Field Data Report 1984-1985, (in preparation).

Bear, J., 1972, Dynamics of Fluids in Porous Media, 2nd ed., American Elsevier, New York, N.Y.

Bowles, J.E., 1984, Physical and Geotechnical Properties of Soils, 2nd. ed., McGraw Hill Book Company, New York, N.Y.

Burton, J.A., Prim, R.C., and Slichter, W.P., 1953, The Distribution of Solute Crystals Grown from the Melt. Part I. Theoretical, The Journal of Chemical Physics, 21(11), 1987-1966.

Campbell, G.S., 1974, A Simple Method for Determining Unsaturated Conductivity From Moisture Retention Data, Soil Science, 117(6), 311-314.

Casagrande, A., 1932, Discussion of Frost Heaving, Highway Research Board Proceedings, Part 1, 2, 168-172.

Chamberlain, E.J., 1983, Frost Heave of Saline Soils, Proceedings of the Fourth International Conference on Permafrost, Fairbanks, Alaska, 1983, 121-126.

Chuoke, R.L., P. van Meurs, and van der Poel, 1959, The Instability of Slow, Immiscible, Viscous Liquid-Liquid Displacement in Permeable Media, Trans. Am. Inst. Min. Metall. Pet. Eng., 288, 188-194.

Cox, G.F.N., and Weeks, W.F., 1975, Brine Drainage and Initial Salt Entrapment in Sodium Chloride Ice, CRREL Research Report 345.

De Jong, E., 1981, Possible Uses of Freeze-Purification in the Reclamation of Saline Soils, Canadian Journal of Soil Science, 61, 317-324.

Doherty, B.T., and Kester, D.R., 1974, Freezing Point of Seawater, Journal Of Marine Research, 32(2), 285-300.

Elder, J.W., 1968, "The unstable thermal interface", Journal of Fluid Mechanics, Part 1, 32, 69-96.

Grange, B.W., Viskanta, R., and Stevenson, W.H., 1974, Solute and Thermal Redistribution During Freezing of Salt Solutions, In: Heat Transfer, 1974, 1, 220-224.

Gupta, S.P., Varnon, J.E., and Greenkorn, R.A., 1973, Viscous Finger Wavelength Degeneration in Hele-Shaw Cells, Water Resources Research, 9(4), 1039-1046.

Hallet, B., 1978, Solute Redistribution in Freezing Ground, Proceedings of the Third International Conference on Permafrost, Edmonton, Canada, 1978, 86-91.

Harrison, W.D., and Osterkamp, W.D., 1976, A Coupled Heat and Salt Transport Model for Subsea Permafrost, Geophysical Institute Report No. UAG R-247, University of Alaska, Fairbanks, Alaska.

Harrison, W.D., and Osterkamp, T.E., 1977, Subsea Permafrost: Probing, Thermal Regime, and Data Analysis, in Environmental Assessment of the Alaskan Continental Shelf, Annual Reports, 17, 424-466.

Harrison, W.D., and Osterkamp, T.E., 1978, Heat and Mass Transport Processes in Subsea Permafrost I. An Analysis of Molecular Diffusion and Its Consequences, Journal of Geophysical Research, 83(C9), 4707-4712.

Harrison, W.D.,and Osterkamp, T.E., 1979, Subsea Permafrost: Probing, Thermal Regime, and Data Analysis, in Environmental Assessment of the Continental Shelf, Annual Reports, 9, 493-580.

Harrison, W.D.,and Osterkamp, T.E., 1981, Subsea Permafrost: Probing, Thermal Regime, and Data Analysis, In: Environmental Assessment of the Alaskan Continental Shelf, Annual Report, (in press).

Harrison, W.D., and Osterkamp, T.E., 1982, Measurements of the Electrical Conductivity of Interstitial Water in Subsea Permafrost, Proceedings of the Fourth Canadian Permafrost Conference, 229-237.

Harrison, W.D., Musgrave,D., and Reeburgh, W.S., 1983, A Wave-Induced Transport Process in Marine Sediments, Journal of Geophysical Research, 88(C12), 7617-7622.

Heller, J.P., 1966, Onset of Instability Patterns between Miscible Fluids in Porous Media, Journal of Applied Physics, 37(4), 1566-1579.

Hillel, D., 1980, Fundamentals of Soil Physics, Academic Press, London.

Hopkins, D.M., and Hartz, R.W., 1978, Shoreline History of Chukchi and Beaufort Seas as an Aid to Predicting Subsea Permafrost Conditions, Annual Report RU 473, BLM/NOAA OCSEAP, Arctic Project Office, University of Alaska, Fairbanks, Alaska.

Horiguchi, K., and Miller, R.D., 1983, Hydraulic Conductivity Functions of Frozen Materials, Proceedings of the Fourth International Permafrost Conference, Fairbanks, Alaska, 1983, 540-508.

Jackson, M.L., 1958, Soil Chemical Analysis, Prentice-Hall, Inc., New Jersey.

Johansen, O., 1977, Thermal Conductivity of Soils, CRREL Draft Translation TL 637.

Kaufmann, D.W., 1960, Sodium Chloride: The Production and Properties of Salt and Brine, Reinhold Publishing Company, London.

Kay, B.D., and Groenevelt, P.H., 1983, The Redistribution of Solutes in Freezing Soil: Exclusion of Solutes, Proceedings of the Fourth International Conference on Permafrost, Fairbanks, Alaska, 1983, 584-588.

Lachenbruch, A.H., and Marshall, B.V., 1978, in Shoreline History of Chukchi and Beaufort Seas as an Aid to Predicting Subsea Permafrost Conditions, Hopkins, D.M., and Hartz, R.W., Annual Report RU 473, BLM/NOAA OCSEAP, Arctic Project Office, University of Alaska, Fairbanks, Alaska.

Lachenbruch, A.H., Sass, J.H., Marshall, B.V., and Moses, T.H. Jr., 1982, Permafrost, Heat Flow, and the Geothermal Regime at Prudhoe Bay, Alaska, Journal of Geophysical Research, 87(B11), 9301-9316.

Lake, R.A., and Lewis, E.L., 1970, Salt Rejection by Sea Ice During Growth, Journal of Geophysical Research, 75(3), 583-597.

Mackay, J.R., 1972, Offshore Permafrost and Ground Ice, Southern Beaufort Sea, Canada, Canadian Journal of Earth Sciences, 9, 1550-1561.

Mahar, L.J., Wilson, R.M., and Vinson, T.S., 1983, Physical and Numerical Modeling of Uniaxial Freezing in a Saline Gravel, Proceedings of the Fourth International Conference on Permafrost, Fairbanks, Alaska, 773-778.

Matava, T., 1986, Settlement of Thawing Permafrost at Prudhoe Bay, Alaska, M.S. Thesis, University of Alaska, Fairbanks, Alaska.

Nakawo, M., and Sinha, N.K., 1981, Growth Rate and Salinity Profile of First-Year Sea Ice in the High Arctic, Journal of Glaciology, 27(96), 315-330.

Nield, D.A., 1968, Onset of Thermohaline Convection in a Porous Medium, Water Resources Research, 4(3), 553-560.

Osterkamp, T.E., 1968, Electrical Phenomena Accompanying the Phase Change of Dilute KCl Solutions into Single Crystal Ices, Ph.D. Thesis, St. Louis University, St. Louis, Missouri.

Osterkamp, T.E., and Weber, A.H., 1970, Electrical Phenomena Accompanying the Phase Change of Dilute KCL Solutions into Single Crystals of Ice, Journal of Glaciology, 9(56), 269-270.

Osterkamp, T.E., 1975, A Conceptual Model of Offshore Permafrost, Geophysical Institute Report UAG R-234, University of Alaska, Fairbanks, Alaska.

Osterkamp, T.E., and Harrison, W.D., 1976, Subsea Permafrost at Prudhoe Bay, Alaska: Drilling Report, Geophysical Report UAG R-245, University of Alaska, Fairbanks, Alaska.

Osterkamp, T.E., and Harrison, W.D., 1977, Sub-Sea Permafrost Regime at Prudhoe Bay, Journal of Glaciology, 19(81), 627-637.

Osterkamp, T.E., and Harrison, W.D., 1978, Subsea Permafrost: Probing, Thermal Regime and Data Analysis, in Environmental Assessment of the Alaskan Continental Shelf, Annual Reports, 11, 570-650.

Osterkamp, T.E., and Harrison, W.D., 1980, Subsea Permafrost: Probing, Thermal Regime and Data Analysis, in Environmental Assessment of the Alaskan Continental Shelf, Annual Reports, 4, 497-677.

Osterkamp, T.E., and Payne, M.W., 1981, Estimates of Permafrost Thickness From Well Logs in Northern Alaska, Cold Regions Science and Technology, 5, 13-27.

Osterkamp, T.E., and Harrison, W.D., 1981, Methods for Equipment for Temperature Measurements in Subsea Permafrost, Geophysical Report UAG R-285, University of Alaska, Fairbanks, Alaska.

Osterkamp, T.E., and Harrison, W.D., 1982, Temperature Measurements in Subsea Permafrost Off the Coast of Alaska, Fourth Canadian Permafrost Conference, 238-248.

Osterkamp, T.E., and Harrison, W.D., 1982, Subsea Permafrost: Probing, Thermal Regime and Data Analysis, in Annual Report to NOAA, ERL, Boulder, Colorado.

Osterkamp, T.E., 1984, Temperature Measurements in Permafrost, Alaska Department of Public Transportation Report No. FHWA-AK-RD-85-11, Fairbanks, Alaska.

Osterkamp, T.E., Peterson, J.K., and Collett, T.S., 1985, Permafrost Thicknesses in the Oliktok Point, Prudhoe Bay and Mikkelsen Bay Areas of Alaska, Cold Regions Science and Technology, 11, 99-105.

Osterkamp, T.E., and Harrison, W.D., 1985, Subsea Permafrost: Probing, Thermal Regime and Analysis 1975 - 1981, Geophysical Report UAG R-301, University of Alaska, Fairbanks, Alaska.

Page, F.W., 1978, Geochemistry of Subsea Permafrost at Prudhoe Bay, Alaska, M.S. Thesis, Dartmouth College, Hanover, New Hampshire.

Page, F.W., and Iskandar, I.K., 1978, Geochemistry of Subsea Permafrost at Prudhoe Bay, Alaska, CRREL Special Report 78-14.

Paterson, L.P. 1984, Fingering with Miscible Fluids in a Hele Shaw Cell, Physics of Fluids, 28, 26-30.

Penman, H.L., 1940, Gas and Vapor Movements in Soil: Part 1; The Diffusion of Vapors Through Porous Media, Journal of Agricultural Science, 30, 437.

Pounder, E.R., 1965, The Physics of Ice, Permagon Press, New York, N.Y.

Rutter, J.W., and Chalmers, B., 1953, A Prismatic Substructure Formed During Solidification of Metals, Canadian Journal of Physics, 31, 15-39.

Saffman, P.G., and Taylor, G., 1958, The Penetration of a Fluid into a Porous Medium or Hele-Shaw Cell Containing a More Viscous Liquid, Proceedings of the Royal Society of America, 245, 312-329.

Sellman, P.V., Lewellen, R.I., Ueda, H.T., Chamberlain, E., Blouin, S.E., 1977, Operational Report: 1977 USA CRREL-USGS Subsea Permafrost Program, Beaufort Sea, Alaska, CRREL Special Report 77-41.

Sellman, P.V., and Chamberlain, E.J., 1980, Permafrost Beneath the Beaufort Sea: Near Prudhoe Bay, Alaska, Offshore Technical Conference, Transactions of the ASME, 102, 35-48.

Sheeran, D.J., Dalton, C.J. and Yong, N.R., 1976, Field Experimentation with Chemical Alleviation of Frost Damage, Conference on Soil-Water Problems, 173-185.

Swift, D.W., Harrison, W.D., and Osterkamp, T.E., 1983, Heat and Salt Transport Processes in Thawing Subsea Permafrost at Prudhoe Bay, Alaska, Proceedings of the Fourth International Conference on Permafrost, 1221-1226.

Swift, D.W., and Harrison, W.D., 1984, Convective Transport of Brine and Thaw of Subsea Permafrost: Results of Numerical Simulations, Journal of Geophysical Research, 89(C2), 2080-2086.

Terwilliger, J.P., and Dizio, S.F., 1970, Salt Rejection Phenomena in the Freezing of Saline Solutions, Chemical Engineering Science, 25, 1331-1349.

Tiller, W.A., Jackson, K.A., Rutter, J.W., and Chalmers, B., 1953, The Redistribution of Solute Atoms During the Solidification of Metals, ACTA Metallurgica, 1, 428-437.

van Bavel, C.H.M., 1952, Gaseous Diffusion and Porosity in Porous Media, Soil Science, 73, 91-104.

Weeks, W.F., 1962, Tensile Strength of NaCl Ice, Journal of Glaciology, 4(31), 25-52.

Weeks, W.F., and Lofgren, G., 1967, The Effective Solute Distribution Coefficient During the Freezing of NaCl Solutions, Physics of Snow and Ice, 1(1), 579-597.

Weeks, W.F., and Ackley, S.F., 1982, The Growth Structure and Properties of Sea Ice, CRREL Monograph 82-1.

Wilson, R.C., 1983, Solute Redistribution and Freezing Rates, M.S. Thesis, Oregon State University, Corvallis, Oregon.

Wooding, R.A., 1959, The Stability of a Viscous Liquid in a Vertical Tube Containing Porous Material, Proceedings of the Royal Society A, 252, 120-134.

Wooding, R.A., 1960, Instability of a Viscous Liquid of Variable Density in a Vertical Hele-Shaw Cell, Journal of Fluid Mechanics, 7, 501-515.

Wooding, R.A., 1969, Growth of Fingers at an Unstable Diffusing Interface in a Porous Medium or Hele-Shaw Cell, California Institute of Technology, Technical Memorandum 69-5.

Zubov, N.N., 1945, Arctic Ice, Moscow, Izdatel'stvo Glavsevmorputi.

Appendix A

UNFROZEN SOIL SOLUTION EXPULSION AND GRAVITY DRAINAGE MODEL

The relative importance of unfrozen soil solution expulsion and gravity drainage as mechanisms for salt transport can be determined from a one-dimensional model. Cox and Weeks (1975) developed such a model for brine expulsion and gravity drainage for the freezing of pure NaCl solutions. It is argued here that unfrozen soil solution drainage in partially frozen saline sand columns may be expected to be similar to brine drainage in sea ice. The smallest scale in sea ice is that of the platelet width which is only somewhat larger than the pore spaces and sand particles in the sand columns. The ice and brine form a more or less continuous skeletonized structure in both sea ice and the sand columns. Unfrozen soil solution and soil particle interaction should be small in the sand columns. The model of Cox and Weeks (1975) was applied to sand columns with the following modifications: substitution of the bulk soil solution salinity, S_b, for the bulk ice salinity S_i and the subscript for unfrozen soil solution, u, for brine, b, in all equations. It is also assumed that the sand matrix is rigid. Since the freezing of soil will only affect the unfrozen soil solution properties, the continuity equations remain the same. Therefore, the salt conservation equation given by Cox and Weeks (1975) becomes

$$\frac{\partial(n\rho_u S_u)}{\partial t} = -\frac{\partial(n\rho_u S_u V)}{\partial z} + \frac{\partial}{\partial z}\left[n\rho_u D_{sw}\left(\frac{\partial S_u}{\partial z}\right)\right] \qquad (A.1)$$

and the unfrozen soil solution conservation equation is

$$\frac{\partial[n(\rho_u - \rho_i) + \rho_i]}{\partial t} = -\frac{\partial(n\rho_u V)}{\partial z} \qquad (A.2)$$

where:

n = relative unfrozen soil solution content, cm^3 (unfrozen soil solution)/cm^3 (unfrozen soil solution and ice)

ρ_u = unfrozen soil solution density, gm/cm^3

ρ_i = pure ice density, gm/cm^3

S_u = unfrozen soil solution salinity, ppt

V = unfrozen soil solution velocity, cm/s

D_{sw} = binary diffusity of salt in water, cm^2/s

t = time, s

z = vertical coordinate or depth, cm.

The assumptions made during the derivation of these equations include:

1) The sand is saturated, i.e. no air in sand, only ice and unfrozen soil solution
2) The pure ice velocity is zero
3) The ice and unfrozen soil solution are in equilibrium.

The initial and final gravimetric water content, W_s, profiles are not considered except for the noting of

assumption 1. The variation in salinity due to explusion of the unfrozen soil solution can be determined from Eqs. A.1 and A.2 if the rate of change of temperature at each position is known. Since the unfrozen soil solution and ice are in equilibrium (assumption 3), the unfrozen soil solution properties S_u and ρ_u can be expressed as functions of temperature only. From Cox and Weeks (1975)

$$S_u = a_1 T + a_2 T^2 + a_3 T^3 \qquad (A.3)$$

where:

$a_1 = -17.5730$

$a_2 = -0.381246$

$a_3 = -3.28366 \times 10^{-3}$.

In addition, the ρ_u profile can be determined from (Zubov, 1945)

$$\rho_u = 1.0000 + 0.0008\, S_u. \qquad (A.4)$$

Substitution of Eq. A.3 into Eq. A.4 yields,

$$\rho_u = 1.0000 + 0.0008\,(a_1 T + a_2 T^2 + a_3 T^3). \qquad (A.5)$$

If salt transport by diffusion is considered negligible, the salt conservation equation (Eq. A.1) reduces to

$$\frac{\partial(n\rho_u S_u)}{\partial t} + \frac{\partial(n\rho_u S_u V)}{\partial z} = 0. \qquad (A.6)$$

Also, if the density of the pure ice is assumed to be constant (ρ_i = 0.917 g/cm^3), then the unfrozen soil solution conservation equation (Eq. A.2) reduces to

$$\frac{\partial(n\rho_u)}{\partial t} + \frac{\partial(n\rho_u V)}{\partial z} = \rho_i \frac{\partial n}{\partial t}. \tag{A.7}$$

Eliminating $\partial V/\partial z$ from Eqs. A.6 and A.7 gives

$$S_u\rho_i \frac{\partial n}{\partial t} + n\rho_u \left[\frac{\partial S_u}{\partial t} + V\left(\frac{\partial S_u}{\partial z}\right)\right] = 0. \tag{A.8}$$

Since S_u is only a function of temperature, then

$$\frac{\partial S_u}{\partial t} = \frac{\partial S_u}{\partial T}\frac{\partial T}{\partial t} \tag{A.9}$$

and

$$\frac{\partial S_u}{\partial z} = \frac{\partial S_u}{\partial T}\frac{\partial T}{\partial z}. \tag{A.10}$$

Substituting Eqs. A.9 and A.10 into Eq. A.8 and solving for $\partial n/\partial t$ gives

$$\frac{\partial n}{\partial t} = -\frac{n\rho_u}{S_u\rho_i}\frac{\partial S_u}{\partial T}\left[\frac{\partial T}{\partial t} + V\left(\frac{\partial T}{\partial z}\right)\right]. \tag{A.11}$$

The unfrozen soil solution velocity gradient may be obtained from Eq. A.7 as

$$\frac{\partial V}{\partial z} = \frac{(\rho_i - \rho_u)}{n\rho_u}\frac{\partial n}{\partial t} - \frac{1}{\rho_u}\frac{\partial \rho_u}{\partial T}\frac{\partial T}{\partial t} - \frac{V}{\rho_u}\frac{\partial \rho_u}{\partial T}\frac{\partial T}{\partial z} - \frac{V}{n}\frac{\partial n}{\partial z}. \tag{A.12}$$

If the unfrozen soil solution velocity at the surface (z = 0) is assumed to be 0, then Eq. A.11 reduces to

$$\left.\frac{\partial n}{\partial t}\right|_{z=0} = -\left[\frac{n\rho_u}{S_u\rho_i}\frac{\partial S_u}{\partial T}\frac{\partial T}{\partial t}\right]_{z=0} \tag{A.13}$$

and Eq. A.12 reduces to

$$\left.\frac{\partial V}{\partial z}\right|_{z=0} = \left[\frac{(\rho_i - \rho_u)}{n\rho_u}\frac{\partial n}{\partial t} - \frac{1}{\rho_u}\frac{\partial \rho_u}{\partial T}\frac{\partial T}{\partial t}\right]_{z=0} . \tag{A.14}$$

Given

$$\frac{\partial T}{\partial t} = f(z,t) \tag{A.15}$$

Eqs. A.11 through A.14 can be solved using a finite difference method where

$$n_{(z,t+\Delta t)} = n_{(z,t)} + \Delta t\left(\frac{\Delta n}{\Delta t}\right)_{(z,t)} \tag{A.16}$$

$$V_{(z+\Delta z,t)} = V_{(z,t)} + \Delta z\left(\frac{\Delta V}{\Delta z}\right)_{(z,t)} \tag{A.17}$$

and

$$T_{(z,t+\Delta t)} = T_{(z,t)} + \Delta t\left(\frac{\Delta T}{\Delta t}\right)_{(z,t)} \tag{A.18}$$

for small Δz and Δt.

Given the initial salinity and temperature profiles at t_1 and the final temperature profile at t_2, the change in salinity and, hence, the final salinity profile due to unfrozen soil solution expulsion can be calculated. The

difference between this profile and the final experimental salinity profile at t_2 is the salinity change attributed to gravity drainage. Since the rate of change of temperature was assumed to be constant, the calculated change in unfrozen soil solution volume or porosity, n, represents an average value over the time period. From Weeks (1962),

$$n = \frac{S_B/\rho_U S_U}{(S_B/\rho_U S_U) + (1 - S_B/S_U)/\rho_i}. \qquad (A.19)$$

Solving Eq. A.19 for S_B gives

$$S_B = \frac{S_U}{1 - (\rho_i/\rho_U)[1 - (1/n)]}. \qquad (A.20)$$

The final salinity profile is calculated from the final calculated n profile using Eq. A.20.

The temperature change with time, $\partial T/\partial t$, (at a specific depth, z) is assumed to be constant and is

$$\partial T/\partial t = \frac{T_{(z,\ \text{final } t)} - T_{(z,\ \text{initial } t)}}{\text{final } t - \text{initial } t}. \qquad (A.21)$$

Taking $\partial/\partial T$ of Eq. A.3 gives

$$\partial S_U/\partial T = a_1 + 2a_2T + 3a_3T^2 \qquad (A.22)$$

and taking $\partial/\partial T$ of Eq. A.4 gives

$$\partial \rho_U/\partial T = 0.0008\ [\partial S_U/\partial T]. \qquad (A.23)$$

Substitution of Eq. A.22 into Eq. A.23 yields,

$$\partial \rho_u / \partial T = 0.0008\ (a_1 + 2a_2 T + 3a_3 T^2). \qquad (A.24)$$

Since the initial n profile is known, the initial $\partial n/\partial z$ profile can also be determined from a forward differencing approximation,

$$\partial n/\partial z \Big|_{z=0} = \frac{n\ (z=1,t=1) - n\ (z=0,t=1)}{\partial z} \qquad (A.25)$$

and the initial $\partial T/\partial z$ profile from

$$\partial T/\partial z \Big|_{z=0} = \frac{T\ (z=1,t=1) - T\ (z=0,t=1)}{\partial z}. \qquad (A.26)$$

The procedure is outlined by the following steps:

1) assume values for the time (Δt) and depth (Δz) increments
2) calculate $\partial T/\partial t$ profile (with depth increment Δz) from Eq. A.21 using the initial and final T profiles and times
3) calculate profiles (with increment Δz) of S_u, ρ_u, n, $\partial S_u/\partial z$, $\partial \rho_u/\partial z$, $\partial n/\partial z$, and $\partial T/dz$ using the initial profiles (t=1) of T and S_B from Eqs. A.3, A.4, A.19, A.22, A.24, A.25, and A.26, respectively
4) calculate $\partial n/\partial t$ (z=0) from Eq. A.13
5) calculate n (z=0, t=2) from Eq. A.16
6) calculate T (z=0, t=2) from Eq. A.18

7) calculate $\partial V/\partial z$ (z=0,t=1) from Eq. A.14

8) calculate V (z=1,t=1) from Eq. A.17

9) calculate T (z=1,t=2) from Eq. A.18

10) calculate $\partial n/\partial t$ (z=1,t=1) from Eq. A.11

11) calculate n (z=1,t=2) from Eq. A.16

12) calculate $\partial V/\partial z$ (z=1,t=1) from Eq. A.12

13) calculate V (z=2,t=1) from Eq. A.17

14) repeat steps 9) through 13) for entire depth of the initial frozen profile.

After completing step 14, the n and T profiles at t=2 will be known. Steps 3 through 10 are repeated for each increment in time, except for the determination of n (in step 3) from Eq. A.19, until reaching the final time. From the calculated n profile at the final time, the S_B profile due to unfrozen soil solution expulsion can be determined from Eq. A.20.

For this study, the depth increment, Δz, was set at 0.1 cm and the time increment, Δt, was varied between 1 and 10 minutes depending on the length of the time interval. Smaller values of Δz and Δt produced little change in the results.

The percent expulsion was calculated from (Cox and Weeks, 1975)

$$\text{percent expulsion} = \left[\frac{S_c - S_1}{S_2 - S_1}\right] 100 \qquad \text{(A.27)}$$

where S_1 and S_2 are the initial and final experimental bulk soil solution salinity values and S_c is the salinity calculated at the final time by the unfrozen soil solution expulsion model.

Appendix B

LIST OF SYMBOLS

BR	bridge reading, mmhos
CC	cell constant, cm^{-1}
C(S,T)	electrical conductivity of solution with salinity S (ppt) at temperature T (°C)
D_{sw}	binary diffusivity of salt, cm^2/s
D	diffusion coefficient, cm^2/s
g	gravitational acceleration, cm/s^2
k	effective distribution coefficient or permeability, cm^2
K	hydraulic conductivity, cm/s
k_F	frozen seabed thermal conductivity, J/m-yr-°C
k_G	thermal conductivity of the mineral grains, J/m-yr-°C
k_I	thermal conductivity of ice, J/m-yr-°C
k^*	equilibrium distribution coefficient with adsorption effects taken into account
K_S	saturated hydraulic conductivity, cm/s
k_T	thawed seabed thermal conductivity, J/m-yr-°C
k_W	thermal conductivity of water, J/m-yr-°C
L	volumetric latent heat of fusion of seawater, J/m^3
L_S	volumetric latent heat of the seabed, J/m^3
L_V	volumetric latent heat of the seabed with no unfrozen soil solution, J/m^3
M_{DS}	mass of the dry soil sample (with salt)
M_S	mass of the salt
M_{SA}	mass of the sample

M_{sL} mass of the dry soil (no salt)

M_{sw} mass of the diluted sample (with distilled water)

M_U mass of the unfrozen pure water

M_w mass of pure water

n unfrozen soil solution content by volume, cm^3 unfrozen soil solution/cm^3 unfrozen soil solution and ice

Ra Rayleigh number

S_A absolute salinity, ratio of the mass of the salt to the mass of the solution

S_{AU} absolute salinity of the unfrozen soil solution

S_b brine salinity, ppt

S_B bulk soil solution salinity, ppt

S_c salinity calculated with only expulsion occurring, ppt

S_D salinity of the diluted soil solution, ppt

S_F salinity of the frozen material, ppt

S_i bulk ice salinity, ppt

S_o initial salinity of the liquid

S_s salinity of the solid

S_T salinity of thawed material, ppt

S_U salinity of the unfrozen soil solution, ppt

t time

T temperature, °C

T_F freezing temperature, °C

T_s seabed or soil temperature, °C

T_T temperature at the ice-bonded permafrost table, °C

v velocity of freezing interface

V velocity

v_A average vertical finger growth rate

V_{AU} absolute unfrozen soil solution content by volume, ratio of the volume of unfrozen soil solution to the volume of unfrozen soil solution and ice

v_b brine volume content, ratio of the volume of brine to the volume of brine and ice, ppt

V_c characteristic velocity, cm/s

v^* effective velocity of the freezing interface

V_U unfrozen soil solution content by volume, ratio of the volume of unfrozen soil solution to volume of the unfrozen soil solution and ice, ppt

W_B bulk gravimetric water content, ratio of the mass of pure water to the mass of dry soil (no salt)

W_U unfrozen gravimetric water content, ratio of the mass of the unfrozen pure water to the mass of the dry soil (no salt)

w_U volumetric unfrozen water content, cm^3 unfrozen water/cm^3 soil

Z ratio of the mass of the dissolved salts to the mass of the solvent or pure water.

α cubical expansion coefficient

β angle (degrees) or temperature gradient

Δ change

δ thickness of the diffuse layer

ε porosity

θ unsaturated volumetric liquid water content, cm^3 water/cm^3 soil

θ_s saturated volumetric water content, cm^3 water/cm^3 soil

κ_s diffusivity of salt through the porous media, cm^2/s

κ_T thermal diffusivity

μ dynamic viscosity of water, g/cm-s

ν kinematic viscosity, cm^2/s

ρ_b brine density, g/cm^3

ρ_i pure ice density, g/cm^3

ρ_s solution density, g/cm^3

ρ_w water density, g/cm^3

ρ_u unfrozen soil solution salinity, g/cm^3

ψ soil water matric potential, cm-water

ψ_m air entry value, cm-water

Appendix C

DEFINITION OF TERMS

BPS - Burton, Prim, and Slichter (1953) theory describing the unidirection freezing of a solid from its melt containing impurities.

brine - unfrozen saline solution.

frozen - in reference to soils means soil in which part or all of the soil solution contains ice.

IBI - mechanically ice-bonded interface.

IBPT - ice-bonded permafrost table.

ice-bearing permafrost - permafrost that contains ice.

ice-bonded permafrost - ice-bearing permafrost in which the soil particles are cemented together by ice.

MASBT - mean annual seabed temperature.

MAST - mean annual surface temperature.

partially frozen - in reference to soils means soil in which not all of the soil solution is frozen.

permafrost - ground that remains at or below 0 °C for at least two years.

seabed - the floor of the sea, sea bottom.

soil solution - liquid phase of the soil water, less formally referred to as brine or pore water.

subsea permafrost - permafrost occurring beneath the sea bottom.

thawed - in reference to soils means soil not containing ice.

WDL - West Dock Line, field site location at ARCO West Dock, Prudhoe Bay, Alaska.